University of Alberta

Development of KMPR-Based Microfluidic Structures for Use in LOC Systems

by

Matthew Reynolds

A thesis submitted to the Faculty of Graduate Studies and Research
in partial fulfillment of the requirements for the degree of

Master of Science

in

Biomedical Engineering

Department of Electrical and Computer Engineering

©Matthew Reynolds
Spring 2014
Edmonton, Alberta

Permission is hereby granted to the University of Alberta Libraries to reproduce single copies of this thesis and to lend or sell such copies for private, scholarly or scientific research purposes only. Where the thesis is converted to, or otherwise made available in digital form, the University of Alberta will advise potential users of the thesis of these terms.

The author reserves all other publication and other rights in association with the copyright in the thesis and, except as herein before provided, neither the thesis nor any substantial portion thereof may be printed or otherwise reproduced in any material form whatever without the author's prior written permission.

Abstract

Lab-on-chip systems will be a major component in the future of health care. These technologies enable point-of-care testing by miniaturizing and improving the efficiency of many diagnostic techniques. Possible applications include the detection of various pathogens using genetic amplification and analysis techniques. Ideally, a system should provide rapid sample-in-answer-out capabilities without requiring a patient to leave their own home.

The goal of this thesis is to advance lab-on-chip manufacturing technologies by using the epoxy-based photopolymer KMPR with the eventual goal of integrating lab-on-chip devices with CMOS technology. In order to produce integrated microfluidics using this material the physical properties of KMPR and the effect of changing processing conditions on those properties was studied. Following this devices were developed consisting of polymeric microfluidic structures (channels, wells and chambers) and integrated metal thin film structures such as heaters and electrodes. Validation of the fabricated devices was performed in order to confirm their operation.

Acknowledgments

I would like to thank Dr. Duncan Elliott, Dr. Dan Sameoto and Dr. Chris Backhouse for acting as my supervisors for the last couple years. Your guidance and expert knowledge helped to guide and focus my work and bring all of this together.

I would also like to thank Dr. Anastasia Elias not only for serving on my committee but also for the access to her equipment and her knowledge to aid in my studies of the mechanical properties of KMPR. I also want to thank Dr. Jeremy Sit for his help and input while serving on my committee as well.

With all the time I spent working in the U of A nanoFab I certainly cannot forget to thank the staff, along with other members of the user community, for their insights and assistance with developing my processes. A big thanks to the ECE machine shop, especially Herbert Dexel, for their assistance in building a variety of parts and holders for my devices.

I would like to acknowledge both Robert Johnstone and Luis Gutierrez-Rivera for their work in establishing the foundation for my work with KMPR. I would also like to thank Jose Martinez Quijada and Saul Caverhill-Godkewitsch for their work in designing and simulating the heater structures that we needed built. Another big thank you needs to go to David Sloan for the help he provided with setting up and running all the different testing equipment we used. I also need to thank Walid Khaled for his assistance with testing the fabrication process.

I thank Teledyne DALSA Semiconductor and NSERC for their generous support of funds so that my research could actually move forward.

Last but not least I'd like to thank my family, especially my parents, for their endless support of me during all of my life and my schooling. I couldn't have gotten through everything without your help.

Contents

1 Introduction **1**

1.1 Why LOC? 2

1.2 Motivation 3

1.3 Factors Involved with LOC Systems 4

1.3.1 Material Choice 4

1.3.2 Thermal Control 6

1.3.3 Fluid Control Systems 7

2 Prior Work In LOC Technologies **9**

2.1 Silicon-Based Chips 9

2.2 Glass-Based Chips 11

2.3 Plastic/Polymer-Based Chips 12

2.3.1 PDMS 12

2.3.2 Photopolymers - SU-8 and KMPR 15

3 Physical Properties of KMPR **17**

3.1 Advantages of KMPR 19

3.2 Effects of Fabrication Parameters on Material Properties 19

3.2.1 Glass Transition Temperature 20

3.2.2 Young's Modulus 24

3.2.3 Creep Behaviour 26

3.2.4 Thermally Induced Cross-linking 28
3.2.5 Thermal Stability 30
3.3 Chapter Summary 31

4 Development of KMPR Microfluidic Devices 32

4.1 Fabrication of KMPR Structures 33
4.1.1 Thickness Uniformity of KMPR Films 33
4.1.2 Thermo-compressive Bonding 36
4.2 Metal Structures on KMPR 41
4.2.1 Metal Deposition on KMPR 41
4.2.2 Fabrication Process for Heaters 53
4.2.3 Characterization of Metal Properties 55
4.3 Fabrication Process 55
4.3.1 Device Wafer - KMPR Floor 56
4.3.2 Device Wafer - Formation of Al Heaters 56
4.3.3 Device Wafer - KMPR Fluidics 57
4.3.4 Carrier Substrate - PDMS Release Layer 61
4.3.5 Carrier Substrate - Fluidic Roof Layer 62
4.3.6 Thermocompressive Bonding 62
4.3.7 Clarification of Exposure Doses 64
4.3.8 Designed Specifications Compared to Actual Specifications 65
4.4 KMPR-Based LOC Design 66
4.4.1 Thermal Requirements for PCR 67
4.4.2 Fluid Control Systems 67
4.4.3 Electrical Connections for Metal Structures 72
4.5 Chapter Summary 75

5 Design and Fabrication Validation **77**
5.1 Heater Functionality and Durability 77
5.1.1 Physical Stability 78
5.1.2 Discussion Of Heater Wrinkling 83
5.1.3 Hotplate Calibrations 86
5.1.4 Electromigration Effects 88
5.1.5 IR Camera Results 90
5.2 Chapter Summary 96

6 Conclusion **99**
6.1 Future Direction 102
6.1.1 Issues Related to Wet Operation of the Devices 103
6.1.2 Airgap Structures 103
6.1.3 Alternate Fabrication Techniques 104

Bibliography **106**

Appendices

A Fabrication Protocols **118**

B Membrane Deflection **149**

C Selective Bonding **162**

D Lithographic Roughening **183**

E Heater Metal Choices **193**

F Dicing Accuracy **198**

List of Tables

3.1 Modulus and Tensile Strength of KMPR 25

3.2 Thermally-Induced Cross-Linking Results for KMPR 29

4.1 Thickness Uniformity of KMPR Films 36

4.2 Stress in Sputtered Metal Films 45

4.3 TiW Deposition Testing 49

4.4 Al Deposition Testing 50

4.5 Cr Deposition Testing 54

4.6 Resistivities of Sputtered Al Films 55

4.7 Values Used in Calculations of Contact Area 73

4.8 Calculations of Electrical Contact Area and Cross-Section Area 74

A.1 Fabrication Parameter Changes Between Batches 138

B.1 COMSOL Simulation Parameters 151

B.2 Simulation Results for Membrane Deflection 152

D.1 Lithographic Roughness Results 189

E.1 Properties of Selected Metals For Possible Heater Metals 194

List of Figures

3.1 T_g vs Exposure Dose 22

3.2 T_g vs Bake Time 23

3.3 T_g vs Bake Temperature 24

3.4 Stress-Strain Curves for KMPR 25

3.5 Creep Results for KMPR 28

3.6 Relaxation Results for KMPR 29

3.7 TGA Curve for KMPR 30

4.1 Fabrication Flow Chart for Bonding 38

4.2 Poor Bonding of KMPR Films 40

4.3 Good Bonding of KMPR 42

4.4 Tape Test Adhesion Results for KMPR and SU-8 43

4.5 Tensile Stress Cracks in Thin Film TiW 47

4.6 Compressive Stress in Thin Film Al 48

4.7 Al Film Wrinkling During Bonding 51

4.8 Avoiding Al Wrinkling During Bonding 52

4.9 Reduction of Al Wrinkling After Bonding 52

4.10 KMPR Cracking During Lift-Off 53

4.11 Fabrication Flow Chart for Device Wafer 58

4.12 Overexposed KMPR Features 61

4.13 Fabrication Flow Chart for Carrier Wafer 63

4.14 Heater Designs 68
4.15 Normally Open Valve Design 69
4.16 Helper Chip 70
4.17 Design Layout for KMPR PC2 71

5.1 Film Wrinkling in Heated Waterbath 81
5.2 Resistance Change of Wrinkled Film in Heated Waterbath . . . 82
5.3 TCR Calibration Results Using Hotplate 87
5.4 Electromigration Failure of Heater Traces 91
5.5 IR Temperature Measurements of Heater 93
5.6 Calibrated IR Temperature Measurements 94
5.7 Adjusted Simulation Results to Confirm IR Temperature Measurements 97

B.1 COMSOL Simulation Geometry 150
B.2 Simulation Result for 0 Posts. 153
B.3 Simulation Result for a Post Placed in the Center of the Chamber. 153
B.4 Simulation Result for 7 Posts. 154
B.5 Simulation Result for 25 Posts. 154
B.6 Simulation Result for 55 Posts. 155
B.7 Simulation Results for a Square Grid of Posts 156
B.8 Simulation Results for a Rectangular Grid of Posts 156
B.9 Simulated Formation of Posts - Rectangular Grid 158
B.10 Simulated Formation of Posts - Hexagonal Grid 158

C.1 SB Result - 60°C PEB 164
C.2 Delamination of KMPR Following 60°C PEB 165
C.3 SB Result - 70°C PEB, 75°C Bonding Temperature 166
C.4 SB Result - 70°C PEB, 90°C Bonding Temperature 168

C.5 Post-Release, PEB at 70°C, Bonded at 85°C, 5750N, 15 minutes. Again the bonding quality was quite poor due to the amount of delaminated area requiring different parameters to be needed for a reliable bonding process. 169
C.6 Bonding at 85°C for 15 Minutes at 5750N 170
C.7 Bonding at 90°C for 15 Minutes at 5750N 171
C.8 Bonding at 85°C for 20 Minutes at 5750N 172
C.9 Substrate bonded at 85°C for 20 minutes at 5750N. The bonding quality would still be considered poor due to the amount of delaminated area. 173
C.10 First Bond for PC5K Chips 174
C.11 Second Bond for PC5K Chips 175
C.12 PC5K Bonding 176
C.13 Filling Test on Bonded Chips 176
C.14 Bonding at 100°C for 15 Minutes with 11500N of Force 177
C.15 Second Bonded Layer of KMPR 178
C.16 Bonding at 80°C 179
C.17 Second Bond Step at 90°C 179
C.18 Second Bonded Layer of KMPR 180

D.1 Optical Profilometer Measurements of Surface Roughness Following Exposure and Baking 185
D.2 Formation Surface Roughness During Fabrication 186
D.3 Fabrication Overview for Lithographic Roughness Tests 188

F.1 Substrate Mounted on Dicing Saw 199
F.2 Dicing Reticle 199
F.3 Rotational Alignment of Dicing Saw 200

F.4 Dicing Lines as Viewed by Saw 201

List of Abbreviations

LOC	Lab On Chip
POC	Point Of Care
μTAS	Micro Total Analysis System
MEMS	Micro Electromechanical Systems
TMAH	Tetramethylammonium Hydroxide
PDMS	Polydimethylsiloxane
PMMA	Poly(methyl methacrylate)
PCR	Polymerase Chain Reaction
qPCR	Quantitative Polymerase Chain Reaction
MCA	Melt Curve Analysis
SP	Sample Preparation
CE	Capillary Electrophoresis
TGA	Thermal Gravimetric Analysis
DMA	Dynamic Mechanical Analysis (or Dynamic Mechanical Analyzer)
T_g	Glass Transition Temperature
PACs	Photo Active Compounds
PEB	Post Exposure Bake
TCR	Temperature Coefficient of Resistivity
SB	Selective Bonding
CW	Carrier Wafer
DW	Device Wafer

Chapter 1

Introduction

Lab-on-a-chip (LOC) technologies have drawn significant attention in recent years [1-10]. Much research has been performed all over the world as many different chemical, biological and life-science applications have driven the need for cheaper and faster analysis equipment. LOC-based systems have enormous potential as point-of-care (POC) diagnostic systems as they are highly efficient genetic analysis platforms [4] due to their high speeds, low costs, good sensitivity, small system size and ease of use [4]. Currently most medical diagnostic tests are performed by highly trained lab technicians using large, expensive equipment. Due to the high cost of the equipment necessary for performing these tests it is not possible to perform many diagnostic tests in point-of-care locations such as local clinics or in areas of the world where fully equipped labs do not exist [5]. Numerous reviews have been written in recent years detailing the state of LOC and μTAS (micro-Total Analysis Systems) research around the world today [3-10] as solutions continue to be developed to overcome the current limitations of medical testing.

This chapter will outline some of the key advantages of LOC technologies and discuss some of the key challenges involved in the development of these

systems.

1.1 Why LOC?

Small, microfluidic-based LOC systems for performing genetic testing are extremely desirable for a number of reasons. The key factor in the effectiveness of these technologies is the small volumes of fluids required for operation. LOC devices have the ability to operate using volumes ranging from microliters to nanoliters, resulting in entire new regimes for performing tests. This smaller volume directly affects the volume of reagents required during tests which is often a significant cost (on the order of $100 per test) for genetic amplification processes [11]. This high cost arises as the biomolecules used must be synthesized for each specific genetic sequence to be amplified. Microfluidic systems utilize volumes that are 10^4 to 10^6 times lower than conventional systems resulting in a negligible reagent cost per test [11]. The reduced volume used in microfluidics also allows for the use of samples that might be too valuable to be used in conventional tests, allowing for a greater range of tests to be performed.

In addition to the reagent benefits, the smaller dimensions used in microfluidic systems results in a highly controllable fluid flow, allowing for improved automation. By including fluid control systems such as microvalves and pumps, these systems can allow for complex movement of the fluid within the devices without requiring manual, physical input from a user. This kind of system allows for parallel operation of various tests on the same chip by using the same samples and reagent supplies multiple times [12].

The use of microfabrication techniques to produce these systems also yields a number of advantages. Most microfabrication processes are easily scaled up

for high volume manufacturing, reducing the cost of LOC technologies. Additionally, modules can be added to systems at a significantly reduced unit cost as long they don't require significant changes to the fabrication process. This allows for LOC systems to utilize a single sample in a wide range of tests for little additional cost. Microfabrication processes also produce very predictable dimensions and material properties which can improve the reliability of test results. The reduced size and cost of LOC systems will also enable a wide range of medical diagnostics to be performed in poor or remote areas instead of requiring fully equipped hospitals and labs [5].

LOC technologies have the potential to change the landscape of modern medical diagnostics by increasing the efficiency and availability of previously limited tests. As research continues to advance these systems, new breakthroughs will allow for wider adoption and use, improving the quality of health care around the world.

1.2 Motivation

The purpose of this thesis is to detail the developments that have been made to our research group's LOC devices over the course of my work. The ideal outcome of this work is to develop a polymer-based LOC device that is capable of performing genetic amplification and detection in a single, integrated chip. Accomplishing this requires an understanding of the physical properties of the polymer materials along with the development of integrated heater structures capable of thermal cycling a sealed volume of fluid to amplify a sample of DNA. This thesis will cover my studies related to the physical properties of KMPR with respect to the fabrication conditions along with the fabrication process development to build the microfluidic structures and the integrated aluminium

heaters for performing genetic amplification. It is hoped that the work in this thesis will lead to a device capable of performing genetic amplification and detection on chip.

1.3 Factors Involved with LOC Systems

LOC systems typically consist of two parts: the small chips on which testing takes place and larger external systems which control the operation of the chips [13]. These external systems are typically more expensive than the chips (though still far cheaper than conventional systems) but may be used repeatedly while the smaller chips may be designed as disposable devices to avoid contamination issues. Although these external systems are important for LOC functionality, the focus of the LOC field is the chips themselves. There are several important factors that we needed to consider when designing and creating our chips [14]:

- What material(s) should they be fabricated from?
- What thermal control elements (heaters, sensors) are to be used?
- What kind of system is required for fluid control during operation?

Answering these questions will be the focus of this thesis with each of these areas being studied.

1.3.1 Material Choice

The first major decision to be made is what material shoudl be used to build our devices. There are currently 3 material types that are primarily used to fabricate LOC devices: silicon [15], glass [16] and polymers [17]. Each have their own advantages and disadvantages related to fabrication and chip

operation. Silicon, thanks to the microelectronics industry, is a very well understood material with a wide range of fabrication processes available for use. Unfortunately silicon is optically opaque in the UV and visible light spectra while the preferred detection mode for LOC systems is optical. In order to use silicon as a chip material windows must be fabricated in the chips to allow for optical access to the sample being analyzed. Also, despite the fact that silicon fabrication processes are very well characterized and precise, processing silicon tends to be too expensive for producing cheap, single-use chips and we have chosen to avoid using this as a material.

Glass chips are popular owing to their high transparency to UV and visible light (allowing for fluorescent measurements to be more reliable), chemical inertness, high dielectric strength (supporting well controlled electric fields for use in electrophoresis) and well-developed surface chemistry processes [18, 19]. Unfortunately glass fabrication also tends to be fairly expensive and can be quite complicated to perform [14] limiting this material's usefulness when producing cheap, mass-produced devices.

Polymer based chips have drawn a lot of attention in recent years as the all-around solution to producing cheap, reliable chips. Two of the most popular polymers to be used for this purpose have been PDMS and PMMA [20, 6] although other polymers such as SU-8 [17, 21] and KMPR [22, 23] have seen recent attention. The main factors pushing polymer-based chips are their low cost and simple fabrication requirements. Polymers also tend to have positive optical, physical and chemical characteristics with respect to the requirements for genetic analysis [15]. However there are still a large number of challenges facing polymer based chips including their long term stability, inherent fluorescent background (interfering with optical/fluorescent detection systems), low glass-transition temperature (compared to Si and glass) and difficulties with

fabricating metal films on their surfaces (for heating/temperature sensing purposes) [14]. PDMS especially, despite its popularity, is known to swell when exposed to solvents, is permeable to gases and is not readily compatible with high-volume manufacturing [15].

Despite the challenges facing polymer-based devices our research group has decided to move forward with using KMPR as a material for producing LOC devices.

1.3.2 Thermal Control

In order to successfully test a sample of DNA, it is important to first increase the amount of sample present to make it easier to detect. The primary process used today for DNA amplification is polymerase chain reaction (PCR). During PCR, the temperature of the sample is cycled through a series of stages corresponding to the denaturing, annealing and extension of the DNA strands [24]. The sample containing the DNA must typically reach temperatures of approximately 95°C to accomplish efficient amplification, requiring accurate temperature control. As a result any LOC system must possess precise thermal control, including both a heating and a temperature sensing element, in order to perform a successful PCR. Also, given that PCR is often the slowest process in genetic analysis systems, it is beneficial to reduce the temperature ramp times as much as possible in order to further reduce the overall analysis time. For POC applications, contact heaters such as Peltier heaters or patterned thin film heaters made from materials such as titanium/platinum [16], aluminium [25] or indium tin oxide [26] are common. Thin film heaters are especially preferred due to their small size and ease of integration and operation.

In our devices we have attempted to integrate a thin film aluminium heater

into the polymer structure of our chips in an attempt to achieve this precise and rapid temperature control.

1.3.3 Fluid Control Systems

One of the key requirements for seamless integration of LOC systems is efficient transport of the sample through the chips [14]. As a sample is moved through a chip to the various stages of processing it is necessary to reduce or avoid any contamination, dilutions or losses in the sample. Many of the different solutions involved in genetic analysis are incompatible with PCR and as such great care is required to avoid contamination. In order to accomplish this sample control some sort of fluid control system is required, often involving electric fields [24, 16], magnetic fields [24], pumps [16] and/or valves. Capture and release structures have also been used in order to collect samples with very high efficiency but can be difficult to implement on-chip [24]. Pumps and electric fields are often simpler structures to implement on-chip but require precise control of the timing in order to properly control a sample, often resulting in low transfer efficiencies.

In designing a pump/valve system for LOC devices there are a large number of factors to consider such as if the valve should be normally open or closed (i.e. the "resting" state), the dead volume, power requirement for actuation, the amount of pressure it can withstand and the complexity and cost of fabrication. Valves can typically be divided into four categories [14]: active mechanical, passive mechanical, active non-mechanical and passive non-mechanical. Out of these 4, active mechanical valves (e.g. electromagnetic, piezoelectric, or pneumatically actuated) are the most common for LOC systems [14] as they have the best performance characteristics, although passive valves may be better suited for certain applications [27].

We have attempted to use a number of different fluid control systems in our devices but have consistently run into problems with building integrated mechanical valves within our devices. Although we have currently settled on an external valve system to control the flow through our chips there is still work being done to develop a valve system that operates directly within the KMPR structures.

The rest of this thesis will cover the work that has been done to develop our KMPR-based LOC systems. Chapter 2 will describe some of the previous work that has been accomplished in the LOC field that we will build off of. Chapter 3 will describe our studies into the mechanical properties of KMPR in order to enable us to build reliable microfluidic structures. Chapter 4 will cover the development of the fabrication process for the devices, along with the development of a thermal control system consisting of an aluminium heater and temperature sensor for performing rapid PCR. Chapter 5 will discuss some of the validation of the devices that has been performed relating the physical and thermal performance of the fabricated devices. The goal of this research is to be able to build a device capable of performing genetic amplification and detection on a single KMPR-based chip.

Chapter 2

Prior Work In LOC Technologies

Virtually all new research is performed using a foundation of knowledge developed by earlier work done in the same or similar fields. This chapter will discuss some of the advancements that have been developed in the LOC field that has led up to the work that is being done today. A convenient sorting system for presenting these advancements is by sorting them based on the primary material used to produce the LOC devices. The materials typically used for LOC systems are silicon, glass and various polymers (PDMS, PMMA, SU-8, KMPR, etc). Early work in the field was focused on silicon based systems although the focus has largely shifted to glass and polymer based systems due to weaknesses inherent to silicon as a material.

2.1 Silicon-Based Chips

Many early examples of LOC technologies were produced using silicon substrates due to the wide range of technologies available for fabrication. The earliest examples of microfluidic LOC systems were demonstrated in the early

1990s [28, 29, 30] as research groups began developing the various aspects of the technologies. It was Manz et al. [31] who first described the concept of a miniaturized Total Chemical Analysis System (μTAS) as a method for performing all stages of an analysis process on a single device. Although miniaturization of the fluidics is the key to improving the speed of analysis, the priority with these technologies is in on improved performance, not the reduction in size. This focus is still used for research in the LOC field today as the development of cheaper, faster and more reliable analysis systems continues.

As with LOC systems in other materials, the focus of development for silicon LOC systems has often been on fluid control systems and chemical detection mechanisms. Early work on silicon systems involved the development of pump systems in order to manipulate samples within the devices. Some of the earliest developments by Van Lintel et al. [28] involve piezo-electric actuated pumps which were capable of unidirectionally controlling the flow of liquids through Si channels by using flap structures to prevent reverse flow. Later research by Zengerle et al. [30] was able to produce bidirectional pumps as well. Manz et al. [29] were also able to demonstrate capillary electrophoresis (CE) on silicon chips, although they determined that at the higher voltages required for efficient CE the voltage breakdown in the semiconductor material proved problematic despite the use of insulating films around the channels. This behaviour caused them to consider using glass as a material due to its superior electrical insulation. CE continues to be a popular technique for genetic detection in LOC systems today, although other techniques have been developed as well. Regardless of the techniques and applications used the focus on improved fluid and sample control has continued to this day in order to develop and fully integrated and automated LOC system.

A further review of silicon-based microfluidics throughout the 1990s was

published by Van Den Berg and Lammerink [32].

2.2 Glass-Based Chips

As the focus in the LOC field shifted away from silicon numerous advancements were made in glass-based chips. Using thin film heaters and temperature sensing elements, Lagally et al. [27] were able to produce chips capable of performing PCR and CE. By integrating a thin film heater and temperature sensor they were able to achieve heating and cooling of the sample in order to amplify DNA in under 15 minutes. By later including a PDMS-glass valve in the system [33] they were able to make a further step towards a fully integrated LOC system. The use of an integrated thin film heater for enabling thermal control for PCR is the technique that we have used when developing our KMPR-based devices discussed in later chapters.

While further building off of this glass-PDMS chip, Behnam et al. [34] were able to integrate sample preparation steps into the chips as well, allowing for the possibility of raw samples (blood, saliva, etc) to be inserted directly into the chips for automated analysis. They were also able to detect the amplified PCR product using a simple lens, filter and photodiode optics system allowing for a far cheaper system to be produced compared to previous devices requiring confocal optics and photomultiplier tubes.

In order to further improve automation of LOC devices Wu et al. [35] were able to bond their glass microfluidics onto printed circuit boards in order to include integrated electronics with their chips. This integration allowed for better automation of the electronic detection of products and opened the door for smaller, cheaper control systems for LOC devices.

Many of the developments that were made using glass-based devices are

a direct inspiration for our polymer-based chips. Our devices attempt to use integrated heaters and valves combined with similar external control and detection systems to produce a functional polymer-based LOC device. By building off of this past work it has allowed us to focus primarily on the new challenges presented when working with polymer structures without also needing to re-develop all of the previous advancements resulting from work in other chip materials.

2.3 Plastic/Polymer-Based Chips

Despite the effectiveness of glass as a material for LOC devices fabrication costs for glass-based chips are still considered to be too high for cheap, mass-produced chips. To overcome this cost factor plastics and polymers are usually considered the best alternative material. Demonstrations have been performed in order to produce simple microfluidic channels in biodegradable plastics [36], hydrogels [37] and polystyrene [38]. PMMA and polypropylene [39, 40] have also been used to produce LOC systems. One of the most popular polymers to be used for microfluidic systems is polydimethylsiloxane (PDMS). Photopolymers such as SU-8 and KMPR have also seen recent attention as structural materials for LOC devices.

Many of the advancements resulting from work on other polymer materials can be readily transferred into our KMPR-based devices and are certainly worth keeping in mind while designing and developing our devices.

2.3.1 PDMS

PDMS is a popular material for LOC systems due to its ease of fabrication by molding techniques. Continuous flow PCR chips have been demonstrated

in PDMS based chips by Joung et al. [41] and Fukuba et al. [26] by using molding techniques to form channels using a master mold of lithographically patterned SU-8. Continuous flow PCR is a variant of typical PCR in which a sample is flowed through a channel consisting of areas heated to different temperatures corresponding to the different temperature steps of PCR. The heating is accomplished in this particular device by using indium-tin-oxide (ITO) thin film heaters fabricated on a glass substrate. The heaters heat large areas of the substrate to the required temperature, and the length of the channel in each heated section is made proportional to the time required for a sample to be kept at that temperature. A sample can then be flowed at a constant velocity through the channels to accomplish the thermal cycling.

Liu et al. developed devices produced from molded PDMS in order to electrochemically determine the location of sample droplets withing the fluidic channels [42]. By eliminating the need for optical detection of the fluid within channels this method can allow for better automation of LOC devices.

Three-dimensional multilayer fluidics in PDMS have also been developed by Zhang et al. [43]. By taking advantage of the transparency and flexibility of PDMS they were able to produce fluidic structures using as many as 6 different layers of PDMS bonded together in a rapid, repeatable and cheap method that is compatible with mass production techniques. Each individual layer was casted using an SU-8 mold and oxygen-plasma bonded to the previous layers. This type of multilayer fluidics creates the possibility of valves and pumps being integrated within the devices further enhancing the automation and efficiency of LOC devices.

Shao et al. developed a pneumatically actuated trapping structure for the capture of microbeads within fluidic channels [44]. Charged microbeads are often used as a capture medium for DNA in order to separate the genetic ma-

terial from the cellular proteins released during cell lysis. By trapping these beads within the channels it is possible to wash away the cellular proteins while minimizing the losses of the sample DNA. They were able to use pneumatic pressure to compress the diameter of the channel to a size smaller than that of the beads, thereby pushing the beads into an adjacent array of pillar structures and trapping them, while fluid is allowed to flow over them through the remaining diameter of the channel. Upon releasing the pneumatic pressure the beads are able to move back into the channel and flow to another part of the device.

In an effort to further improve the control of DNA, Sheng and Bowser [45] developed a nanoporous membrane in a PDMS microfluidic device in order to allow for the size-selective transport of DNA. Molded PDMS channels are separated by a porous polycarbonate membrane in order to facilitate the transport of DNA. The pores in the polycarbonate membrane are large enough to allow for a strand of DNA to pass through. The pores are small enough that larger DNA strands are slower to cross the membrane and by manipulating the flow rates and the buffer strength it is possible to control the transport of DNA by preventing larger strands from crossing the membrane.

Lounsbury et al. developed a PDMS/PMMA microfluidic device capable of processing a raw sample (buccal swab) and performing a PCR in under 45 minutes [40]. The devices use single-actuation valves and external IR heating during processing. Although these devices are an important step forward in the LOC field there is still much room for improvement with respect to manufacturability, integration, automation and speed of processing. A method of detecting the PCR product is also required to be integrated with the system before a true "sample-in-answer-out" system can be realized.

2.3.2 Photopolymers - SU-8 and KMPR

The negative photopolymers SU-8 and KMPR have also seen recent attention as materials for microfluidic structures. Negative photopolymers are a class of photoresist material which exhibit increased chemical resistance following exposure to UV light. UV exposure activates photo-sensitive chemicals within the resist layer that serve to change the physical structure of the resist (typically by increasing the level of cross-linking between the polymer chains). Fluidic structures are produced in these materials by using photolithography to directly pattern thin films, allowing for high resolution patterns with high contrast ratio walls (nearly 90° angle between channel floor and walls) for fluidic channels. By bonding layers of the material together it is possible to form closed channels and chambers as well as creating the possibility of 3D valve structures.

The first demonstration of full-wafer bonding with SU-8 was demonstrated in 2004 [46], allowing for the production of three dimensional fluidic channels in a fast, reliable process performed at temperatures low enough to be compatible with a wide range of technologies, including CMOS devices. PCR has also been performed in SU-8 devices [17] in order to demonstrate the compatibility of the material with the amplification process although the heater structure was fabricated directly on the glass substrate. This style of bonding processed has also been used for the production of SU-8 based integrated SP, PCR, CE devices that are designed for operation in point-of-care situations [21].

KMPR-based microfluidics have also seen development in recent research. Directly patterned fluidic channels have been produced by photolithography with parts of the KMPR combined with an absorbing dye to form a filter to improve fluorescence detection [22]. A multilayer bonding technique, using a thin film of KMPR as a bonding agent, has also been developed to produce

three-dimensional KMPR structures [47]. This method can be applied to improve the bonding quality for highly cross-linked films compared to typical thermo-compressive methods and has even been shown to allow up to 6 layers to be bonded on one substrate.

A number of the developments that have been listed in this chapter were applied during the development of our KMPR-based LOC devices, while many of the remaining techniques could prove useful for future development and as such should be kept in mind when designing new devices. With a background of the previous advancements in the field established it is possible to move forward with the development of new devices.

Chapter 3

Physical Properties of KMPR

LOC devices, by definition, require physical chips to be built in order to fulfill their functions. In order to produce these microfabricated systems it is necessary to understand the physical properties of the material that is to be used and only once this information is obtained is it possible to move forward with building structures that have the ability to function as designed while minimizing unexpected behaviour. With this in mind the first step before attempting to develop any LOC devices using KMPR is to study the properties of the material.[1]

KMPR is an epoxy based negative photoresist developed by Microchem Corp. and Nippon Kayaku Co. Ltd. in 2004 for fabricating MEMS devices [49]. It is a high contrast, chemically amplified (for improved the response to UV exposure), thick film photoresist designed to have similar imaging properties as SU-8, another negative resist from Microchem. It has been used in a number of different areas such as microfluidics [50, 22], RIE (reactive ion etching) masking layers [51, 52], electrodeposition molds [53, 54, 55, 56], proton beam

[1] A version of this chapter has been published. M. Reynolds, A. Elias, D. G Elliott, C. Backhouse, and D. Sameoto, "Variation of thermal and mechanical properties of KMPR due to processing parameters," Journal of Micromechanics and Microengineering,vol. 22, p. 125023, Dec. 2012.

writing [57] and radiation imaging detection [58].

Our research group in particular is interested in producing microfluidic structures using KMPR for the purpose of performing genetic amplification and testing. These applications require extensive use of closed microfluidic structures and suspended membranes along with actuating structures and membranes to act as valves. These structures require accurate control over the material properties in order to utilize a thermo-compressive bonding process and to minimize unwanted deflection of any suspended membranes such as chamber roofs and air gaps.

Most of the past work done with KMPR focuses on the lithographic properties of the material but one key area that has seen very little research is the thermal and mechanical properties of KMPR. Only a single published paper could be located studying the elastic modulus and hardness of KMPR [59] and none could be found studying its thermal properties such as stability at high temperatures and glass transition temperature. Also no work could be found studying the effect of processing conditions on these properties, unlike SU-8 which has been studied quite thoroughly in this regard [60]. Without this information it is difficult to create predictable MEMS and microfluidic structures using KMPR and developing reliable fabrication protocols is even harder. In order to rectify this situation various properties of KMPR were studied including Young's modulus, glass transition temperature (T_g, the temperature at which the polymer chains become mobile while still maintaining a solid film), creep behavior, thermal stability and the thermal conditions under which KMPR cross-links without UV exposure. Different exposure doses, bake times and bake temperatures were studied in order to determine their effect on these material properties.

3.1 Advantages of KMPR

Although KMPR was designed to have lithographic performance matching that of SU-8 it does have numerous advantages over it and other polymers. KMPR can be developed using TMAH-based aqueous developers instead of the solvent-based developers required by SU-8 and it is easily stripped even after hard baking the film [59, 61]. It also has better moisture resistance than SU-8 [62] demonstrating stable adhesion after exposure to high humidity conditions for several days. KMPR may be spun up to 100μm thick in a single spin, displays better adhesion to substrates than SU-8 [58, 63], requires less stringent baking conditions to avoid cracking than SU-8 [59] and has good chemical, plasma and dry etch resistance [51]. As a structural material KMPR has been shown to facilitate bonding between layers while maintaining its sidewall profiles [50]. KMPR also provides strong adhesion for metal films deposited onto it [47] which is often a key weakness of polymer-based materials and therefore allows for resistive heaters and temperature sensors to be fabricated directly within the polymer structures. Given these advantages we decided to move forward with attempting to build LOC devices out of this material.

3.2 Effects of Fabrication Parameters on Material Properties

Glass transition temperature measurements were taken using a dynamic mechanical analyzer (DMA 8000 from PerkinElmer Inc.) to locate the peak of the tan delta curve (which is measured by applying a small, oscillating force to a sample and studying the phase lag between the applied force and the displacement of the sample) for KMPR prepared under different processing

conditions. Using a model 5943 Instron tensile tester Young's modulus was calculated using a stress-strain curve for the KMPR samples and creep was studied by applying a fixed stress to the sample and measuring the increase in strain over time. KMPR's resistance to thermal cross-linking (cross-linking without UV exposure) was also studied by baking samples at a range of temperatures and times and comparing the development times. Thermal stability of KMPR at high temperatures was also studied using a thermal gravimetric analyzer (Q500 TGA from TA Instruments). Exposure doses in this chapter are calculated using only the intensity of the 365nm emission of a mercury lamp as KMPR has been reported to respond primarily to wavelengths between 350 and 400nm [23].

3.2.1 Glass Transition Temperature

In polymer materials the glass transition temperature (T_g) is the temperature at which the polymer chains are able to slide past each other without the material actually melting. Qualitatively this causes the material to experiences large amounts of plastic strain while experiencing small amounts of mechanical stress. This effect is important when building mechanical structures using polymers as the structures may permanently deform if stressed while they are heated.

The T_g was measured with respect to three different fabrication parameters: exposure dose, post exposure bake (PEB) length and PEB temperature. Graphs of the results can be seen in Figures 3.1 - 3.3. Figure 3.1 shows that exposure doses above 2 J/cm^2 have a minimal effect on the T_g, with a sharp increase of T_g as a function of dose at lower exposure intensities. This type of behavior is expected given that the UV exposure serves to convert the photo-active chemicals (PACs) in the resist to acids which then catalyze the

cross-linking reactions in the resist. For doses above 2J/cm^2 these results indicate that most, if not all, of the PACs have been activated and higher doses cannot further increase the cross-linking rate. This same behavior has been demonstrated with SU-8[60]. The peak dose required to fully convert all of the PACs present will vary based on film thickness due to the absorption of the UV light by the KMPR.

It should be noted that patterning KMPR with doses as high as 2J/cm^2 will reduce the resolution of lithography due to scattering, reflection and diffraction effects causing exposure in areas that would otherwise be unexposed. Because of this effect it is not possible to pattern microfluidic structures with a sufficiently high exposure dose to achieve a stable T_g. To avoid this problem while still achieving a stable T_g it is possible to first expose the KMPR at a lower exposure dose (to ensure sufficient pattern resolution) and developing the film before then re-exposing the now patterned film to activate the remainder of the PACs. This two-step exposure will allow for resolution of the lithography to be maintained without sacrificing the physical stability of the film.

It is also important to be aware of the change in dose that will be required if the substrate material changes or if the film thickness changes significantly. These dose values were determined for a 20 μm thick film deposited on a glass substrate. Other substrate materials will result in a different amount of UV radiation being reflected back through the KMPR film increasing the effective exposure dose experienced by the film. Thicker films will also result in a greater amount of energy being absorbed by the resist requiring a higher exposure dose to activate all of the PACs in the film.

Figure 3.2 shows the effect of the post exposure bake (PEB) time on the T_g of KMPR. Baking temperatures of 120°C and 200°C were compared, with an exposure dose of 4J/cm^2, chosen to ensure all of the PACs in the resist were

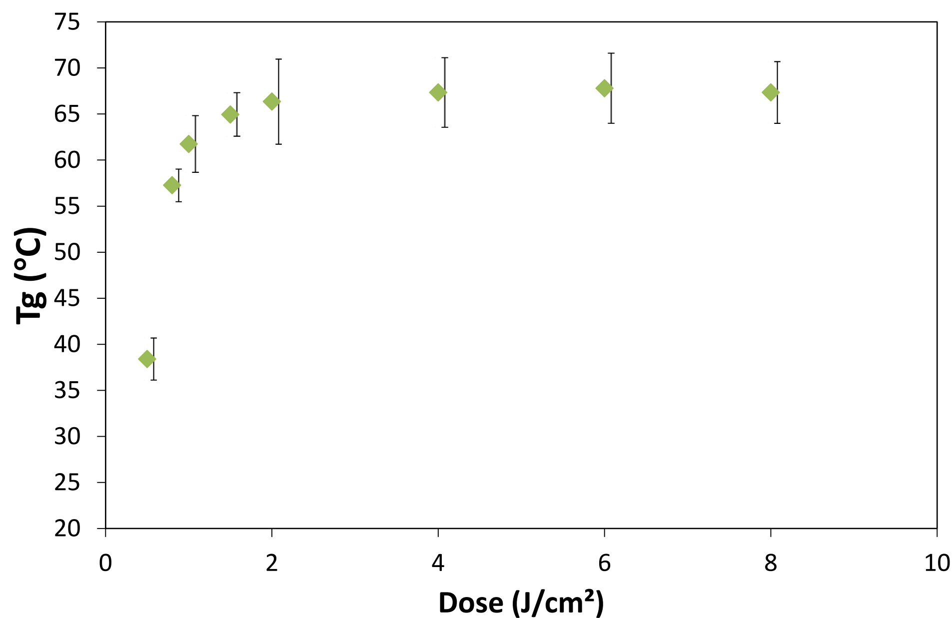

Figure 3.1: T_g as a function of exposure dose, with baking conditions of 100°C for 2 h. Error bars (for this and subsequent figures in this chapter) are calculated using the standard deviation from the average of all samples tested with the same processing conditions. Each T_g measurement in this chapter was taken with 3 or 4 samples. The T_g reaches a plateau for exposure doses above 2J/cm^2, indicating that all PACs in the resist have been activated.

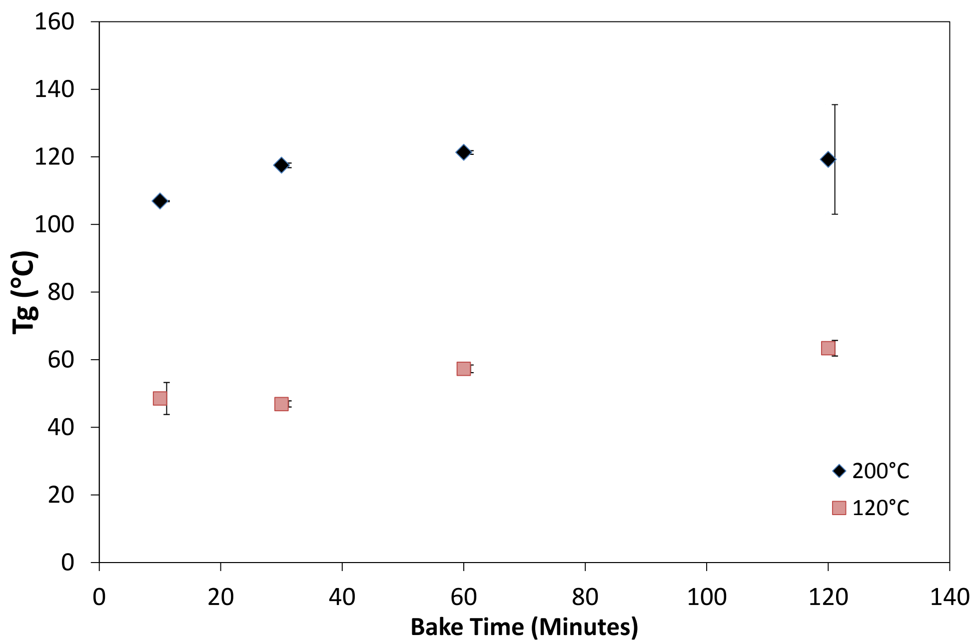

Figure 3.2: T_g as a function of bake time with an exposure dose of 4 J/cm^2 and baking temperatures of 120 and 200°C. The T_g is mostly independent of baking time, even for bake lengths as short as 10 minutes, implying KMPR cross-links very quickly after UV exposure and baking.

converted to acid. These results show that, unlike SU-8 [60], KMPR exhibits very little change in T_g between bake times of 10 minute and 2 hours. It is also worth noting that the T_g of KMPR peaks at a temperature much lower than the PEB temperature (after a 20 minute bake the T_g of SU-8 is typically equal to the baking temperature [60]). KMPR cross-links much faster than SU-8 under the same conditions but does not reach the same level of stability at higher temperatures. Any bakes longer than 60 minutes should ensure a reliably cross-linked film.

The greatest factor affecting the T_g of KMPR (based on these measurements) is the PEB temperature used in processing the resist. Figure 3.3 shows the T_g of KMPR varying from 39°C for an 80°C PEB to 128°C for a PEB at 250°C. The T_g for a PEB of 150°C was 115°C, with the change in T_g being minimal at higher PEB temperatures. This trend is similar to what has been

found for SU-8 [60] where the T_g increased approximately linearly with bake temperature up to 200°C at which point the cross-linking reactions begin to reach their limit. According to these results baking temperatures of at least 150°C should ensure reliable film properties for fabricated structures.

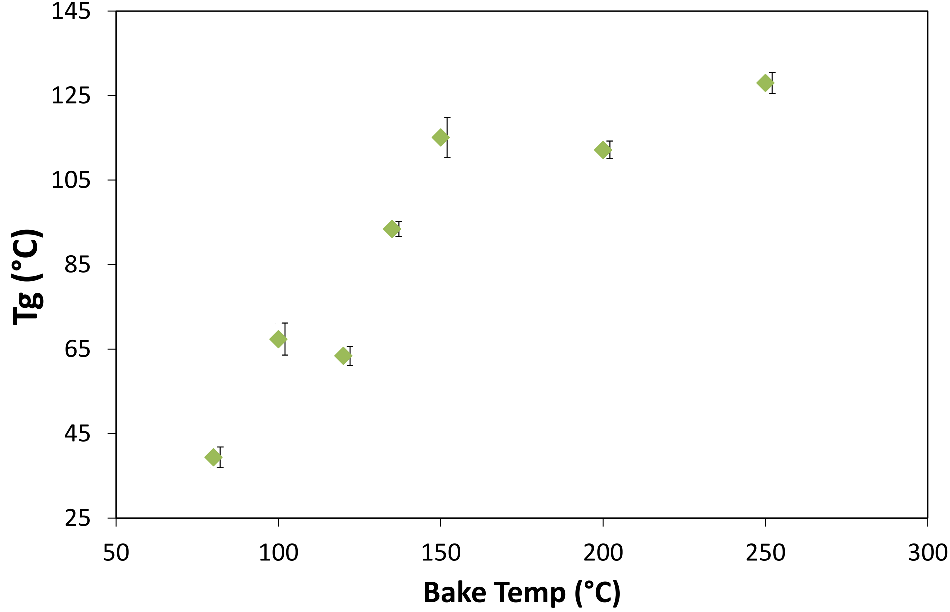

Figure 3.3: T_g as a function of bake temperature with an exposure dose of 4 J/cm^2 and a baking time of 2 h. The T_g increases significantly as a function of baking temperature up to temperatures of 150° before reaching a plateau at higher temperatures, indicating the cross-linking reactions have reached their peak.

3.2.2 Young's Modulus

Young's Modulus was measured using three processing conditions: 2 J/cm^2 dose and 100°C hard bake for 1 hour, 2 J/cm^2 dose and 150°C hard bake for 1 hour and 2 J/cm^2 dose and 200°C hard bake for 1 hour (Figure 3.4). The sample prepared at 100°C had a measured modulus of 2.0 +/- 0.2 GPa while the samples prepared at both 150°C and 200°C exhibited a modulus of 2.7 +/- 0.1 GPa. The tensile strength and elongation of the samples are listed in Ta-

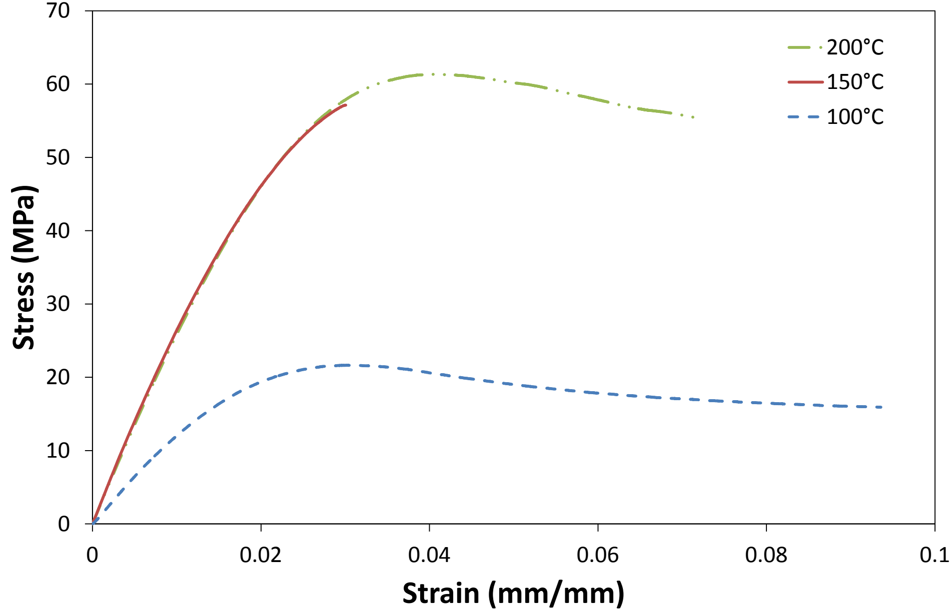

Figure 3.4: Stress-Strain curves for KMPR exposed to 2 J/cm^2 of UV light and baked at the indicated temperature for 1 hour. With the cross-linking reactions having reached their peak, the samples baked at 150°C and 200°C exhibited consistent modulus values and the sample baked at 200°C exhibited a slightly higher tensile strength and maximum strain prior to failure. The modulus is determined according the initial slope of the stress-strain curve.

Table 3.1: Young's modulus and maximum tensile strength (MTS) of KMPR with comparisons to SU-8, with the KMPR values being determined by the stress-strain curves shown in Figure 3.4.

		Bake Temp [°C]	Young's Modulus [GPa]	MTS [MPa]	Elongation at MTS
KMPR		100	2.0 +/- 0.2	21.6 +/- 1.7	3.1 %
		150	2.7 +/- 0.1	57.1 +/- 0.8	3.0 %
		200	2.7 +/- 0.1	61.3 +/- 4.6	4.0 %
SU-8	[64]	80	2.1 +/- 0.2	46 +/- 10	1.6 %
	[60]	95	2.4	52.6	3.8 %
	[60]	200	2.4	73.1	5.2 %

ble 3.1. Under similar processing conditions, SU-8 and KMPR exhibit similar room temperature modulus values, maximum tensile strength and maximum elongation [60, 64]. These modulus measurements are similar to previously reported Young's modulus values for KMPR under similar conditions [59] with the variation (2 GPa instead of 1 GPa) likely arising from the different processing conditions (5 minute bake compared to 1 hour bake). These results suggest that baking temperatures between 150°C and 200°C should yield a consistent modulus although baking at 200°C allows for a greater tensile strength and maximum strain.

3.2.3 Creep Behaviour

It is important to consider any possible plastic deformations experienced by KMPR in response to a constant applied stress, also known as creep. Unless these deformations are accounted for long-term operations of any devices will be difficult to control. Creep behavior in KMPR was studied using 3 different processing conditions. All samples were exposed to a UV dose of 2 J/cm^2 and baked for 1 hour at 100°C, 150°C or 200°C. The amount of creep experienced by KMPR is expected to decrease as the temperature of the processing is increased due to the increased cross-linking level increasing the mechanical stability. The level of creep, C, is determined by measuring the change in strain experienced by a sample experiencing a constant level of stress and calculated using equation 3.1. The samples were strained by applying a stress equal to half of the ultimate tensile strength of the sample (determined using another sample from the same substrate). While holding the stress constant the change in strain was measured for 15 minutes. Creep results for each of the processing conditions are shown in Figure 3.5.

$$C[\%] = \frac{\varepsilon_f - \varepsilon_i}{\varepsilon_i} \tag{3.1}$$

C = Percent Creep, ε_f = Final Strain [%] and ε_i = Initial Strain [%]

Samples baked at 100°C with an applied stress of 14 MPa ($\varepsilon_i = 0.54$ %) displayed a creep of 138.9 % over 15 minutes. Samples baked at 150°C with an applied stress of 32 MPa ($\varepsilon_i = 0.95$ %) exhibited a creep of 34.7 % over 15 minutes. Samples baked at 200°C with an applied stress of 34 MPa ($\varepsilon_i = 1.12$ %) had a measured creep of 23.2 % over 15 minutes. These creep results are larger than creep results for SU-8 which have been determined to be between 3 % [64] and 10 % [65].

Along with creep it is also important to determine the relaxation of the material once the stress has been removed. Relaxation is typically measured by applying compressive stress to the strained material, but this cannot be done with thin films since the film will simply buckle under the applied stress. To work around this problem the relaxation of a thin film is determined by leaving a small residual tensile stress on the material and measuring the change in strain [64]. Relaxation was measured on a sample prepared at 100°C and stressed with 13.8 MPa for 5 minutes to induce creep. The measured creep after 5 minutes was 97 %, at which point the applied stress was reduced to 1.38 MPa and held for 15 minutes to allow the sample to recover. The % relaxation, R, was measured (calculated with equation 3.2) to be 44 % (Figure 3.6). This value is similar to reported recovery rates for SU-8 [64] suggesting that KMPR is able to recover nearly as well as SU-8 despite experiencing a much higher level of creep.

$$R[\%] = \frac{\varepsilon_i - \varepsilon_f}{\varepsilon_f} \tag{3.2}$$

R = Percent Relaxation, ε_f = Final Strain [%] and ε_i = Initial Strain [%]

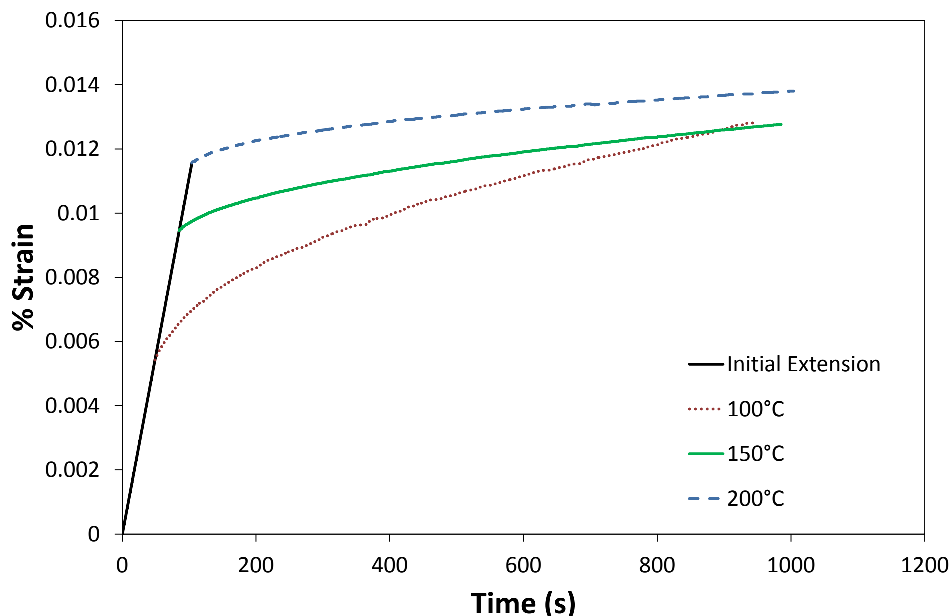

Figure 3.5: Creep results for samples exposed to 2 J/cm^2 and baked for 1 hour at the indicated temperatures. The samples were strained at a rate of 0.2 mm/min up to half their maximum tensile stress (measured separately) and the change in strain was measured while the stress was held constant for 15 minutes. The results show that KMPR becomes more resistant to creep as the cross-linking level of the material increases.

3.2.4 Thermally Induced Cross-linking

In most fabrication processes KMPR only cross-links when exposed to UV light. KMPR can also be cross-linked in the absence of UV light by using high temperature baking steps. This can have particular importance when determining what baking conditions can be applied prior to developing a KMPR film. In order to study this thermally-induced crosslinking the developing time of a film is used to determine if cross-linking is occurring. As the KMPR begins

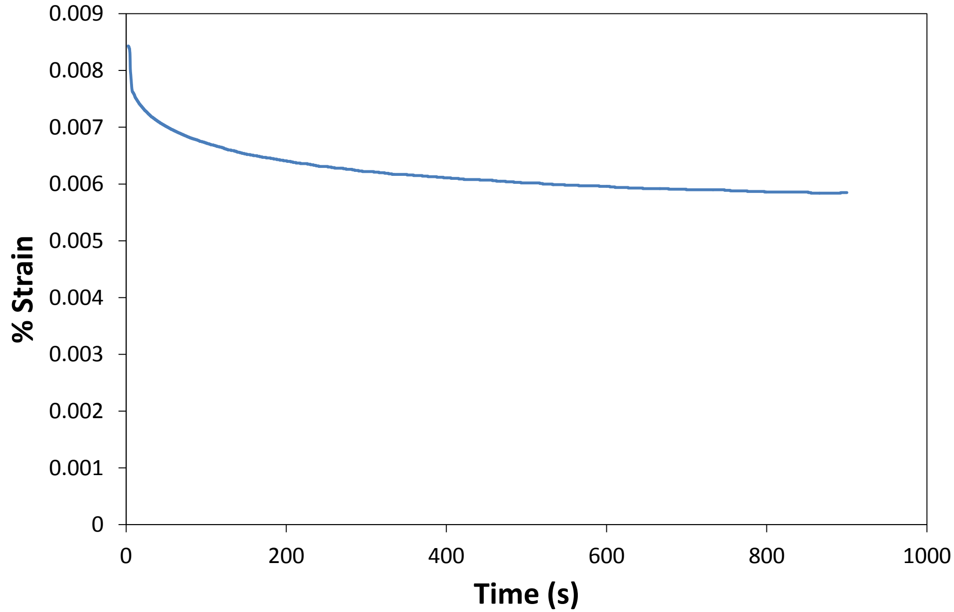

Figure 3.6: Relaxation results for a sample baked at 100°C and strained at 13.8 MPa for 5 minutes (97 % creep). Relaxation was measured with an applied tensile stress of 1.38 MPa. The measured recovery was 44 %.

to cross-link the developing time will increase dramatically and development will stop altogether once the reactions have proceeded sufficiently. A control sample post-exposure baked at 100°C for 5 minutes was used to determine a baseline develop time. Table 3.2 summarizes the results for these tests.

Based on these results unexposed KMPR will cross-link when heated to 150°C. Baking at temperatures no higher than 120°C for less than an hour

Table 3.2: Thermally-induced cross-linking results for KMPR.

Bake Temp	Bake Time	Develop Time	Did Sample Develop
100°C	5 minutes	8 minutes	Yes
100°C	60 minutes	13 minutes	Yes
120°C	30 minutes	20 minutes	Yes
120°C	60 minutes	30 minutes	Yes
120°C	120 minutes	21 hours	No
150°C	10 minutes	21 hours	No

should avoid any problems with development beyond slowing the development slightly. If higher temperature bakes are required they should be performed after development is finished.

3.2.5 Thermal Stability

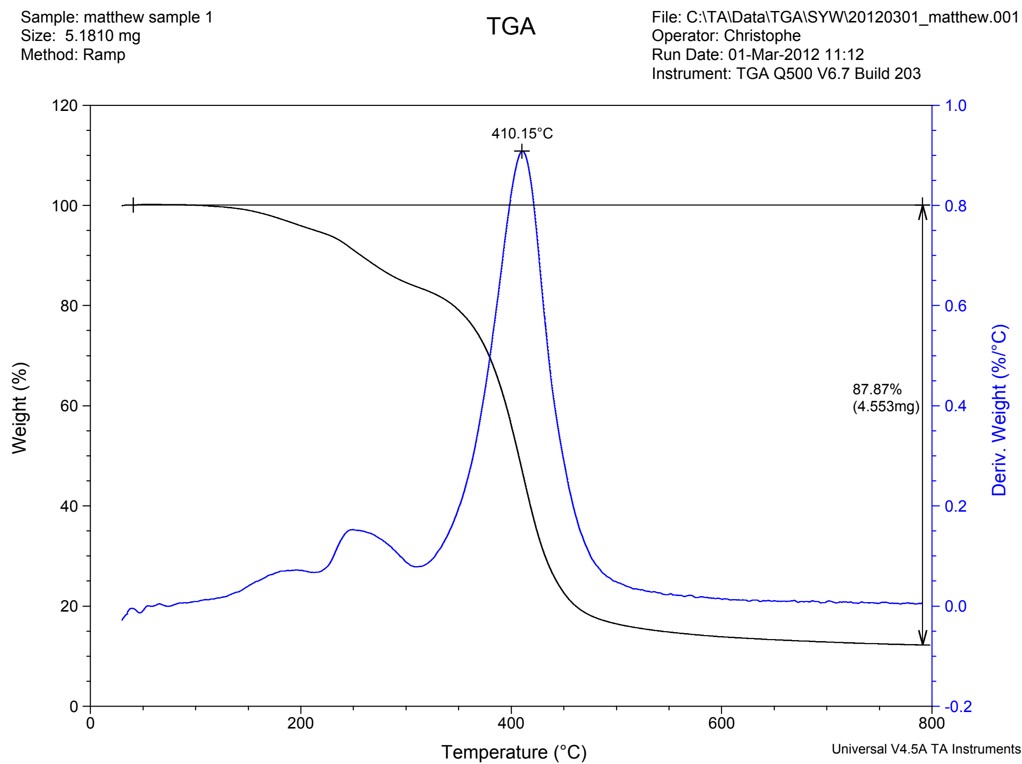

Figure 3.7: TGA curve for KMPR. Operating conditions: N_2 atmosphere, 20°C/min ramp. There is a 5 % drop in mass around 200°C as the KMPR polymer chains begin to breakdown.

It has already been shown that baking KMPR at higher temperatures serves to increase and stabilize the cross-linking level of the material. What has not been shown is how stable KMPR is at high temperatures. Thermal gravimetric analysis (TGA) was used to measure mass loss of KMPR over a large range of temperatures. Unlike SU-8, which is stable beyond 300°C [60], a cross-linked

film of KMPR at 200°C will have already experienced a 5 % loss of mass, with most of its mass being lost between 350 and 450°C (Figure 3.7). The tested samples had been baked at 100°C for 2 hours prior to being tested and as such it is unlikely that this initial 5 % drop is a result of solvent evaporating but is actually a degradation of the polymer chains. With these results in mind temperatures greater than 200°C should be avoided when processing KMPR.

3.3 Chapter Summary

The information presented in this chapter can be used to provide an understand of the physical properties of KMPR during fabrication. Using this information we are able to develop a process capable of producing reliable microfluidic structures. Of particular interest is the determination of a range of processing times and temperatures that will produce reliable mechanical properties. It has been determined that ideal processing conditions for stable, well-crosslinked KMPR is to apply an exposure dose of at least 2 J/cm^2 (for a 20 μm thick film on glass) and a hard-bake lasting at least 60 minutes at a temperature between 150 and 200 °C. Temperatures above 200 °C should be avoided due to degradation of the material. It has also been observed that an exposure dose of 2 J/cm^2 results in a loss of lithography resolution due to scattering effects. Because of this limitation, if both high resolution and a stable T_g is required when fabricating a device it is necessary to use a 2-stage exposure process. Further discussion on this issue is carried out in Chapter 4. With an understanding of the properties of KMPR established we were able to move into building our LOC devices.

Chapter 4

Development of KMPR Microfluidic Devices

While understanding the physical properties of KMPR is a good start for any fabrication process there are still a number of other factors that are involved. Developing a microfabrication process, especially when using a new material, is a time-consuming challenge. In order for any devices developed here to be useful for a real-world POC application it is necessary for a stable, reliable process to be developed that covers every step of manufacturing and packaging. High yields are especially important to ensure cost-efficient fabrication for commercial sale of a product and therefore the fabrication parameters must be tightly controlled to ensure uniformity of the films and structures that are produced.

This chapter will start by covering the challenges related to spinning sufficiently uniform films before moving onto discussing the development of a thermo-compressive bonding process and the fabrication of integrated heaters into the polymer structures. These developments will then be applied to the design of a LOC device.

4.1 Fabrication of KMPR Structures

Although spin processes for photoresists are generally well defined and understood, KMPR being a relatively new material is not very well characterized. Additionally the requirements for a thermo-compressive bonding process are much more rigid than typical spin processes usually involve requiring special attention to be paid when establishing spin protocols. Once the spin protocols were defined it was possible to move onto developing a process for thermo-compressive bonding layers of KMPR together.

4.1.1 Thickness Uniformity of KMPR Films

One of the first processing steps when working with KMPR is the spin-coating step. Spin-coating is a well used process for applying thin films of a wide range of organic photoresists which are purchased in liquid form. The resist material can be poured onto the center of a substrate and spun, often at several thousand RPM, in order to produce a uniform thin film which can then be used for photolithography. Although most spin processes produce films with a reasonably uniform thickness in order for a thermo-compressive bonding process to achieve intimate contact a very high degree of uniformity is required. Given the modulus values for KMPR measured in Chapter 3 a quick calculation shows that the pressure required to deform a 20 μm thick film by even 1 μm is 135 MPa. Based on experience with this type of bonding applying a pressure of at least 2.5 MPa results in a majority of substrates breaking during bonding. Although on the surface this would suggest a uniformity of better than 10nm is required for guaranteed perfect contact without breaking the substrate, experiments have shown that a thickness uniformity of better than 1 μm across the entire substrate will still achieve high quality bonding.

This result can be accounted for by considering the softening of the KMPR when heated beyond its glass transition temperature during bonding.

Our research group's initial solution to the uniformity problem was to use a volume of up to 25 mL KMPR per spin step in order to achieve the required 1 μm uniformity. Using a more reasonable 5-10 mL per spin with our previous spin process would typically result thickness variations of 2 μm or more for a film at least 20 μm thick. Given that KMPR costs around $1/mL this high volume of resist becomes a major component of the cost of fabricating these devices. It was considered necessary to reduce this required volume by modifying the fabrication protocol to produce the required uniformity of 1 μm without requiring such large volumes of resist material.

Microchem Corp, the supplier of KMPR, recommends a spin process [23] involving 1 mL of KMPR for every inch of substrate diameter spread for 5-10 seconds at 500 RPM immediately followed by a spin step for 30 seconds at the speed required to achieve the desired thickness (either using their spin curves [23] or by creating new curves to account for environmental differences affecting the spin results). Following the spin step a soft bake is performed between 95 and 100°C for a length of time determined by the film thickness (again following their suggested bake length or determining a suitable length). This process, although a reasonable starting point, does not yield the required uniformity and changes needed to be made.

It should be noted that when spin-coating a substrate with a resist the outer edge of the substrate will have excess resist piled up (referred to as an edge bead). It is standard practice to avoid using up to a 1 cm wide area around the edge of a 4" silicon substrate in order to avoid the increased thickness. When using KMPR the edge bead can be easily removed by ensuring the edge of the substrate is not exposed (and therefore not cross-linked) resulting in the edge

bead being removed during development.

Studies have been performed comparing the effects of the various spin parameters on the thickness uniformity of SU-8 (another negative photo-polymer from Microchem)[46]. By maximizing the acceleration of the spin steps and increasing the spin time of the process it has been shown that it is possible to achieve a thickness uniformity of less than 1 % in SU-8 [46], which is a uniformity that would be acceptable for working with a 20 μm thick film.

In addition to changes to the spin process studies have shown that gravity also plays a role in film uniformity [66, 67] with an uncured film having reduced uniformity if left to rest on a surface that is not level [67]. This fact required care to be shown with ensuring a substrate is held level following spinning but prior to curing.

Using these two factors the process was modified as follows:

- 5 mL of KMPR was used per spin instead of 25 mL.
- The spread step was increased to 2000 RPM with a 1 second ramp time and the minimum duration necessary to coat the entire substrate (typically 2-3 seconds).
- The substrates were allowed to sit for 1 minute in between the spread and the spin steps to allow gravity to encourage the resist to settle and better remove any non-uniformities.
- The spin step was ramped at between 300 and 400 RPM/second and the spin lasted 60 seconds (spin speed depended on desired thickness).
- The substrates were left to sit for 2 minutes after spinning to once again allow gravity to encourage the resist to reflow and improve uniformity prior to curing the films..
- The substrates were soft-baked (to remove excess solvent) at 100°C on a hotplate (bake duration was determined based on film thickness).

Table 4.1: Thickness uniformity results for spinning KMPR films. The films were spun at the listed speed for 60 seconds prior to soft-baking, exposure and development. Thickness measurements were performed at different positions around the substrate and the average and standard deviation was determined for each substrate that was prepared. Films prepared with a spin speed of at least 1500 RPM displayed a uniformity better than 1 μm, which is the targeted uniformity for achieving bonding.

Spin Speed [rpm]	Mean Thickness [μm]	Variation [μm]	Variation [%]
1000	61.3	1.7	2.8
1500	37.3	0.4	1.1
4000	16.1	0.3	1.9

As shown in Table 4.1 this spin process resulted in an average thickness of 61.3 μm (average non-uniformity of 1.7 μm) for spin speeds of 1000 RPM and average thickness of 37.3 μm (average non-uniformity of 0.4 μm) for spin speeds of 1500 RPM and an average thickness of 16.1 μm (average non-uniformity of 0.3 μm) for spin speeds of 4000 RPM. Although this results in a non-uniformity of greater than 1 μm for thicker films the non-uniformity for 20-30 μm thick films (the thicknesses being considered for this process) is less than 0.5 μm. Uniformity could be further improved by increasing the ramp rate of the spread step (at the risk of substrates flying off the chuck), by allowing the film to settle longer prior to baking or by heating the substrates slightly while allowing the films to settle in order to reduce the viscosity.

4.1.2 Thermo-compressive Bonding

In order to produce sealed microfluidic channels in our devices it is necessary to use either sacrificial release layers or have a reliable bonding process. Since our process involves directly creating the fluidic channels within the KMPR, sacrificial layers are impractical leaving us with a bonding process as our most effective option. Channel floors and walls can be fabricated using a multi-layer

spin process but roof layers must be fabricated on a separate substrate and bonded on top. The bonding process involves using a hot embosser system to simultaneously heat 2 layers of KMPR and press them together in order to induce the two layers to crosslink across the interface between them (Figure 4.1). For this process to work the layers must be in intimate contact (hence the high level of uniformity in the previous section) and requires the films to not be highly crosslinked. A bonding temperature exceeding the glass transition temperature of the films is also considered to be beneficial as it will allow the films to deform slightly in order to come into better contact. Other bonding processes could potentially be used as an alternative to this bonding process such as lamination or using a thin film of uncrosslinked KMPR as a bonding layer[47].

Initial work with the bonding process involved both films being baked for 30 minutes during fabrication, one film at 100°C and the other at 130°C, prior to being bonded at 110°C for 15 minutes with a force of 23 kN. This process was developed prior to learning the information discussed in Chapter 3 and it was expected that the films would be able to cross-link together due to the bonding temperature being higher than the baking temperature of one of the films and therefore enabling further cross-linking reactions to occur. The high force was used to compress the films into uniform contact. This bonding process lacked reliability, especially when bonding multiple films to the same substrate, suffering from low bonding quality (low percentage of area bonded, Figure 4.2) and would sometimes result in the substrates breaking under the high pressure. With the information gained in Chapter 3 the next step was to modify the fabrication conditions to produce a pair of films that are better suited for the bonding process (by lowering their T_g and thereby enabling more cross-linking across the bonding interface as well as allowing the films

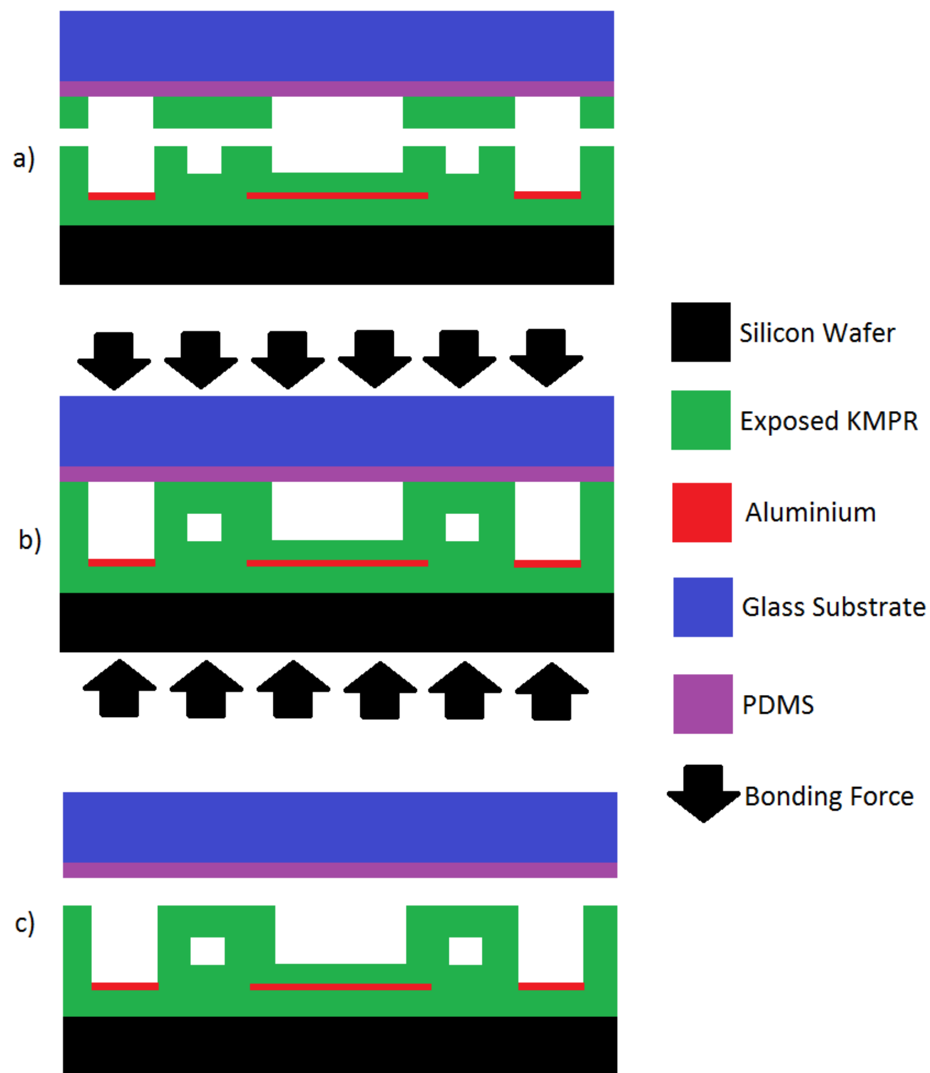

Figure 4.1: Flow chart for the thermocompressive bonding of the Si device wafer and the glass carrier substrate in order to produce closed microfluidic channels. Following bonding the glass substrates were released from the KMPR by taking advantage of the poor adhesion between the PDMS and KMPR films.

to better conform to eachother to achieve better contact) in order to reduce delamination (Figure 4.3) and to avoid breaking of the substrates (by reducing the bonding force required).

Using the information gained from studying the physical properties of KMPR some changes could be made to the bonding process to improve its reliability. The first change to be made was the length of the PEBs applied to the films. Figure 3.2 suggests that even a 30 minute bake will stabilize KMPR and therefore reduce the bonding effectiveness. To avoid this the PEB time was kept to 5 minutes for any films to be bonded together. This bake time allows for the exposed KMPR to crosslink enough to allow the film to be developed. The next parameter to be changed was the PEB temperatures. Figure 3.3 shows the relation of glass transition temperature (which can be taken as a relative measure of crosslinking) and indicates that lower temperature bakes should help us in two ways: a lower T_g should allow the films to deform slightly during bonding for improve contact and lower crosslinking should improve the bonding strength. Temperatures of 100°C are now used for baking both films as lower temperatures introduce difficulties related to contrast and resolution during development.

With these changes made to the film fabrication in order to produce uniform, lightly crosslinked, low T_g films for bonding, some changes could also be made to the bonding step to improve the yield. A bonding temperature of 100°C with these new film parameters has proven sufficient to provide effective bonding with over 90% of the bonded area being clear of any voids or delamination (Figure 4.3), although higher temperatures could be used if bonding strength proves to be an issue in the future. The bonding pressure was also reduced to 10 kN (from 23 kN) in order to reduce the breaking of substrates. Additionally if the bond strength is insufficient following this process, resulting

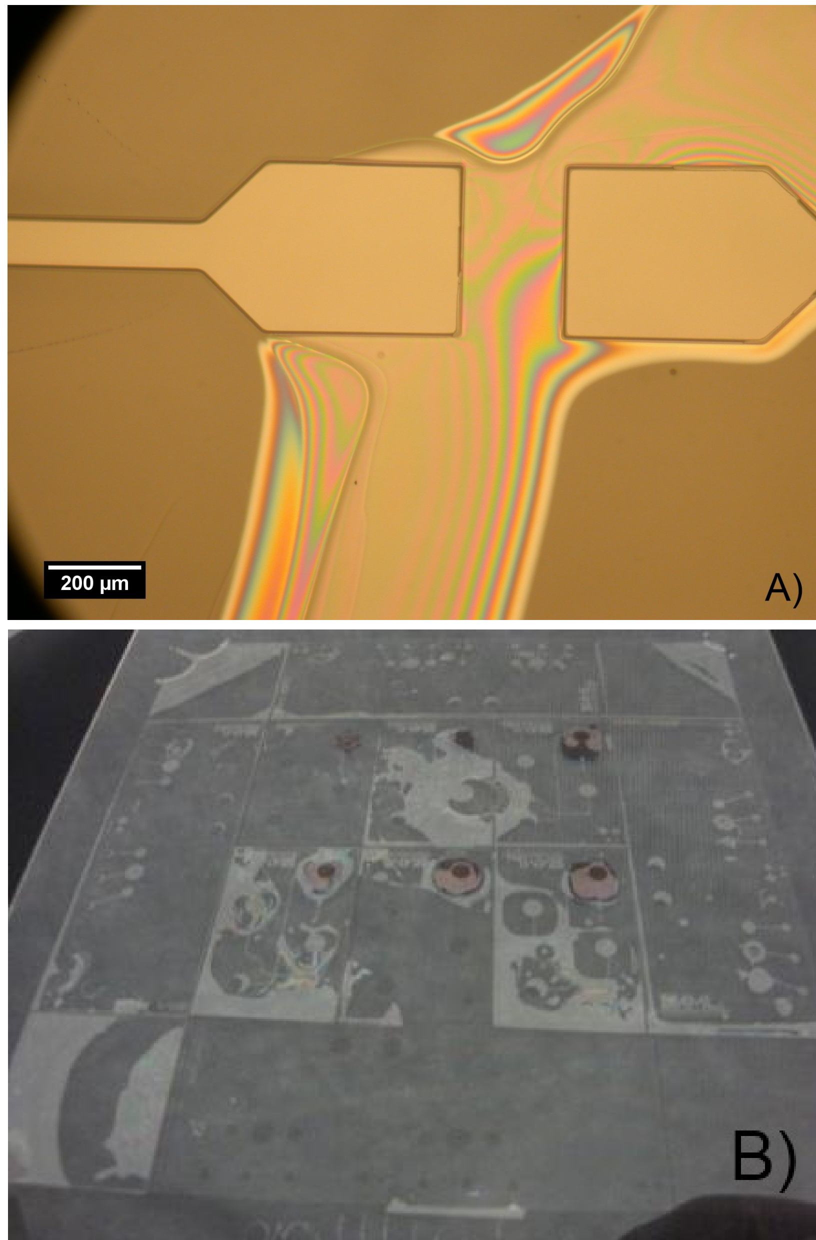

Figure 4.2: In cases of poor bonding quality voids can clearly be seen around the KMPR structures. Image A shows a microscope view of delamination effects around fluidic structures while image B shows a full substrate view (4” glass) of poor bonding where some areas did not release from the carrier substrate at all while other areas show large amounts of delamination.

in the bonded film delaminating when the fluidics are sealed and pressurized, a higher temperature bake (150-180°C) using a hotplate can be applied after bonding is completed to improve the bond strength by encouraging more crosslinking reactions across the bonding interface.

Various other techniques, variations and applications of bonding were also studied and are discussed in Appendix D.

4.2 Metal Structures on KMPR

One of the key parts of these devices is the integrated heaters and temperature sensors that will allow for PCR thermal cycling. In order to reduce the power required and improve the rate of temperature change the heaters should be placed as close to the PCR chamber as possible which means embedding the heaters within the polymer itself. Depositing a metal onto a polymer film poses a number of problems related to film stress, cracking, adhesion and reliability. This section discusses the work that was done in order to fabricate heater structures within KMPR devices.

4.2.1 Metal Deposition on KMPR

Depositing metal films onto polymer surfaces typically results in a number of issues that do not arise when depositing onto a silicon or a glass surface. The first problem is one of film adhesion. Polymeric materials provide notoriously poor adhesion for metal films deposited onto them [68] often resulting in the deposited metal delaminating from the surface during use. In the case of these structures any delamination would result in a complete failure of the heaters. Fortunately, unlike with SU-8 and many other polymer materials, metal films show excellent adhesion to KMPR. Figure 4.4 shows a tape test comparing the

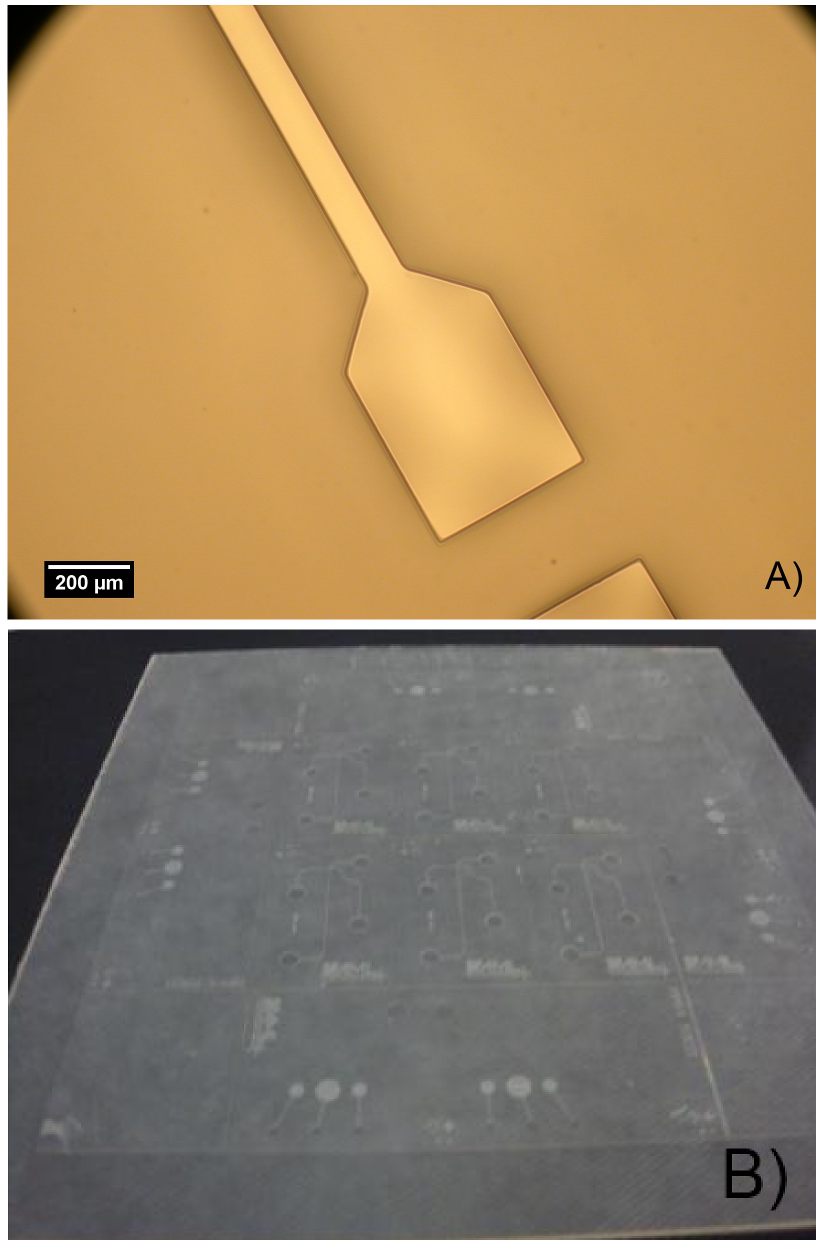

Figure 4.3: When good bonding and contact is achieved (by improving the film uniformity and reducing the cross-linking level of the films to be bonded) there are little-to-no visible voids present in the KMPR structures (goal is to have greater than 90% of the bonded area to have no signs of delamination). Image A is a microscope view of the area surrounding the fluidic structures, while image B shows a full substrate view following bonding.

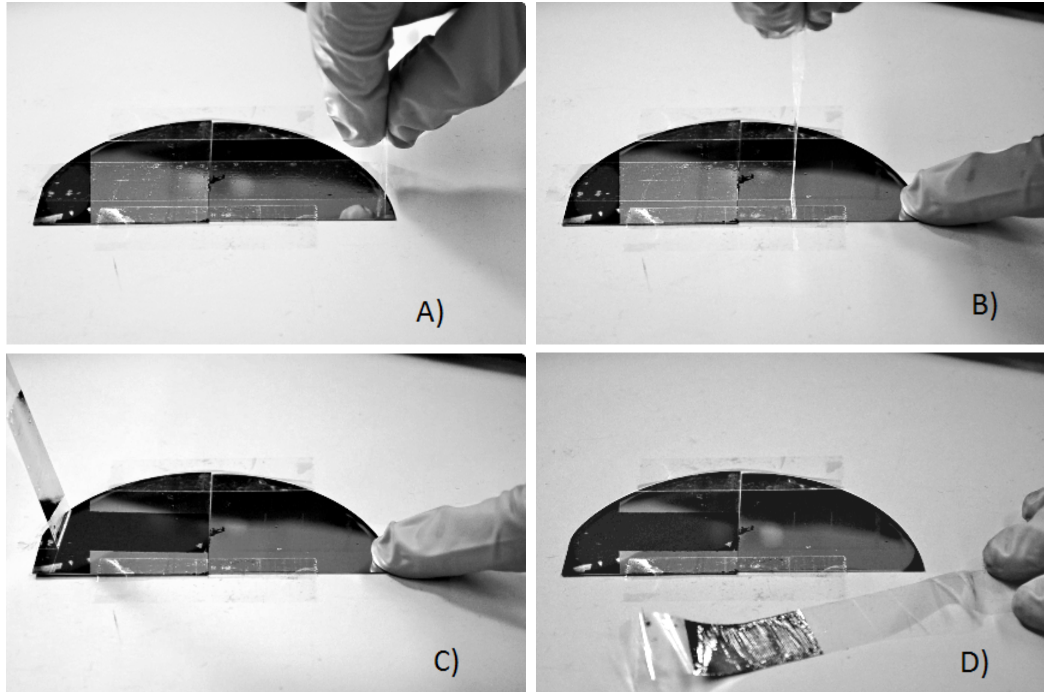

Figure 4.4: Tape test results. The quarter substrate (4” Si substrate) on the left is coated with an SU-8 film while the quarter on the right is coated in a KMPR film. Both polymers were soft-baked at 100°C. Both pieces had 100nm of Al sputter coated onto the surfaces at the same time with a deposition pressure of 7mTorr and power of 300W (deposition voltage of 400V). A single piece of tape was applied to both substrates and removed in one continuous motion. The Al film was completely removed from the SU-8 but remained attached to the KMPR.

difference in adhesion of 100nm of sputtered Al to an SU-8 surface compared to a KMPR surface. The metal films were deposited onto each substrate at the same time to ensure the only variable involved was the difference in surface. Scotch tape (Grand and Toy brand) was used to attempt to remove the Al films by applying a single piece of tape to both substrates and peeling off the tape in a single, continuous motion at an approximately 90 degree angle. The Al film was easily removed from the SU-8 coated substrates while the film deposited onto the KMPR exhibited stronger adhesion to the polymer surface than it did to the tape.

However adhesion is not the only factor affecting metal film viability on

polymer substrates. The difference in thermal expansion coefficients, combined with stress within a deposited film, can also result in cracking of the films after deposition or after heating the substrate following deposition. Given that these films are to be used to produce resistive heaters any cracking in the films would render them non-operational due to the loss of a conductive pathway through the devices. In order for these devices to function it was necessary to ensure that a film could be deposited without the metal cracking even when heated to over 100°C. The stress present in a sputtered metal film can be varied by changing the deposition pressure of the sputter process [69] as shown in Table 4.2 (data collected by University of Alberta Nanofab staff). The difference in thermal expansion coefficients also introduces additional film stress, especially when depositing metal onto polymer films due to the localized heating of the polymer surface during sputter deposition. Tests were performed in order to qualitatively determine the suitability of both Al and TiW films sputter coated onto a KMPR film (results discussed later in this section). These tests involved varying the Ar pressure during deposition between 2 mTorr and 13 mTorr (thereby varying the film stress from the sputtering process) in order to find a range of conditions for which the metal films were able to avoid cracking.

All work related to film stresses was only done qualitatively as at the time it was considered sufficient to have only a general idea of what deposition conditions would result in a smooth, continuous film. Although we did have data on film stress for metal films on a bare silicon substrate (Table 4.2) we were not confident in the reliability of the same technique for measuring the film stress due to the effects of the thick polymer film between the metal and the substrate. Since at the time a qualitative analysis of the film stress was considered sufficient the effort was not undertaken to measure and analyze the data for metal film stresses when deposited onto KMPR. More recent

work has revealed a number of possible concerns with respect to film stresses when operating our devices at high temperatures in the presence of moisture (discussed in Chapter 5). Given this new information it would be beneficial for further research into a quantitative analysis of the film stresses in order to gain a greater understanding of the interactions between the KMPR and the metal films. It may be possible to obtain at least some of this information using the Flexus system present in the nanoFab, combined with any necessary analysis of the data to interpret the information, or other techniques such as deflection of freestanding cantilevers or beams could be used although this would require significant process development to achieve.

Table 4.2: Stress in Sputtered Metal Films as a Function of Ar Pressure. Negative stress indicates compressive stress. Stress is calculated by measuring the curvature of the Si substrate after film deposition onto a bare silicon wafer using a Flexus 2320 thin film stress measurement tool.

Material	Ar Pressure [mTorr]	Film Stress [MPa]
Gold	12	10.1
"	7	-11.4
"	2	-50.1
TiW	13	-10.5
"	7	3200.4
"	2	-2080.0
Al	7	-70.9

The other consideration for designing and fabricating metal films was electromigration. Using these films as resistive heaters requires high current densities to achieve effective Joule heating. Passing high current densities through thin films of metal is known to result in connectivity failures due to collisions between the electrons and metal atoms resulting in metal atoms being pushed from their lattice positions, resulting in the formation of voids in the metal films and eventually resulting in open-circuit failures [70]. Some metals, such as aluminium, are known to be particularly susceptible to these failures. In

choosing an appropriate metal for these devices, it was necessary to balance a number of considerations such as the resistivity, the temperature coefficient of resistivity (TCR), patternability, cost, electromigration resistance and film stress.

After considering the options it was decided that either a TiW alloy (sputter target is W/Ti, 90/10 wt%) or aluminium were the best options. TiW is the preferred option given its good electromigration resistance, high resistivity and high TCR, however TiW films tend to have high levels of stress after deposition which could make undamaged films hard to create unless a set of deposition conditions can be determined to reduce the stress sufficiently. Aluminium was also a possibility due to its low stress films and acceptable resistivity and TCR, but electromigration is a potentially serious concern with the electromigration threshold for Al typically being considered to be around 1 mA/μm^2 [71]. A further list of other suggested heater materials is discussed in Appendix E.

With a preference for using TiW, due to the superior electrical properties, the first tests looked at the feasibility of producing stable films on KMPR surfaces. As shown in Table 4.2 TiW under certain deposition conditions possesses a lot of film stress but should have at least 2 different deposition pressures at which the stress is minimized assuming that the curve of film stress as a function of film stress is continuous. Stress in deposited films will usually manifest itself in one of two ways, tensile or compressive. Tensile stress in the films results in widespread cracking (Figure 4.5) whereas compressive stress results in widespread ridging across the films (Figure 4.6).

In order to determine a set of deposition conditions under which TiW can be deposited without damage the Ar pressure during deposition was varied between 2 mTorr and 13 mTorr. Unfortunately, despite using this range of deposition conditions (Table 4.3) no conditions could be found where the de-

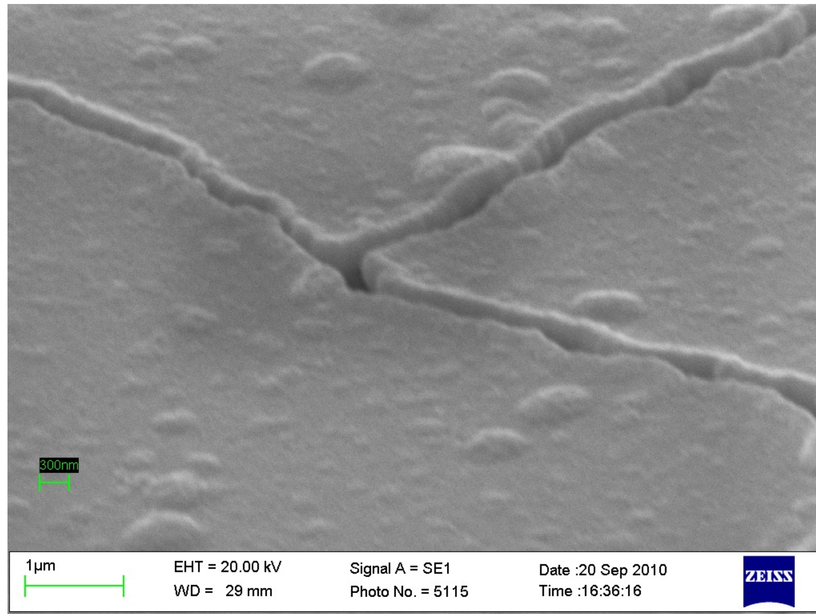

Figure 4.5: SEM image of TiW cracking immediately following deposition due to tensile film stresses. The KMPR film was approximately 50 μm thick and had been baked at 130°C for 30 minutes. TiW films deposited at deposition pressures between 1 and 14mTorr experienced this type of cracking either immediately following deposition or following heating to 100°C after deposition was completed. The TiW film was 200 nm thick and deposited at 200 W of power. The depositing pressure for this particular film was 7 mTorr.

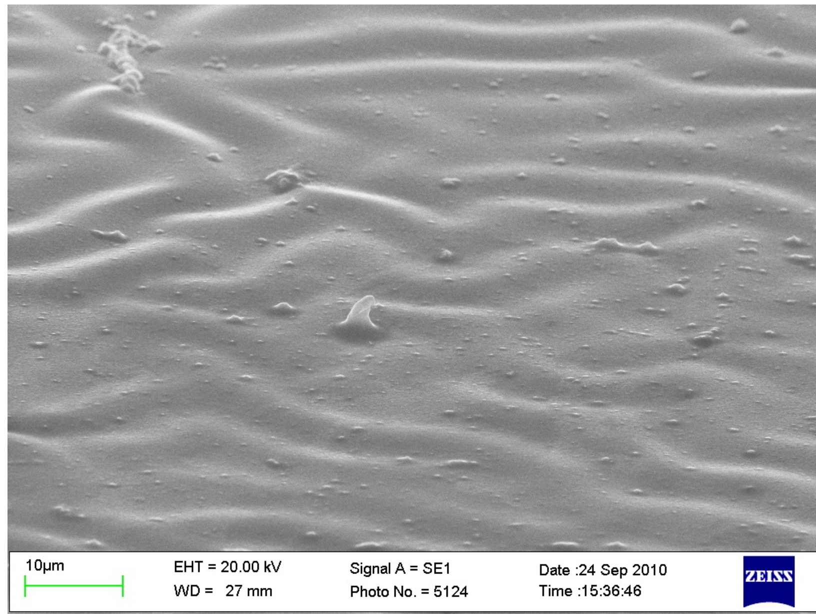

Figure 4.6: SEM image of ridging in an Al film due to compressive film stresses. The KMPR film was approximately 50 μm thick and had been baked at 130°C for 30 minutes while the Al film was 200 nm thick and deposited at 300 W. This kind of behaviour was seen for films deposited with a deposition pressure of 6mTorr or less. Al films deposited with a pressure of at least 7mTorr did not experience this wrinkling.

posited TiW film was able to withstand heating (on hotplate after deposition was completed) up to 100°C without cracking. Table 4.2 suggests that the film stress should be compressive at pressures around 2 mTorr and 13 mTorr, although testing of the films deposited on KMPR (instead of silicon) suggests that the stress is always tensile in the pressure ranges tested. This change is likely due to different interactions of the TiW film with the surface of the KMPR film when compared with the surface of a bare silicon wafer. With these problems related to TiW films, Al was studied as an alternative metal.

Table 4.3: Results from testing the deposition of TiW metal films on KMPR surfaces for a range of deposition pressures. Some films were damaged immediately following deposition, while some films were only damaged after annealing the films at 100 degrees for 1 hour. It must be mentioned that the KMPR these films were deposited on were not hard-baked to maximize their T_g. Each film was 200 nm thick and was deposited at 200 W of power. The difference in film behaviour from the results in Table 4.2 is most likely caused by the change in surface from silicon to KMPR, resulting in different stresses being generated.

Ar Pressure [mTorr]	Qualitative Result
2	Cracked film
3	Cracked film
4	Cracked film
4.5	Cracked film
5	Cracked film
5.5	Cracked film
6	Cracked film
6.5	Cracked film
7	Cracked film
9	Cracked film
12	Cracked after annealing
12.5	Cracked after annealing
12.7	Cracked after annealing
12.8	Cracked after annealing
12.9	Cracked after annealing
13	Cracked after annealing

Al films were also studied in a similar manner as the TiW films. Deposition

pressures between 3mTorr and 13mTorr were studied for a qualitative analysis film quality as a function of deposition pressure. The results of the tests are show in Table 4.4. From those tests it was discovered that films deposited with an Ar pressure of at least 7mTorr and a deposition power of 300W were able to produce films with no signs of stress, even following annealing of the films at 100°C. Following these tests thin film Al heaters were produced and tested on KMPR by other colleagues from our research group [68] using a deposition pressure of 7mTorr. These heaters were able to achieve repeatable resistances when calibrating using a temperature controlled waterbath and were able to use Joule heating to achieve heating up to 165°C for several hours without failing.

Table 4.4: Results from testing the deposition of Al metal films on KMPR surfaces for a range of deposition pressures. Although lower pressures exibited film wrinkling following deposition the higher pressures resulted in smooth, continuous films even after annealing at 100°C. It must again be mentioned that the KMPR these films were deposited on were not hard-baked to maximize their T_g. Each film was 200 nm thick and was deposited at 300 W of power.

Ar Pressure [mTorr]	Qualitative Result
3	Film Wrinkled
5	Film Wrinkled
6	Film Wrinkled
7	Smooth, Continuous Film
9	Smooth, Continuous Film
11	Smooth, Continuous Film
13	Smooth, Continuous Film

A problem was discovered when first attempting to integrate the Al films with the thermo-compressive bonding process. It was discovered that following the bonding process parts of the Al films would wrinkle (Figure 4.7). This wrinkling was likely caused by the low T_g of the floor layer of KMPR due to the initial fabrication process only using a 120°C bake step. This low T_g,

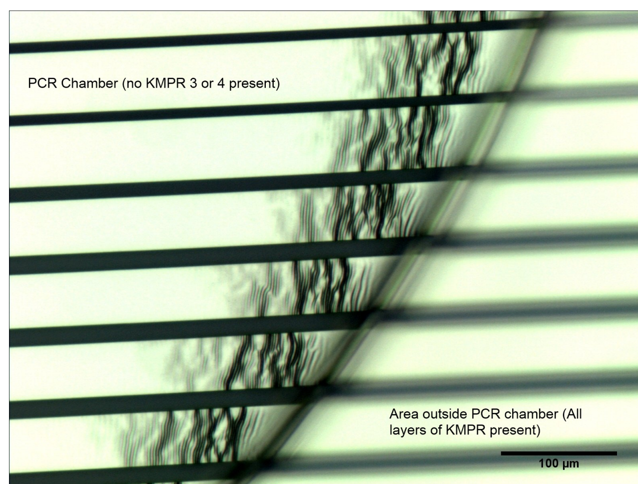

Figure 4.7: Wrinkling of Al film near the edges of KMPR features following bonding. The left portion of the image is a section of the design with only two layers of KMPR present, compared to the 4 layers of KMPR present on the right portion of the image. As a result of this difference, the areas with less KMPR are not directly exposed to the applied pressure during bonding, causing some wrinkling in the KMPR and the metal layers during the bonding process. This wrinkling was avoided in later fabrication by increasing the PEB temperature for the KMPR floor.

combined with the temperature and pressure of the bonding process, resulted in the formation of wrinkles in the metal in areas where the presence of the fluidic structures resulted in uneven pressure being applied to the metal. This uneven pressure resulted in the KMPR, along with the Al film, being "pushed" into the areas of lower pressure leading to wrinkling. This effect was avoided by performing a high temperature (180°C) bake on the KMPR film prior to depositing the metal film in order to increase the film's T_g (Figure 4.8). Subsequent layers spun on top of this highly cross-linked film have no issues with adhesion between layers. It was also discovered that baking the wrinkled chips at 100°C for 20 minutes on a hotplate following the bonding process served to smooth out the wrinkles in the KMPR (Figure 4.9), likely due to a relaxation of the film stresses.

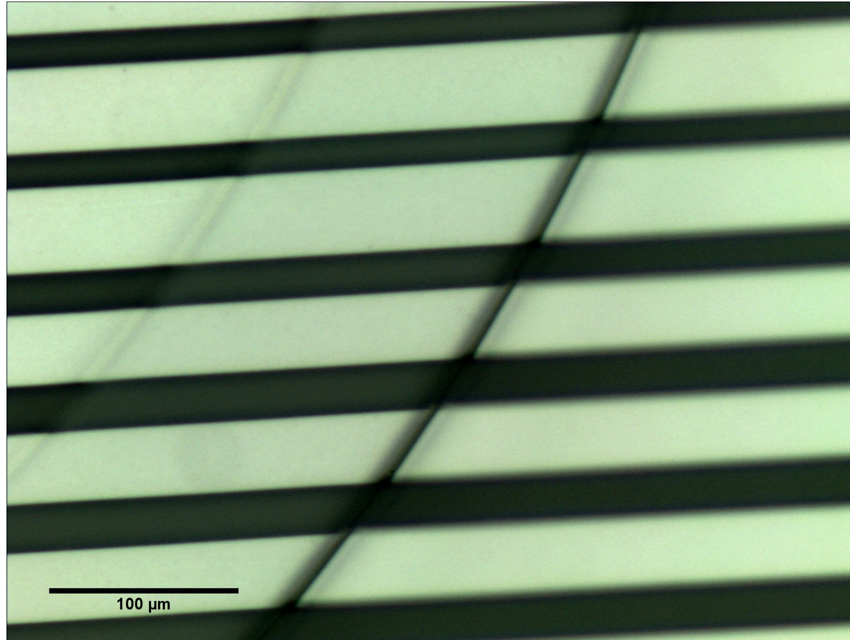

Figure 4.8: By baking the bottom layer of KMPR at 180°C prior to depositing the Al film the wrinkling resulting from the bonding process is reduced due to the increased resistance of the KMPR film to physical deformation.

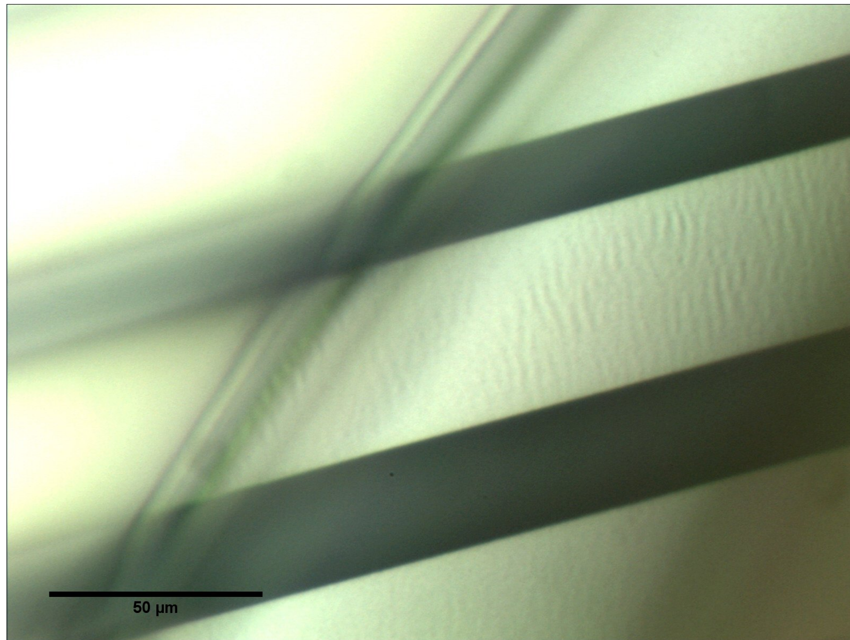

Figure 4.9: Baking completed chips (chips possessing the wrinkled metal shown in Figure 4.7) at 100°C actually served to smooth out the wrinkling in the Al that arose during the bonding process.

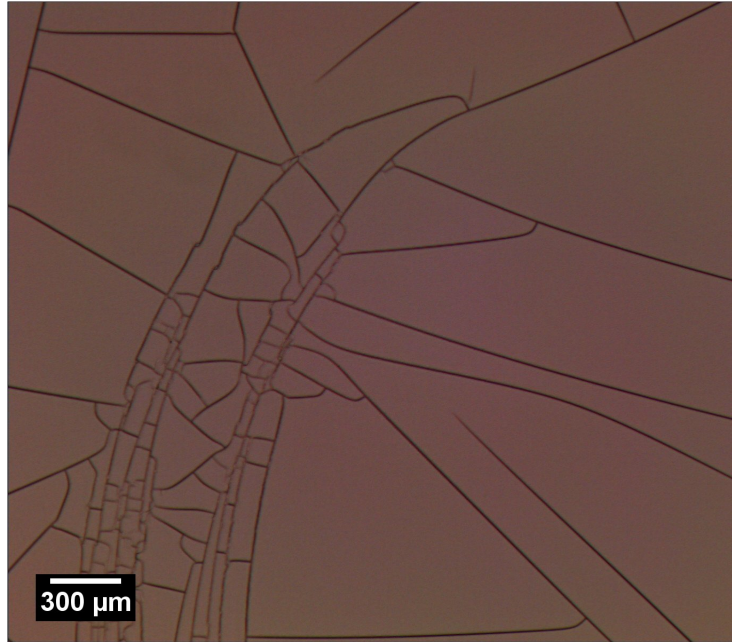

Figure 4.10: Cracking of a KMPR film when placed in an ultrasonic bath of acetone for a lift-off process. The interactions between the KMPR and the acetone are sufficient to crack and damage any exposed KMPR during lift-off.

4.2.2 Fabrication Process for Heaters

In order to remain compatible with the rest of the fabrication process there are two options considered for patterning the Al films: etching (wet or dry) and lift-off. Either option should be sufficient for our needs but a lift-off process was decided upon for patterning the metal in order to avoid having to modify the heater design to account for an isotropic etch step. The main problem to account for with a lift-off process was that KMPR films will crack when placed in an ultrasonic bath of acetone (Figure 4.10). To avoid this problem a thin (50nm) Cr protection layer was first sputter deposited and patterned on top of the KMPR. A stable Cr film could be deposited by using a deposition pressure of 8.5 mTorr (instead of the usual 7 mTorr) and patterning the Cr film (wet etch) prior to the Al deposition allowed for the properties of the Al film to be unaffected by interactions with an underlying Cr film. This deposition

pressure for Cr was determined by first depositing a number of films while varying the deposition pressure between 6 and 10 mTorr in order to find a range of pressure that avoid cracking in the Cr film following deposition (Table 4.5). 8.5 mTorr was determined based on pressures between 8 and 9 mTorr being free of cracking. Following sputter deposition the lift-off process would take 10-15 minutes in acetone per substrate to remove the excess Al (using a microscope to confirm the end point) followed by a minute of Cr etch to remove the remaining Cr. Initial results using this fabrication process were very successful however over time additional problems have arisen related to the KMPR floor cracking during the lift-off process. Increasing the thickness of the Cr film to 100nm as well as applying a hard-bake step to the lift-off resist has helped to reduce the problem but cracking continues to be a persistent problem. In future work it may be beneficial to either re-develop the fabrication process using a photoresist better optimized for a lift-off process or to develop and use an etch process as an alternative for patterning the metal in order to avoid the exposure of KMPR to sonication in acetone.

Table 4.5: Results from determining a deposition pressure allowing for a Cr protection film to be deposited onto KMPR without cracking. Each film was 50nm thick and was deposited at 300W of power.

Ar Pressure [mTorr]	Qualitative Result
6	Film Cracked
7	Film Cracked
8	Smooth, Continuous Film
8.5	Smooth, Continuous Film
9	Smooth, Continuous Film
10	Film Cracked

Table 4.6: Resistivities of Sputtered Al Films at Different Deposition Pressures Before and After Annealing for 2 Hours (200nm thick films). The underlying KMPR film had been baked at 130°C for 30 minutes prior to deposition. Note that the sample at 5mTorr was wrinkled after deposition and annealing, but a resistivity could still be measured.

Pressure	Deposit ρ (Ω-nm)	Post Anneal ρ	Anneal Temp
5 mTorr*	34 Ω-nm	34 Ω-nm	100°C
7 mTorr	177 Ω-nm	166 Ω-nm	100°C
9 mTorr	199 Ω-nm	197 Ω-nm	100°C
11 mTorr	163 Ω-nm	159 Ω-nm	100°C

4.2.3 Characterization of Metal Properties

An important consideration for the heaters is their resistivity and response to annealing effects. For this application a higher resistivity is beneficial as it allows a lower current to be used in order to achieve the same power density. In general the resistivity of a thin film increases for thinner films [72] and measurements of Al resistivity agree with that trend. Table 4.6 shows a list of resistivities of Al films deposited under different deposition pressures before and after annealing. Resistivities were measured using a 4-point probe. From these results it's clear that the resistivities are stable even after annealing for 2 hours at 100°C and the resistivity at deposition pressures of at least 7 mTorr are high enough for the operation of the heater designs, a fact which would interact favorably if higher deposition pressures are required in the future to handle any issues related to film wrinkling or cracking.

4.3 Fabrication Process

Using the information that has been discussed up to this point the next step was to build a full fabrication process that can be used to produce LOC devices. This protocol was able to produce devices with a yield up 75% based on

non-delaminated bonding (qualitative analysis of the bonded devices, compare Figures 4.2 and 4.3, with a target of at least 90% of the wafer area lacking visible voids) and the survival of the Al heaters (no cracking, successful electrical connection with expected range of resistances across the heater). A more detailed fabrication protocol can be seen in Appendix A.

4.3.1 Device Wafer - KMPR Floor

4" silicon substrates were used to fabricate the devices. Substrates were prepared by first cleaning them in a fresh, hot piranha solution (3:1 H_2SO_4 (96%):H_2O_2 (30%)) for 15 minutes. The substrates were then rinsed with de-ionized (DI) water and spun dry. They were then placed on a hotplate at 100°C for 15 minutes to be dehydrated. KMPR 1025 was spun onto the substrates at 4000 RPM and soft-baked at 100°C for 10 minutes on a hotplate (Figure 4.11 a). This spin speed results in a KMPR thickness of 20 μm when spinning on a 4 inch round silicon substrate, compared to the thickness of 16.1μm when spinning on a 4 inch square glass substrate that was reported in Table 4.1. After cooling the substrates the KMPR was blanket exposed (ABM mask aligner with a mercury light source) to activate the PACs in the film using an exposure dose of 1,333 $\frac{mJ}{cm^2}$ (this exposure dose is equivalent to the 2000 $\frac{mJ}{cm^2}$ discussed in Chapter 3 as these films were produced on a Silicon substrate instead of a glass substrate), calculated using the 365 nm line intensity of the UV source. After exposure the substrates were baked at 180°C for 60 minutes to ensure the film is well crosslinked (Figure 4.11 b).

4.3.2 Device Wafer - Formation of Al Heaters

In order to protect the KMPR floor during the lift-off process a 100nm layer of Cr was sputtered onto the KMPR film using an Ar deposition pressure of

8.5 mTorr (Figure 4.11 c). The Cr film was patterned by using HPR 504 positive photoresist (Figure 4.11 d) and a wet etch process (commercial Cr etchant from Fujifilm Electronic Materials USA was used containing a mixture of Ceric Ammonium Nitrate, Nitric acid and water) in order to remove any Cr from the areas where the heaters were to be formed (Figure 4.11 e). The HPR 504 was left on the substrate to act as the lift-off resist. A 180 nm thick Al film was sputtered onto the substrates with an Ar deposition pressure of 7 mTorr (Figure 4.11 f). In order to meet the target resistance values for the heaters we required a film thickness between 160 nm and 180 nm (based on resistivity measurements from previous films deposited). Witness samples (clean and bare 4 inch silicon substrates) were used prior to deposition in order to calibrate the deposition rate, but variations in the deposition rate between runs (despite controlling for factors such as the sputtering gun used and the placement of the wafers in the sputtering chamber), combined with the non-uniformity of the film thickness across the substrate, made it difficult to achieve a film thickness with an accuracy better than this range. If a more accurate thickness is required in the future than more effort would be required to improve the control over the deposition rate.

After deposition lift-off was performed by sonicating the substrates in acetone for 10-15 minutes until the lift-off was complete (Figure 4.11 g). Following lift-off the remaining Cr was removed by wet etching (Figure 4.11 h).

4.3.3 Device Wafer - KMPR Fluidics

A KMPR film acting as the floor to the fluidic channels was spin coated on top of the heater structures using the same spin process previously used (Figure 4.11 i). The film was patterned by UV exposure (same dose as previously) through a glass/Cr photomask in order to avoid cross-linking the film above

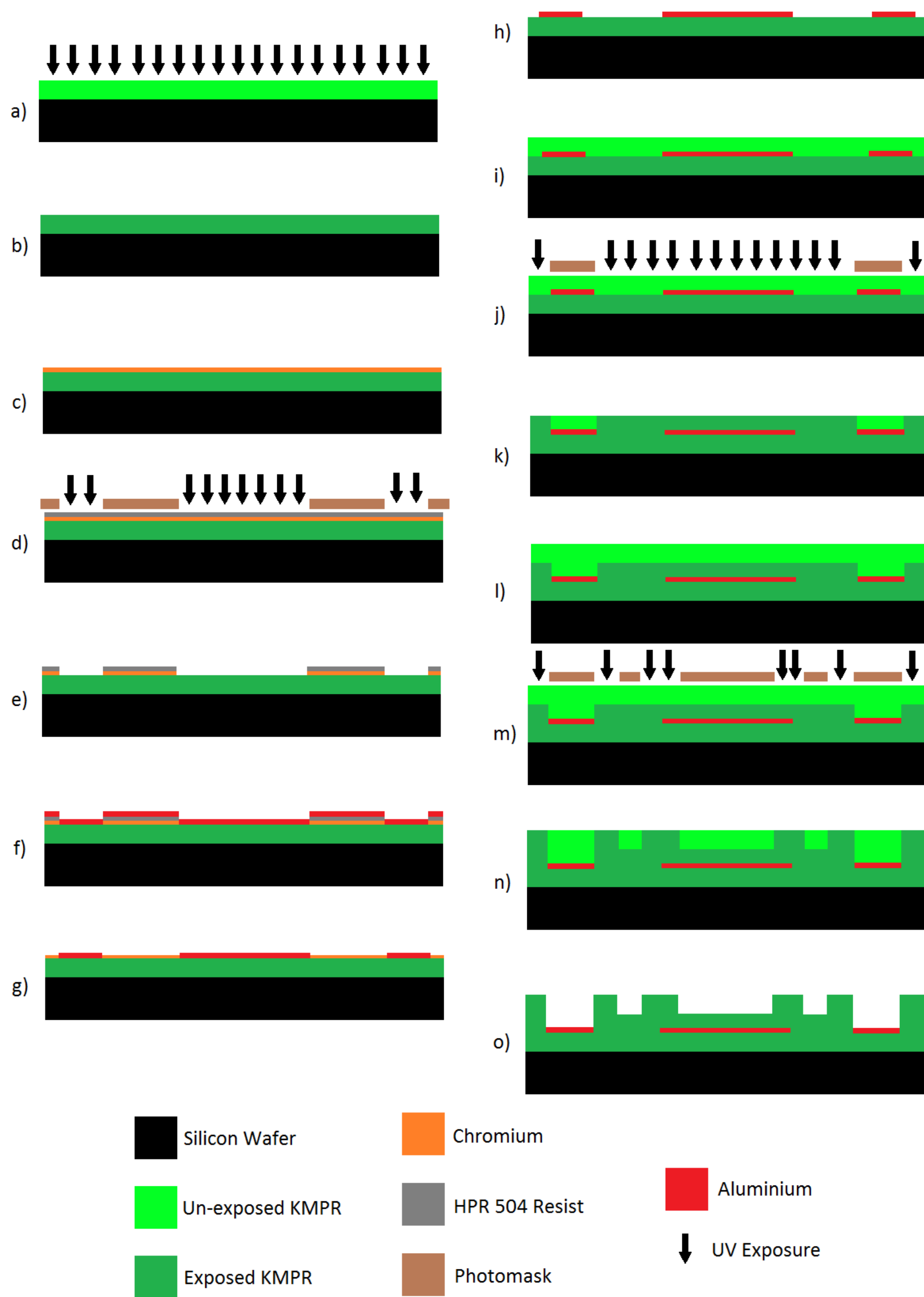

Figure 4.11: Flow chart for the fabrication of the device wafer consisting of 3 layers of KMPR and the Al film for resistive heaters.

the electrical access pads in the devices (Figure 4.11 j). Such a high exposure dose was possible to use in this layer as the only features to be developed were the contact pads for the heaters which were large enough avoid any issues related to resolution. The substrates were then given a post exposure bake (PEB) for 5 minutes at 100°C to lightly cross-link the film but the film was not developed yet (Figure 4.11 k). Another KMPR film was spun on top of the previous layer (same spin protocol yielding the same thickness) in order to produce the fluidic structures (Figure 4.11 l). After patterning the film (UV dose of only 600 $\frac{mJ}{cm^2}$ in order to achieve sufficient resolution to pattern the 100 μm features in the layer) to form the required structures (Figure 4.11 m), the substrate was again placed on a hotplate for a 5 minute PEB at 100°C (Figure 4.11 n). Both films were then developed using SU-8 developer for 4 to 5 minutes (to avoid damage caused by TMAH to the exposed Al films) (Figure 4.11 o).

The exposure dose for the fluidic layer (as well as the roof layer fabricated later) was kept lower than the dose used for the first 2 layers of KMPR in order to avoid resolution problems as mentioned in Chapter 3. In the first 2 batches of fabricated devices (the different batches are described in Appendix A) the exposure dose for all layers was the same in order to achieve a maximum physical stability. A device from the first batch was tested immediately following fabrication to ensure the channels were opened by performing a fill test (applying a drop of water to an input well and checking to ensure the water is able to flow into the channel by capillary forces). This first device successfully passed the fill test, and given similar results in previous development it was assumed that the channels were sufficiently formed to enable fluidic operation. It was only after the second batch of chips was tested that it was observed that every device tested was having issues with liquids entering the channels. The

devices were inspected with an SEM (Figure 4.12) and it was discovered that overexposure was indeed an issue with these devices and that it was only by chance that the first device tested had passed a fill test. Given this information batch 3 was fabricated by reducing the exposure doses for the KMPR layers containing fluidic features. An exposure dose of 600 $\frac{mJ}{cm^2}$ was used for the fluidic channels and a dose of 900 $\frac{mJ}{cm^2}$ was used for the fluidic roof (since the roof was fabricated on a glass substrate the two doses are equivalent as discussed later in this section). 2 devices from this batch were randomly chosen (in an effort to keep most of the devices clean for use in later tests it was desirable to limit the number of devices tested) and tested to ensure proper filling and they were both successful in passing the fill test (drops of water placed on the input wells were able to fill into the channels using only capillary forces). Batch 4 also had 3 devices tested at random and all were again able to fill properly using the same fill tests. Given the information presented in Chapter 3 it is expected that these layers will have a reduced and possibly unreliable T_g due to the lower exposure dose. Although this lower dose would likely improve the bonding strength (due to the films being able to deform better under pressure and achieve closer contact), there has not been any evidence to suggest that the lower T_g has had any negative effect on the operation of the chips. It has been suggested that the lower T_g would result in channel collapse during bonding but the 100% success rate in fill tests on devices from batches 3 and 4 has not provided any evidence that this is happening. In addition, past work by our research group with KMPR used fabrication conditions that would yield similar, if not lower T_g values, combined with higher bonding pressures, also didn't experience any issues with channel collapse during bonding [47]. Based on this information the lower exposure doses used in this fabrication process do not appear to have any negative effect on the operation of the chips. If in

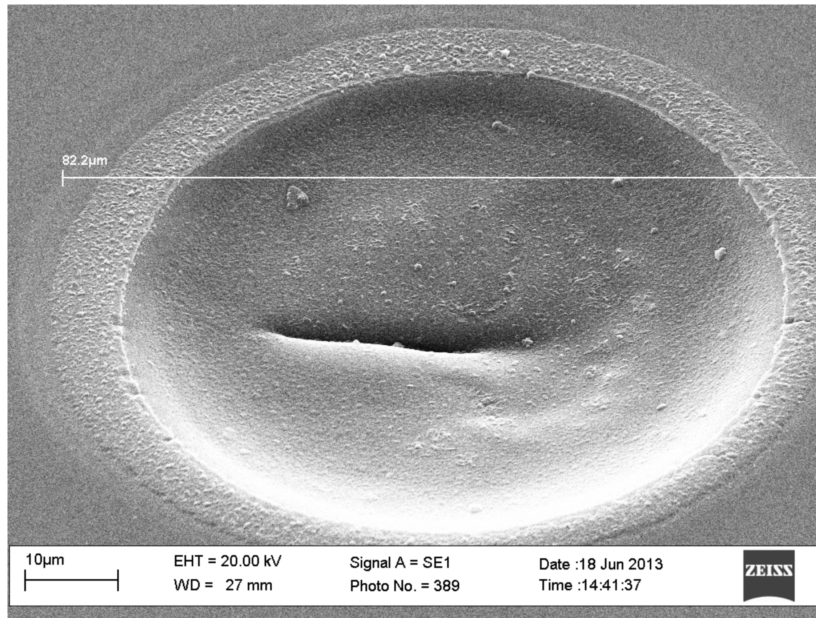

Figure 4.12: SEM image of an over-exposed fluidic via. As a result of the high exposure dose (2 J/cm^2) the opening in the KMPR did not properly develop resulting in a sealed channel. Reducing the exposure dose to 600mJ/cm^2 (900mJ/cm^2 for glass substrates due to reduced reflection of UV light off substrate) when patterning the fluidic layers avoided this problem.

the future it is desirable for the T_g of the 2 fluidic layers to be increased then the 2-stage exposure described in Chapter 3 can be used to achieve both high resolution and a stable T_g.

4.3.4 Carrier Substrate - PDMS Release Layer

4" square Borofloat glass substrates were used for fabricating the roof layer of KMPR. The substrates were first piranha cleaned for 15 minutes prior to rinsing in DI water, spin drying, and dehydrating on a hotplate at 100°C for 15 minutes. PDMS (Sylgard 184) was prepared by mixing the base and curing agent in a 10:1 ratio and degassing under a light vacuum (-20 mmHg). The PDMS was spun onto the glass substrates at 3000 RPM to form a 5μm film before being placed into a vacuum oven at 110°C for 1 hour to cure the film

(Figure 4.13 a). A 10nm thick, 0.5 cm wide gold border was sputtered onto the edges of the substrates in order to avoid de-wetting effects of the KMPR films fabricated on top of the PDMS.

4.3.5 Carrier Substrate - Fluidic Roof Layer

KMPR 1025 was spun onto the substrates at 4000 RPM (resulting film thickness when spinning on PDMS was 25 μm instead of 20μm) and a 3-stage soft bake was used to avoid de-wetting effects: 10 minutes at 50°C, 10 minutes at 80°C and 20 minutes at 100°C (Figure 4.13 b). This process produced a KMPR film thickness of 26 μm. The KMPR was patterned by UV exposure (900 $\frac{mJ}{cm^2}$ in order to achieve sufficient resolution for the 100 μm features in the layer; this dose is equivalent to a 600 $\frac{mJ}{cm^2}$ dose on a Silicon substrate) to form the fluidic wells and electrical access pads (Figure 4.13 c). A 5 minute PEB at 100°C was performed to lightly cross-link the KMPR prior to development in MF-319 for approximately 8 minutes (Figure 4.13 d, e).

4.3.6 Thermocompressive Bonding

Bonding of the KMPR layers was performed using a Jenoptik Hex02 hot embosser system. The bonding stack was assembled, from bottom to top, with a 6” quartz glass plate, polycarbonate (PC) piece (cut to the same radius of the patterned KMPR), Si device wafer, glass carrier substrate, and PC piece (same as the previous PC piece). Alignment of the features was performed under a microscope and was targeted to be within 5 μm across the entire substrate (Figure 4.1 a). The PC pieces acted to spread the applied bonding force across the substrates while minimizing the torque applied in order to avoid shattering the substrates. Bonding was carried out at 100°C with a force of 10 kN for 15 minutes (Figure 4.1 b). After bonding, when the substrates had

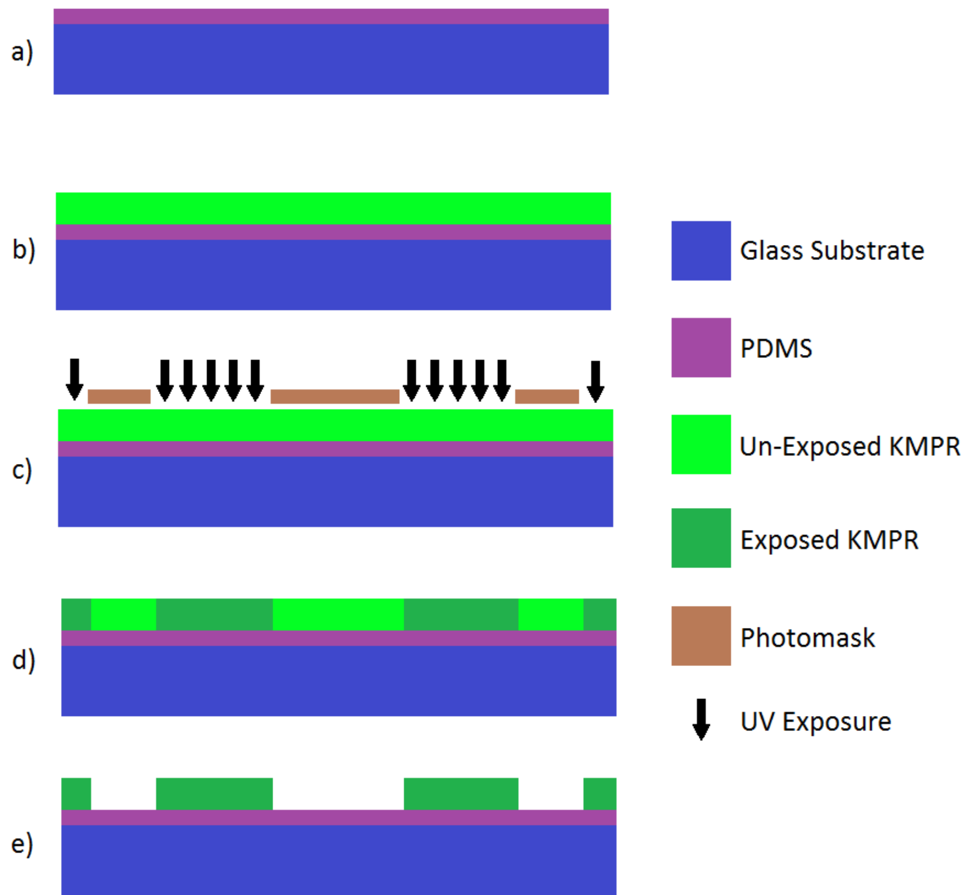

Figure 4.13: Flow chart for the fabrication of the glass carrier substrate consisting of the roof layer of KMPR fabricated on top of a PDMS release layer.

been allowed to cool to room temperature, a scalpel was be inserted carefully between the Si and glass substrates slowly working around the edges of the substrates in order to release the carrier substrate without breaking the Si wafer (Figure 4.1 c). If bonding was successful, with at least 90% of the KMPR area bonding, there was no problem releasing the KMPR from the PDMS. After release the chips were ready to be individually diced using a Disco DAD 321 dicing saw. The details of the dicing process are discussed in Appendix F.

4.3.7 Clarification of Exposure Doses

There are a number of different exposure doses that have been mentioned in this protocol and in order to avoid confusion the variations will be explained here. In Chapter 3 it was determined that an exposure dose of 2000 $\frac{mJ}{cm^2}$ was sufficient to activate all of the PACs in a 20 μm thick film of KMPR on a glass substrate. Based on information provided in the KMPR data sheet [23], films produced on a silicon substrate require only two-thirds the dose of a film deposited on a glass substrate due to the reflection of the UV light off of the substrate surface. Due to this effect an exposure dose of 1333 $\frac{mJ}{cm^2}$ is sufficient to activate all of the PACs in a 20μm thick film of KMPR on silicon.

It has also been noted that this high of an exposure dose limits the resolution of lithography to scattering and diffraction effects during exposure. In the case of the fluidic channels, fabricated on the silicon device wafer, this limits the exposure dose to 600 $\frac{mJ}{cm^2}$. For the fluidic roof layer (fabricated on the glass handle substrate) this is equivalent to a dose of 900 $\frac{mJ}{cm^2}$. This lower exposure dose allows for sufficient resolution during lithography, but also results in not all of the PACs being activated. Although it hasn't been necessary, it is possible to activate the remainder of the PACs in the film by performing a second, blanket, exposure step sometime after the film has been developed. This 2

stage exposure allows for both an increased T_g in the film while still maintaining the necessary lithographic resolution to pattern microfluidic channels.

4.3.8 Designed Specifications Compared to Actual Specifications

Based on private communications within our research group the following list of specifications was created for the fabricated devices:

- Devices should be able to pass a tape test to qualitatively confirm bonding strength.
- Devices should be able to pass a fill test, as described previously, in order to ensure channels are not sealed.
- Heater resistance should be between 20 and 30 Ω, though resistances up to 33 Ω are acceptable, in order to remain compatible with the current controlling electronics. This resistance must also remain sufficiently stable during operation in order to provide a temperature measurement accurate to within 1°C.
- Chips should be diced to within 100 μm of the designed dimensions. Further discussion of the dicing specifications are discussed in Appendix F.

As mentioned earlier, 3 devices from the last batch of chips were chosen at random and subjected to a tape test and a fill test. All of the tested devices passed both tests (no delamination during tape test, channels were able to fill using capillary forces when a drop of water was placed in the input well). Only 3 devices were tested as these tests have a high probability of contaminating the chips that are tested. The heater resistances were all measured to be

between 24 and 32 Ω, missing the target range but still within the acceptable range of resistances. As mentioned earlier this variation of resistances is due to the non-uniformity of the sputtering process along with the non-uniformity of the sputtering rate between runs that has resulted from our fabrication. Further work could be performed in order to further improve this uniformity if it is required. All of the chips were also had measured device dimensions within 80 μm of their designed values based on micrometer measurements.

The specification related to the ability of the heaters to remain stable when operating at PCR temperatures (up to 95°C) in the presence of moisture has encountered problems and will be discussed in the next chapter.

4.4 KMPR-Based LOC Design

With the fabrication process developed the next step was to establish the design of the microfluidic structures. The 3 main processes required for genetic analysis that need to be included in a full LOC device are sample preparation (SP), amplification (by polymerase chain reaction, PCR) and detection. This current generation of KMPR devices focuses on rapid PCR and detection using either capillary electrophoresis (CE) or quantitative PCR (qPCR). SP is being developed separately and will be integrated into later designs.

The required design elements for PCR include the ability to produce a uniform, controllable temperature profile throughout the PCR chamber for temperatures up to ∼95°C (depending on the PCR reagents used), the ability to load the chamber without trapping bubbles, to seal the chamber during operation and to remove the PCR product following thermal cycling. Within these separate requirements there are a number of design decisions to be made.

4.4.1 Thermal Requirements for PCR

PCR is performed by cycling a volume of sample through 3 different temperature ranges several times. In each cycle the amount of product produced is increased. The reagents and enzymes used in PCR operate in narrow temperature ranges and as such the temperature uniformity of the sample volume must be tightly controlled for reliable amplification [73]. In order to accomplish this thermal control on chip there are a lot of factors to consider related to heat flow throughout the chips. As discussed in section 4.2 the easiest way to control the temperature of the PCR chamber is to have the heater placed as close as possible to the chamber. Furthermore in order to reduce the power required to heat the chamber (necessary for future CMOS integration) it is also important to have a thermal resistance between the heater and the silicon substrate (which acts as a heatsink). There were two options considered for achieving this thermal resistance: an airgap between the heater and the substrate or a thick floor of KMPR. Given the complications related to building an airgap in these structures (some of which are discussed in Appendix B) this generation of chips is using a 13 μm thick layer of KMPR to provide some thermal resistance. The heaters themselves were designed in such a way as to produce a uniform uniform temperature throughout the entire chamber by determining the power density distribution created by current passing through the heater traces. The designs of the heaters were created by Jose Martinez-Quijada and Saul Caverhill-Godkewitsch and as such won't be discussed here, but the final designs can be seen in Figure 4.14.

4.4.2 Fluid Control Systems

Fluid control is the other important consideration in LOC systems, allowing for the sample and products to be loaded and moved where they need to be in

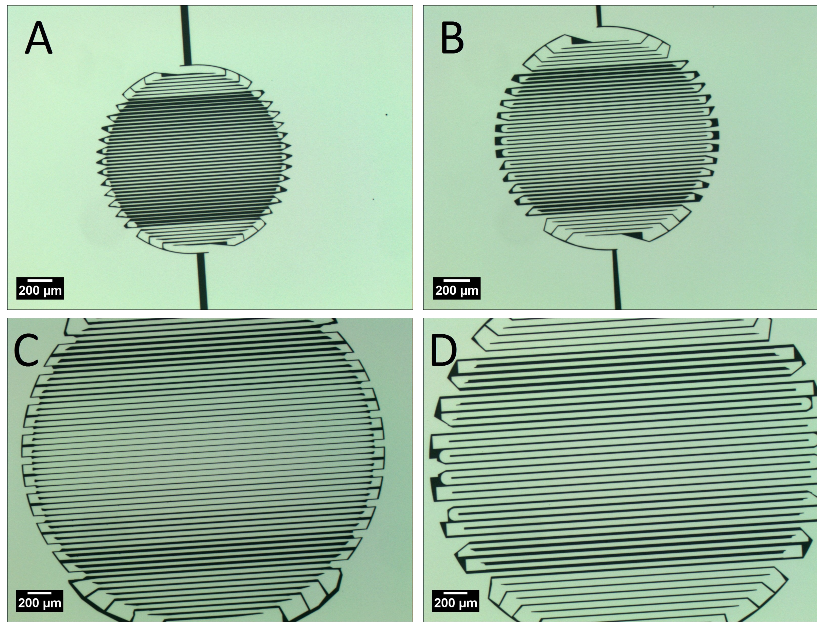

Figure 4.14: 4 different heater designs were created. The bulk of the images is the Al thin film, with the black areas being the space between the heater traces. A and B are designed for a 500 μm radius PCR chamber while C and D were designed for a 1200 μm radius PCR chamber.

the chip at various stages of processing and analysis. In the case of these chip designs, which do not include an SP stage, the concern is to be able to load the sample into the chamber, seal it and possibly inject the sample for CE. The biggest challenge here is to be able to seal the sample within the PCR chamber during thermal cycling. Ideally valves would be present surrounding the PCR chamber which would be sealed (pneumatically, electro-statically, etc.) during PCR however building valves within a KMPR structure has proved to be a challenge. In order to have reliable, integrated, normally-closed valves it is necessary to bond KMPR layers together in such a way as to have selectively poor bonding in the valve area. Normally closed valves are preferred as they are best able to seal without leaking issues. Unfortunately this type of bonding strategy is extremely difficult to achieve in practice. After an extended effort to achieve this selective bonding (see Appendix C for details) the concept was

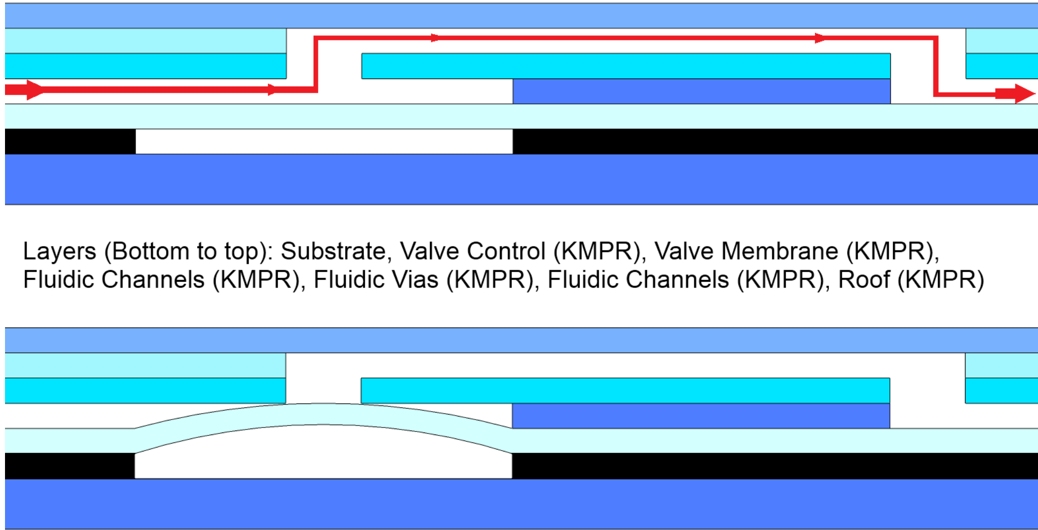

Figure 4.15: Profile view of a normally-open valve using multilayer fluidics in a 6-layer fabrication process. The red line indicates the direction of fluid flow through the valve. When no deflection is induced in the membrane fluid is free to flow through the valve. Only by actively deflecting the membrane can flow be blocked. Deflection of the membrane could be achieved using penumatic pressure acting on the bottom of the membrane, or some combination of pressure and electrostatic forces. This valve type would not suffer the same issues as normally-closed valves with respect to the valves bonding closed.

abandoned in favor of other strategies.

The first alternative strategy proposed was to use multi-layer fluidics to achieve a normally-open valve that would still produce a reliable, leak-proof seal (Figure 4.15). This type of valve would require no new fabrication processes to be developed as a multi-layer bonding process had already been developed as part of previous selective bonding research (see Appendix C). Challenges would still exist in ensuring good seals around channels and the fluidic vias and the actual sealing capability is unconfirmed.

Another proposed method for sealing the PCR chamber involves the use of external valves as part of a helper-chip package.

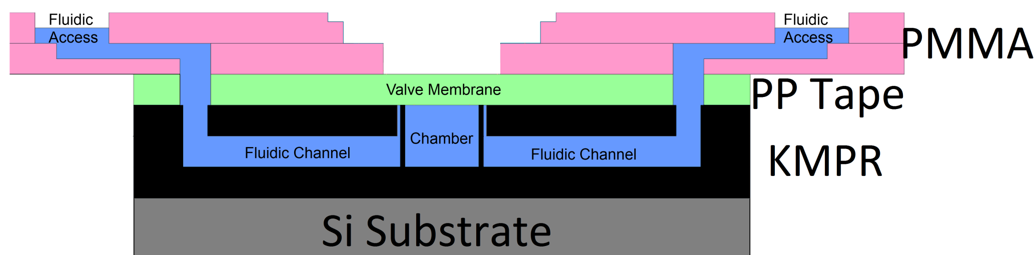

Figure 4.16: Profile view of a helper chip valve. The polypropylene tape used to attach the PMMA helper chip to the KMPR chip is also used as the valve membrane and is controlled by pneumatic pressure in the chamber above the valve membrane.

PMMA Helper Chips

Research collaborators at the University of Waterloo are working to develop a laser cut poly(methyl methacrylate) (PMMA) chip that will improve the interface between the small fluidic access wells in the KMPR and the larger sample volumes that are to be tested. This helper chip can also be modified to include a pneumatically controlled membrane that can serve to seal a PCR "well" fabricated in KMPR (no roof layer is fabricated over the PCR chamber) as shown in Figure 4.16. Fluidic access to the chamber is achieved through vias placed on either side of the PCR chamber which are connected to fluidic channels.

The current generation of chips use the external valve and as such the final design was made accordingly (Figure 4.17). The design is split into three sections, from left to right: sample loading, PCR chamber and CE/output channels. The sample loading channel has two output wells and a via in the middle for access to the PCR section of the chip. By having two wells it is possible to flow fluid through the channel after sealing the PCR chamber to avoid any contamination from leftover sample during loading. The PCR chamber does not have a fabricated roof but rather relies on the external helper chip to seal the chamber and the nearby vias during thermal cycling.

The channels on the right side of the design allow for the PCR product to be removed from the chip through one of the wells or allows for CE to be performed by using the long channel as the separation channel.

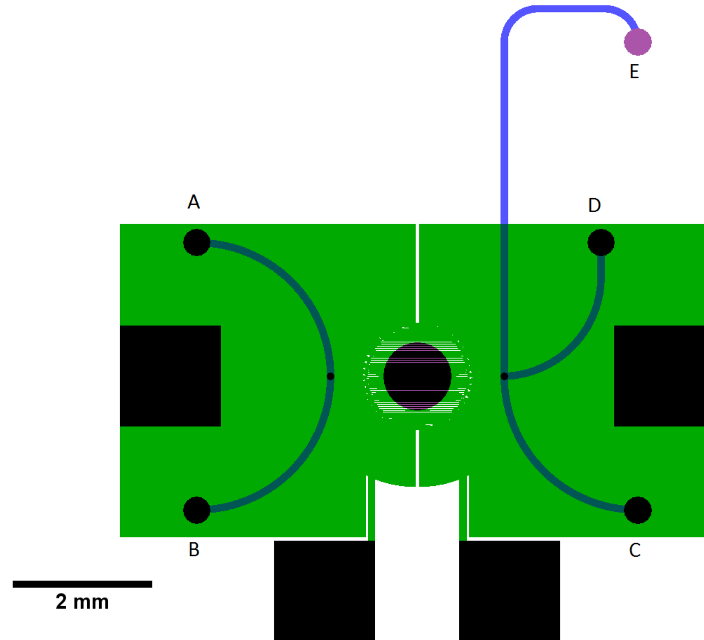

Figure 4.17: Top down layout of the current generation of LOC devices. From left to right the sections are designed for sample input, thermal-cycling for PCR and product output/detection. The channels are 100 μm wide, with the vias being 100 μm diameter circles. The channel running between well "A" and well "B" is designed for use in loading the sample into the chip with a via in the mid-point of the channel to allow access to the PCR chamber through the external valve. The reason for the second well in this section is to allow for the channel to be flushed and cleaned after the PCR chamber is sealed. If no CE is to be performed either well "C" or "D" can be used to unload the sample from the PCR chamber (by flowing fluid through the device from either well "A" or "B"). The combination of wells "C", "D" and "E" also provides a standard platform to CE to eventually be performed, with product injection occurring by running current between wells "A" and "D", and separation occurring by running a current between wells "C" and "E". Detection would occur along the top portion of the channel, which is closest to the edge of the chip.

4.4.3 Electrical Connections for Metal Structures

With the chips designed and built interfacing methods needed to be considered. Fluidic interfaces are being developed using a helper chip concept by other colleagues but the electrical interface also required development. The preferred connection technique for previous designs has been to use spring-loaded "pogo" pins (Mill-Max Manufacturing Corp. Part number 0906-1-15-20-75-14-11-0) to connect to the exposed connection pads on the chips. This method presents two possible issues: high current densities around the connection points leading to electromigration problems and mechanical scratching in the electrical pads every time a connection is made.

To determine if electromigration around the connections is going to be a problem the current densities flowing out of the connections must first be determined. Contact area (required to determine current density) between the pogo pins and the aluminium pads was approximated using Hertzian contact theory between two elastic bodies which is based on the following equation:

$$r = \left(\frac{3LR}{4E^*}\right)^{\frac{1}{3}} \tag{4.1}$$

With: r=Contact radius, L=Load, $R = \left(\frac{1}{R_1} + \frac{1}{R_2}\right)^{-1}$, $E^* = \left(\frac{1-\nu_1^2}{E_1} + \frac{1-\nu_2^2}{E_2}\right)^{-1}$. R_1 and R_2 are the radius of curvatures of the 2 contacting materials, E_1 and E_2 are the Young's modulus of the two materials and ν_1 and ν_2 are the Poisson's ratios of the materials. This method results in a reasonable approximation of the contact area which is sufficient for this purpose.

Two sets of calculations were used in order to simplify the situation: the first set of calculations assumes that the aluminium film is not present and the pogo pin is being pressed directly into the KMPR while the second set assumes the pin is being pressed into a thick (infinite) piece of aluminium (neglecting

Table 4.7: Summary of mechanical properties used in calculations. The Radius of the pins (gold and nickel) are approximated using a microscope image of the tip. The Poisson's ratio of KMPR is assumed to be that of SU-8 as no data is available for KMPR.

Material	E [GPa]	ν	Radius of curvature (R) [m]
Gold	79	0.44	0.00126
KMPR	2.7	0.22	∞
Aluminium	70	0.35	∞
Nickel	200	0.31	0.00126

the KMPR completely). The actual case falls somewhere in between, likely being closer to the first situation given the small (100nm) thickness of the aluminium film.

In these calculations material 1 is the pogo pin which is listed by the supplier as having a gold coating 510nm thick over nickel. Given that the Young's modulus of gold (79 GPa) is higher than that of both aluminium (70 GPa) and KMPR (2.7 GPa) it also assumed that the nickel bulk of the pin (E = 200 GPa) has little effect on the contact area, but the change in the contact area resulting from assuming the pins are made entirely of nickel was also calculated. Table 4.7 presents a list of the values used for the calculations.

The calculation results for the radius of the contact area are listed in Table 4.8 based on the material assumptions used. The results show that the difference between a gold pin and a nickel pin is small (the softer material deforms better, dominating over the deformation of the hard pin), especially into the KMPR surface which is likely to be closest to the true situation. Now that these radius values have been calculated they can be converted into an electrical cross-section for calculating the current density out of the pins by noting that all current flowing out of the pins must pass through the cross-sectional area with a height equal to the thickness of the Al film and a width equal to the circumference of the contact area. The calculated values are shown in

Table 4.8: Calculation results for pogo pin contact radius, cross-section area and current densities, listed according to material assumption used. The 4 assumptions are a gold or Ni pin pressed into an infinite block of KMPR or Al.

Material Assumptions	Contact Radius [μm]	Cross-section Area [μm^2]	Current Density [$\frac{mA}{\mu m^2}$]
Au pin into KMPR	58.6	36.8	9.0 - 12.7
Au pin into Al	23.3	14.6	22.7 - 31.9
Ni pin into KMPR	58.3	36.6	9.1 - 12.7
Ni pin into Al	21.2	13.3	25.0 - 35.0

Table 4.8 using an Al thickness of 100nm to determine the cross-section area.

These cross-sectional areas correspond to a range of current densities based on the current requirements for the different heater designs currently used (currents between 332 mA and 466 mA). For each material assumption the range of expected current densities when running the different heater designs at full current is given in Table 4.8.

Given that J_{max} for the heaters is designed to fall between 13.66 $\frac{mA}{\mu m^2}$ and 26.67 $\frac{mA}{\mu m^2}$ the cases where the Al film is neglected should not produce any extra difficulties with respect to electromigration problems (i.e. the heater traces will fail before the connections do) but if the actual contact areas end up closer to the Al-only assumption there may be problems resulting from electromigration that would require extra effort to work around. The effect of the silicon substrate has also been neglected in these calculations under the assumption that the KMPR film is thick enough to minimize the effect of the high modulus substrate on the deformation. Even for the case of a gold pin pressing into the KMPR surface (the case with the highest contact area, and therefore highest deformation) the pin will be pressing less than 1.5 μm into the 15 μm thick KMPR film which indicates that the effect of the silicon should be minor, although it may result in a slight increase in the current density

leaving the pins especially if the thickness of the KMPR floor is reduced.

In an effort to further reduce the current density at the connection points a number of alternatives have been considered. Initially a conductive silver epoxy was applied to the electrical access pads in an effort to spread out the current entering the Al as well as to protect the pads from any scratches caused by pressing the pins into the thin metal. Unfortunately the silver epoxy utilizes small silver particles to carry the current resulting in a number of high current density locations which resulted in the fusing of the connections when operated at high currents. Other possible connection mechanisms include low temperature solder materials, low melting point metals and even wirebonding (assuming it could be accomplished without damaging the KMPR). Positive results have been achieved using Field's metal (32.5 % Bi, 51 % In, 16.5 % Sn, melting point of 62°C, supplied by Rotometals Inc.) as a connection material. Connections are achieved by placing a small amount of solid metal onto each of the contacts pads before heating the entire chip to 65°C to melt the metal onto the contact pads. After cooling the chip to room temperature the pogo pins are then pressed down onto the connection pads and secured in placed prior to re-heating the chip to 65°C in order to increase the contact area between the pins and solder metal. Once the chips are cooled once more the devices are ready to be used. This type of connection has proven to be reliable for longterm operation of the chips avoiding fusing or electromigration problems around the connection points.

4.5 Chapter Summary

This chapter has described the work that has been done to design and build KMPR-based microfluidic devices. Using information from the previous chap-

ter on the physical properties of KMPR a viable fabrication process was developed to allow for the production of sealed microfluidic channels by using a thermo-compressive bonding process to create a roof layer without the use of sacrificial support layers. KMPR films have been spun with thickness uniformity better than 1 μm across an entire 4" Si wafer allowing for improved bonding quality with greater than 90 % of the bonding area achieving intimate contact during bonding. Aluminium heaters have also been fabricated within the KMPR structures providing separation of the heater structures from the silicon substrate and allowing for reduced power consumption when operating the heaters. All of these details have been combined to create a new LOC system design for performing genetic amplification and detection.

Chapter 5

Design and Fabrication Validation

With the fabrication process worked out and the chips fabricated the next stage is to test the durability and functionality of the chips, especially the heater structures. This chapter discusses the heater durability during operation, thermal uniformity results and temperature coefficient of resistance (TCR) results of the chips. This work will enable the future operation of these chips for PCR, CE and melting curve analysis (MCA).

5.1 Heater Functionality and Durability

The heaters are the most fragile structures in these devices given their thin metal traces fabricated on potentially unstable surfaces and the high current densities that will be applied to them. The heaters must be capable of withstanding any expansion or wrinkling in the KMPR during operation along with being able to sufficiently withstand the designed current densities that will lead to electromigration problems during any long-term operation of the chips. In order for these heaters to be useful they must be able to run at

95°C with consistent resistivity for at least a single, full PCR process (lasting at least several minutes), but in order to aid the development process they should run for at least several hours to allow for re-use of chips and for the performance of qPCR and MCA analysis. It was also necessary to study the operation of the chips in order to verify the TCR of the chips as well as the thermal uniformity produced by the heater. The first stage of testing involves measuring the TCR of the heaters in order to allow for the the temperature of the heaters to be measured during operation. By connecting the heaters in a 4-point mode during operation it is possible to measure both the applied current and the voltage drop across the heater. With these values measured Ohm's law allows for a real-time calculation of the heater resistance during heating. By tracking the increase in the heater resistance during heating the average temperature of the heater can be determined according to the TCR of the heater metal, therefore providing real-time temperature feedback of the system. After the TCR was determined an infrared (IR) camera was used in order to directly measure the thermal uniformity of the heater during operation. Lifetime tests have also been performed to determine what kind of issues are likely to be faced with respect to electromigration.

5.1.1 Physical Stability

In order for these heater devices to be useful they must maintain their physical (and therefore electrical) properties during operation. In the past most polymer-based LOC systems using thin film metal structures have deposited the metal films directly onto either a glass or silicon substrate with the polymer fluidics built on top [41, 17]. This setup provides a rigid surface for the metal structures in order to avoid any deformation or damage as the temperature changes but also increases the power required to heat the fluidics due to the

high thermal conductivity of the substrates compared to the polymer structures. By moving the heater structures from the surface of the substrate (as was the case for our research group's previous LOC devices [16]) directly into the polymer films the power required to heat the system is reduced (thanks to the increased thermal insulation provided by the polymer film) at the cost of reduced physical stability. As mentioned in the previous chapter KMPR provides exceptional adhesion of metal films compared to other polymeric materials however its low glass transition temperature (discussed in Chapter 3) could result in the film wrinkling or cracking when the chips are heated.

The first tests related to the physical stability of the films during operation of the chips involved calibrating the TCR using a temperature-controlled waterbath (Haake Phoenix II C35P). The expected calibration process was to use a temperature-controlled waterbath with the temperature controlled to better than 0.1°C to produce a uniform, known temperature throughout the device while measuring the change in resistance. Chips were loaded into a custom-designed connection jig and connected in order to achieve 4-point resistance measurements. The chips were then placed into a plastic bag (Foodsaver 1 gallon vacuum sealing freezer bags) and the end of the bag was tied shut with the electrical wires running out the mouth of the bag. The bag was then inserted into the waterbath with the mouth of the bag remaining outside of the bath to prevent moisture from entering and shorting out the connections. The waterbath was then ramped through several different temperatures between room temperature and 80°C (allowing time for the temperature to stabilize at each step) and a resistance versus temperature curve was produced in order to determine the TCR of the heater.

Although this calibration process has been used in the past by our research group to successfully study the operation of Al heaters fabrication on KMPR

[68], with the current design of devices it was discovered that when heating the chips to 80°C in the waterbath the metal film experienced serious wrinkling (Figure 5.1). Since this same behaviour is not seen when heating the devices on a hotplate (which actually served to smooth out the film following bonding as mentioned in the previous chapter) it is assumed that the wrinkling is the result of some combination of the increased temperature and the high humidity that would result from the situation even with the chip enclosed in a plastic bag to isolate the devices from the warm water. Theories as to this behaviour will be discussed shortly.

This wrinkling proved to have a major effect on the resistance of the heaters. Figure 5.2 shows the resistance (4-point measurement using a Hewlett Packard 34401A multimeter) over time resulting from placing a chip in the waterbath and holding the temperature at 80°C for 5 hours compared to placing a chip on a hotplate at 100°C for the same length of time. The heater in the water sees a 29% increase in its resistance over the 5 hour test. The change in resistance is not likely due to any annealing effects in the Al film as the change in resistance would have been seen in both samples, but is rather likely caused by the deformation of the metal film caused by the KMPR softening due to the absorption of moisture. This softening would cause the films to deform as any residual stress in the Al or KMPR films would attempt to relieve themselves. This wrinkling occurred for PEB bakes of the KMPR floor layer with temperatures of 120°C, 150°C and 180°C.

Experiments performed by collaborators at the University of Waterloo with heating fluids within the PCR chamber have reached temperatures of over 50°C without experiencing the same increase in heater resistance but have yet to be tested at temperatures up to 95°C. Our testing has indicated that the heater films and the KMPR consistently wrinkle after several minutes of heating up

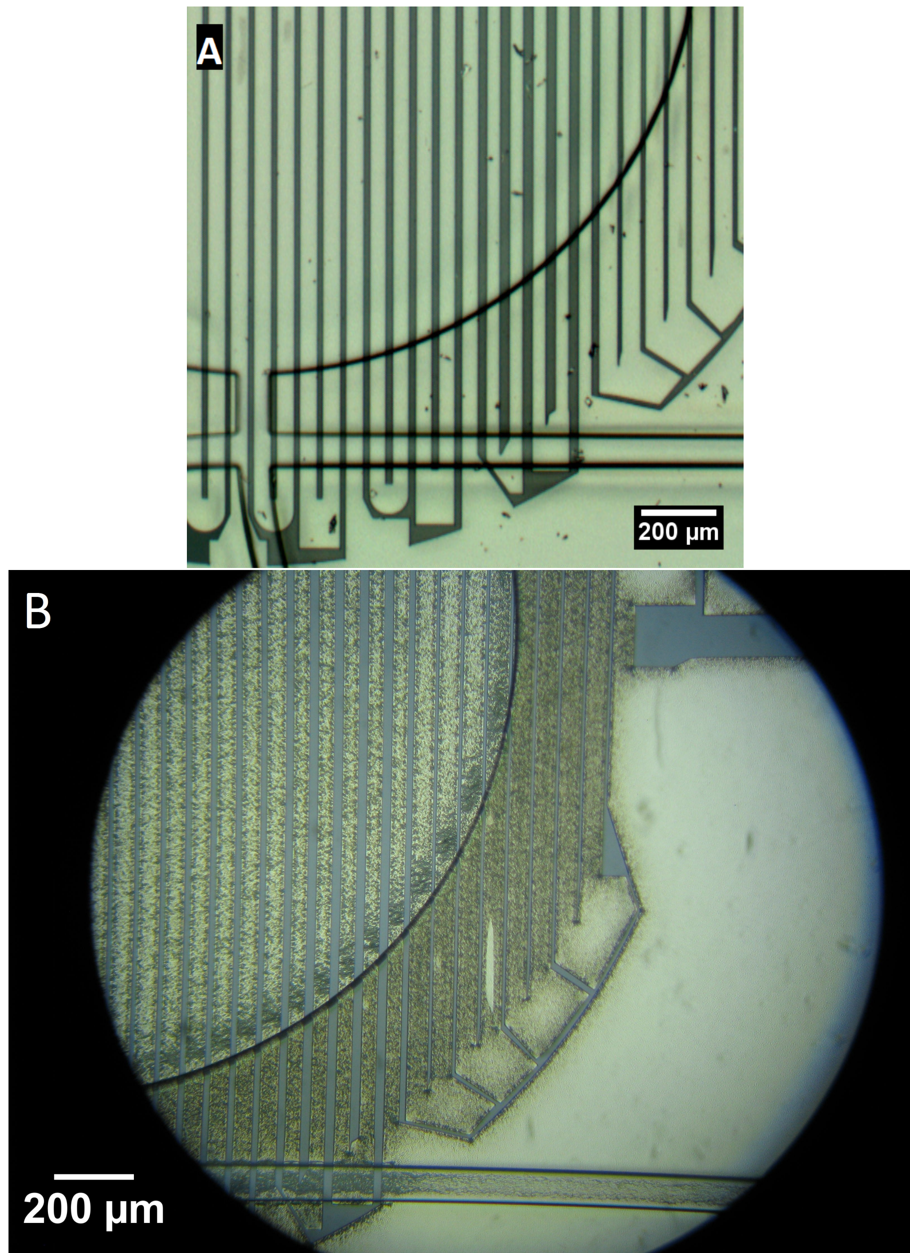

Figure 5.1: Heater film before and after heating in a waterbath at 80°C. Slight wrinkling of the metal can be seen around the edges of KMPR features before heating (image A) but after heating the much of the film is heavily wrinkled (image B). This wrinkling does appear to be concentrated around the edges of the aluminium features (the majority of the area of the large contacts are smooth whereas the heater traces and the edges of the contacts are drastically changed between the two images) possibly indicating that moisture is diffusing through the KMPR underneath the aluminium and causing the wrinkling or buckling of the film. Given that the larger areas of Al are untouched this issue does appear to be one of the Al reacting with the moisture otherwise all of the Al would be responding the same way.

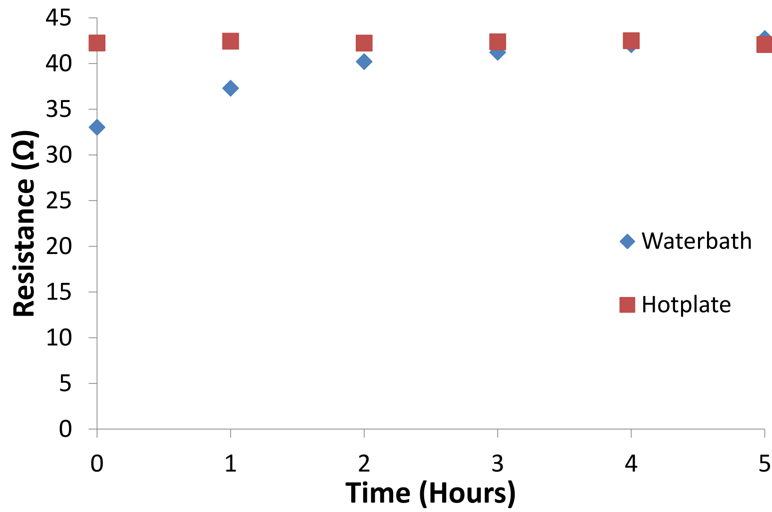

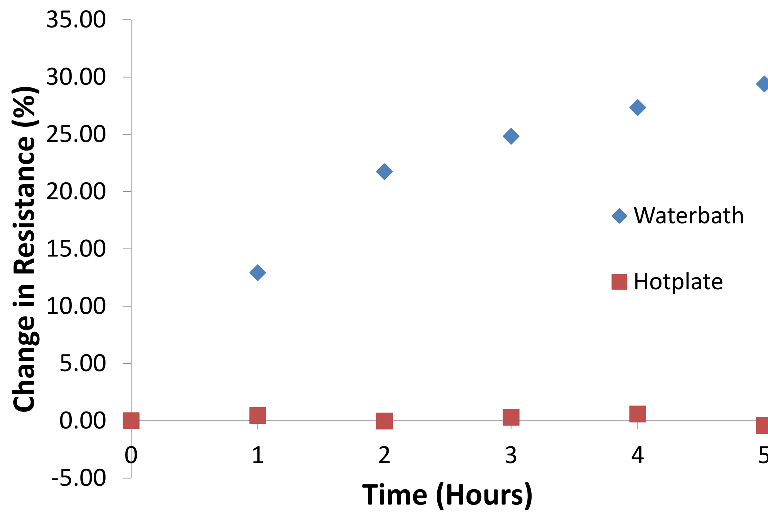

Figure 5.2: Resistance change of a heater placed in a waterbath at 80°C and another placed on a hotplate at 100°C. The chip placed in the waterbath experienced a 29% change in resistance over 5 hours, while the chip on the hotplate experienced a negligible change in resistance. The difference in the initial resistance values is due to a combination of the higher temperature experienced by the chip on the hotplate, and a slightly different film thickness arising from the sputtering process. The change in resistance from the waterbath test is attributed to the wrinkling experienced by the film during operation, which is most likely caused by softening of the KMPR upon exposure moisture resulting in any residual stresses in the Al film working to deform the films in an attempt to relieve the stress.

to PCR temperatures in the presence of moisture regardless of the amount of baking, or the temperature of baking, experienced by the film prior to exposure to the moisture. This issue will either severely limit or outright prevent any applications of these heaters related to PCR. This is a serious concern that must be addressed in future development of these devices.

5.1.2 Discussion Of Heater Wrinkling

This wrinkling of the heater structures during wet operation is a major concern for the ultimate functionality of these devices. The current fabrication process as it has been developed is not capable of producing a heater structure capable of operating in the presence of moisture and changes need to be made in order for these devices to accomplish reliable genetic amplification. What is more troubling is that the current devices have encountered this issue where previous devices fabricated by our research have been able to function in the same waterbath conditions [68].

Based on the information we currently possess it seems that the wrinkling is most likely due to some combination of the KMPR softening while absorbing moisture during the waterbath testing and residual stress in the metal film. Figure 5.1 suggests that the wrinkling is mostly localized near the edges of the aluminium features, possibly indicating that any moisture diffusing into the KMPR is limited in the distance it can diffuse over the course of the testing and that the metal film serves to block diffusion through it.

As a point of mention, this wrinkling problem is considered to be different from the wrinkling that initially arose during the bonding process (discussed in Chapter 4). In early fabrication work, before the PEB temperature of the floor layer of KMPR was increased, the metal film wrinkled during the bonding process as a result of the uneven forces that were applied due to the patterned

layers of KMPR above the heaters. That problem was solved by increasing the cross-linking level of the KMPR floor to provide a a more rigid surface to resist the pressure differences during bonding. The wrinkling of the metal during wet operation is most likely caused by residual stresses in the Al and/or the KMPR films after fabrication. As the KMPR is heated and absorbs more water it is likely softening and residual tensile stress in the metal would result in wrinkling.

SU-8 has been studied and has been shown to increase in volume while absorbing water by diffusion [74, 75] as well as suffering from a reduced modulus [76]. This volume increase introduces compressive stress into the polymer material causing it to wrinkle in an attempt to relieve the stress, on top of any wrinkling resulting from residual stress in the films from the fabrication process.

It may be possible to adjust the deposition parameters of the aluminium film in order to produce a slightly tensile stress in order to prevent wrinkling when the KMPR softens, although cracking of the film may result instead. It would be beneficial in future research to study the film stress in metals deposited onto KMPR as it would provide additional information to expand this hypothesis and possibly reach a solution.

It may also be possible to avoid this wrinkling if a moisture barrier can be introduced to block the KMPR floor from absorbing any moisture from the PCR chamber during operation. Although it may be possible to utilize some other thin polymer layer such as parylene C or polypropylene [77] as a blocking layer it is likely that an inorganic blocking layer, such as an additional metal film, would be required to provide a diffusion resistance significantly higher than that of KMPR. The advantage of using another metal film in between the heater and the PCR chamber is that it would likely serve to further

spread out the heat flux into the chamber, yielding an even greater temperature uniformity. Any of these changes would require a significant redesign of the process but would increase the possibility of the devices functioning for an extended period of time in a moist environment.

Another possibility for avoiding the wrinkling problem is to replace the floor layer with a more physically stable material that still provides sufficient insulation from the Si substrate to avoid a significant increase in power consumption. It is possible that another polymer such as SU-8 would be capable of handling the diffusion of moisture into the film while still maintaining sufficient stability to prevent wrinkling of the metal.

These hypotheses do not answer the question as to why our previous work did not experience these issues. It may be beneficial to study the differences between the two fabrication processes to identify the reason why this problem has only now arisen. Differences in the film thicknesses and fabrication conditions may have led to change in behaviour. The previous work done with these materials [68] used a thicker KMPR film, a lower PEB temperature and time, and had the heater patterned by wet etching instead of lift-off. The difference may also have arisen due to the age of the KMPR used in the process, as the devices tested in this thesis were produced using a supply of KMPR slightly over a year old (stored in a freezer to improve shelf-life), although the age of the KMPR used for the original tests is not known. Any of these differences may have resulted in a change in behaviour due to changing different stresses and material properties. It may also be the case that the more rigid KMPR resulting from the current process is actually a detriment to the operation of the heaters. The softer KMPR from our previous work may have served to better absorb any residual stresses in the metal films and actually served to prevent the wrinkling problem. If this is the case then it may be possible to

find a balance of KMPR mechanical properties to allow the heaters to survive the bonding process (our previous work did not include a bonding process) but to also allow the KMPR to be soft enough to absorb any residual stress from the metal films and prevent their wrinkling and damage during operation.

5.1.3 Hotplate Calibrations

Despite the current problems related to wrinkling in a moist environment it is still beneficial to study the operation of the currently fabricated heaters in order to confirm their simulated functionality and to provide feedback that can be used to improve future designs. Fortunately, as shown in Figure 5.2, placing the chips on a hotplate at 100°C for several hours has a negligible effect on the resistance allowing for the heater resistances to be calibrated with respect to the heater temperature. Although the same level of thermal control cannot be achieved using a hotplate for the calibrations by using a thermocouple to confirm the temperature of the hotplate surface it is possible to determine the temperature of the heater by running a COMSOL simulation to relate the temperature of the bottom of the chip to the temperature of the heater film.

Calibration results for one of the heaters on a hotplate is shown in Figure 5.3, with the calibration consisting of resistance measurements at 22°C, 40°C, 60°C, 80°C, 100°C and again at each of those temperatures while ramping down. Unlike with the waterbath calibration, the measurements are extremely consistent, with a variation of less than 0.2 Ω at all points. Calibration was performed using thermal paste (T630 thermally conductive form-in-place gap filler, Parker Hannifin Corp) to ensure good thermal contact between the chip and the hotplate and the resistance was measured in 4-point mode to eliminate any variations in the contact resistance. The resistance versus temperature measurements can be converted to the TCR of the metal by a geometric factor

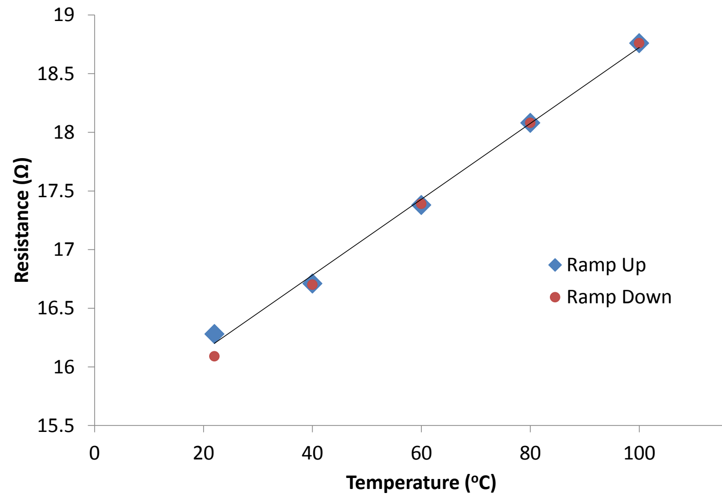

Figure 5.3: Heater calibration using a hotplate. The chip is heated from room temperature (22°C) to 100°C and then cooled back to room temperature with the resistance measured (4-point measurement) in 20 degree increments (with the first measurement at 22°C instead of 20°C). The TCR value resulting from this graph is 0.002 K^{-1}.

specific to each individual heater design. In the case of the device measured in Figure 5.3 the TCR of the metal was determined to be 0.00204 +/- 0.00004 K^{-1} and has been confirmed within error on several different devices, including devices from a separate sputtering process. If this consistency of TCR is maintained it will allow for the calibration of chips to be greatly simplified in future devices as the TCR for each individual device would not need to be measured. This consistency of TCR also allows for increased confidence in any temperature calculations (important for reliable temperature control) and allows chips to be calibrated by using only a room temperature resistance measurement for each chip.

5.1.4 Electromigration Effects

As discussed in Chapter 4 electromigration is a potential concern with regards to the operation of aluminium resistive heaters. High current densities passing through the heater traces will introduce stresses within the metal resulting in the formation of voids and open circuit failures of the heaters. There are two potential locations where electromigration could prove to be a concern: the heater connections and the heater traces themselves.

Initial operation of the chips used either pogo pins directly pressing into the electrical connection pads or used a small amount of silver conductive epoxy to improve the connection area. Unfortunately these techniques yielded inconsistent results with some connections failing within moments of current passing through the pins and some connections lasting several hours prior to failure. In both of these cases the limiting factor in the lifetime of the chips was the durability of the connection points. Based on the calculations made in Chapter 4 this suggests that the connection area between the pogo pins and the Al pads is closer to the worst case calculations (where the current density through the connections would be higher than the current density in the heater traces, causing the connections to be the first point of failure). In addition silver epoxy seems to have minimal effect with reducing the input current density due to the small silver particles creating areas of high localized current density. In an effort to move past this problem all chips now use a small amount of low-temperature solder coating the Al pads to effectively spread the input current across the pads. Since this technique has been applied the lifetime of the chips has been limited by the electromigration in the heater traces during operation.

Lifetime tests were performed in order to determine the length of time the resistive heaters could be used prior to electromigration failures occurring. As

shown in Figure 4.14 4 different heater designs were produced and a lifetime test was performed on a chip of the design which utilized the highest current density to achieve heating. Electrical connections to the chip were made using Field's metal (32.5% Bi, 51% In, 16.5% Sn: melting point 62°C) as a low temperature solder and spring loaded "pogo" pins pressed into the metal. The chip was connected in a 4-point mode in order to facilitate current and voltage measurements during the test. The target resistance (corresponding to the target temperature due to the TCR of aluminium) during the test was determined by heating the chip on a hotplate to 95°C and measuring the resistance of the heater, which was found to be 11.43 Ω. The voltage and current applied to the heater was controlled in order to achieve and maintain the target resistance, and therefore the target temperature, during the test. These conditions were held until the heater failed.

The current applied to the heater during the test was 314 mA (voltage of 3.59 V, power supplied by an Agilent E3647A DC power supply operating in current control mode) corresponding to a maximum current density of 14.2 mA/μm^2. The current was held steady (approximately 3.3% variation in current, with the resistance controlled within 0.2%) for 41 hours and 25 minutes until the first failures occurred in the heater tracks (the change in current due to failing trace occurred over a period of time of less than 1 minute). By using this same control system to drive the heaters this variation in resistance equates to a temperature control of 1.1°C (based on Figure 5.3), which is just barely outside of the target temperature accuracy of 1°C that was stated in the previous chapter but a more accurate heater controller should be able to reduce this further during an actual PCR. Heater failures occurred as a result of void formation within the heater traces in the areas of highest current density resulting in open circuit failure (Figure 5.4). This lifetime will allow for

these chips to be used not only for PCR (assuming the wet operation problems can be solved) but also for MCA and qPCR without fear of failure. The heaters should also be capable of multiple uses assuming the chips can be sufficiently cleaned in between tests. Although tests haven't yet been performed on the other device designs the maximum current densities required to achieve a temperature of 95°C on those devices is 25-50% lower than the design that was tested. Given that electromigration is approximately proportional to the current density squared (Equation 5.1, [71]) the other designs should have significantly longer lifetimes. If lifetimes do prove to be a problem the current density can be further reduced by increasing the thickness of the metal film (serving to increase the cross-sectional area of the heater tracks). Even increasing the film thickness to 200 nm would reduce the maximum current density in the tracks to less than 10 mA/μm^2 without any appreciable effect on the thermal uniformity of the system.

$$\text{Mean time to failure} = \frac{Ae^{\frac{E_a}{kT}}}{J^n} \tag{5.1}$$

Where A is a film dependent scaling factor, J is the average current density, n is a constant close to 2, E_a is the activation energy, k is Boltzmann's constant and T is the temperature.

With the TCR of the heaters determined along with an understand of the lifetime limitations of the heaters the next step of testing is to study the thermal uniformity of the heaters during operation.

5.1.5 IR Camera Results

Since these chips are designed to have uniform heating within the chamber for PCR thermal cycling it is necessary to confirm that the heating is accom-

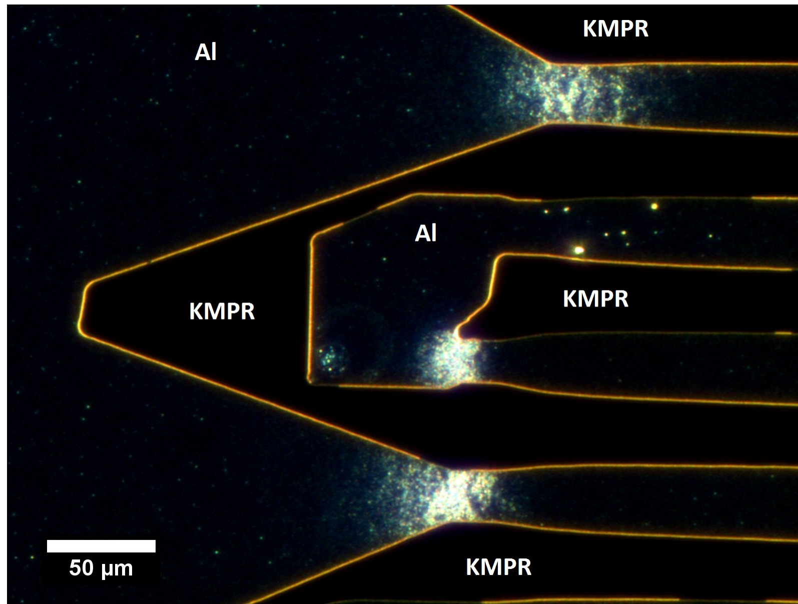

Figure 5.4: Void formation as a result of electromigration effects in the heater traces. The voids are formed in the thinnest parts of the traces where the current density is highest during operation. These images were taken after the heaters failed due to open circuit formation.

plished as expected. Measuring the thermal uniformity of this kind of system is extremely difficult and although the plan is to use the resistance of the heaters as an indirect measurement of the chamber temperature this only provides the average temperature without providing any information as to the uniformity within the chamber. It is preferred that a method be used that is able to give the spatial thermal uniformity with a resolution of better than 10 μm allowing for the spacing between heater traces to be resolved as well. In order to accomplish this a high resolution IR camera (FLIR SC5600-M) was used to view the chips during operation. The challenge of using an IR camera in order to measure temperature without knowing the emissive properties of the material is that the absolute temperature of the system cannot be determined with certainty. However since the primary interest in these measurements is the temperature uniformity of the chamber it is much simpler to determine the

relative temperatures throughout an image by calibrating the images using a measurement taken while everything is at a known temperature (i.e. room temperature prior to running any current through the heater).

In order to obtain images the chips to be imaged were loaded into a custom designed jig with the electrical connections achieved by pressing pogo pins into a silver conductive epoxy. The jig consists of a solid block of aluminium with recesses machined into it for the chips to fit into allowing for the chips to be reasonably heat-sunk. Power was applied to the chips in order to produce Joule heating and the heaters were imaged using the IR camera to confirm the behaviour of the chips. The camera captured images at 10 frames per second in order to provide real-time feedback on the heating. The settling rate of the chip temperature in response to a change in the supplied power was confirmed with the temperature changing from 95°C to room temperature in less than 2 frames when the power was turned off. The heating rate of the chip matched the cooling rate with any change in temperature again occurring within 2 frames of the power being changed.

Some raw images taken by the camera can be seen in Figure 5.5. The images show the increased temperature to be primarily limited to the area above the heater elements which is expected given the design. However some inconsistencies can be seen, especially visible at lower temperatures where there is a cold spot in the image on the right side of the image. This area (which was consistent across all images) is attributed to the reflected image of the cooled detector of the IR camera itself. Given that this cold spot is constant it is possible to calibrate it out of the images by realizing that the entire chip is at a uniform temperature (room temperature) prior to the application of any current through the heater. A calibrated image of the heater at full current is shown in Figure 5.6 (no calibrated image at room temperature is shown as it

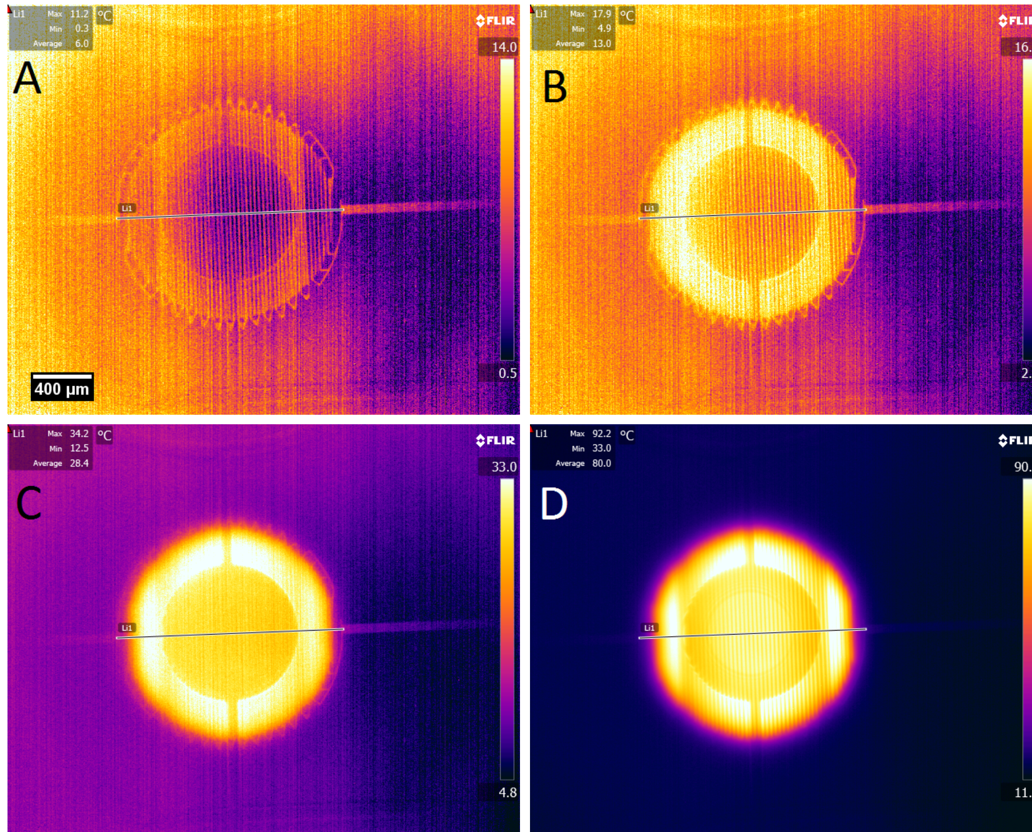

Figure 5.5: Raw images taken by the IR camera. The image A is at room temperature (no current flowing) with the other 3 images showing the chip with increasing current levels flowing through the chips.

is simply a uniform color/temperature).

There are still a couple concerns with the temperature profile of the calibrated images. First the temperature variation between the KMPR above any heater traces and the KMPR without any underlying heater traces is larger than expected (the temperature profile in Figure 5.6 shows a variation of around 4°C compared to a simulated difference of about 1°C) and the area "outside" the PCR chamber (but still within the heater radius) is measured as slightly hotter than the area "inside" the PCR chamber, which is opposite the expected behaviour. To address these differences it was necessary to consider what it was the camera was measuring the temperature of. The simulations

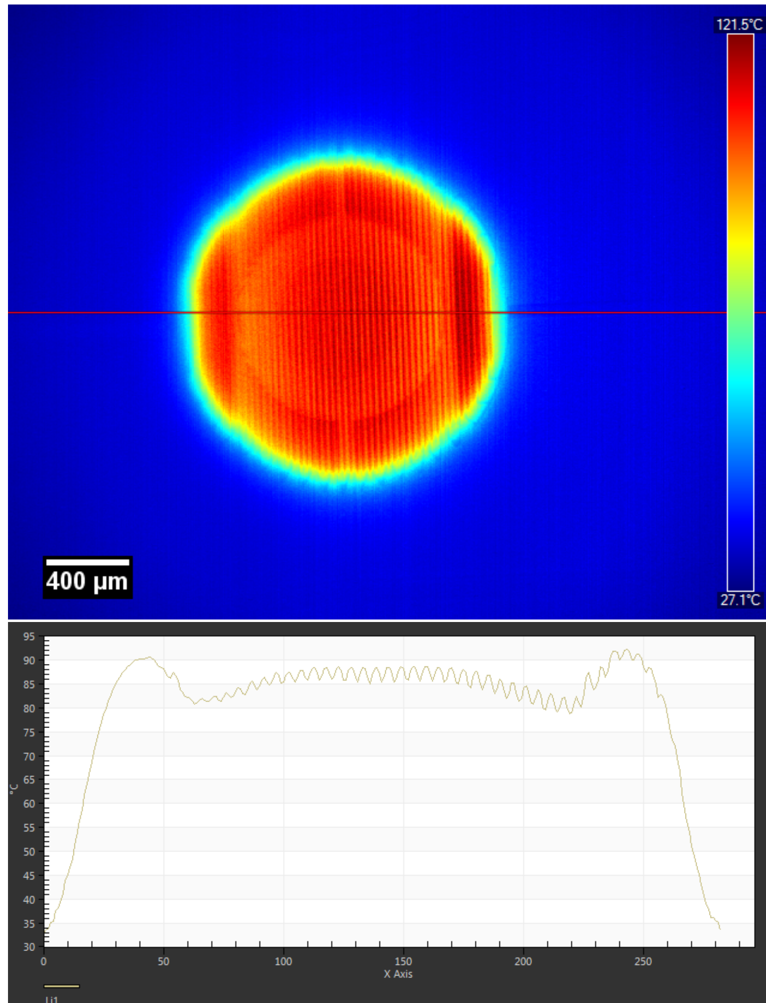

Figure 5.6: Calibrated IR camera image to account for the room temperature variations of the raw images. The bottom image is the temperature profile taken across the width of the heater area showing the measured temperature uniformity. The temperature of the image was calibrated by using a room temperature image (where the entire image was at a known temperature) to calibrate the temperature of each pixel to remove any effect of background temperature variations. The result still doesn't take into account variation in emissivity across the image resulting in exaggerated temperature differences across the different parts of the image.

assumed that the camera is able to measure the top surface of the KMPR without any effect being introduced by the reflective metal film embedded in the KMPR. It is more likely that KMPR is partially transmissive at IR wavelengths and therefore the temperature measurements at each point of the image are a combination of the temperature profile throughout the volume of the KMPR. On its own this does not explain the temperature variations seen in the calibration but when the metal film embedded in the KMPR is taken into account we can begin to predict these changes. Unlike KMPR the Al film is a very reflective surface and as such the camera is likely unable to see any KMPR beneath the metal (which also happens to be the coldest KMPR in the device) and instead would see any KMPR above the metal reflected back to the camera increasing the intensity of the radiation seen by the detector. Using the assumption that KMPR is partially transmissive and that Al is highly reflective a MATLAB script was written to "calibrate" the simulated temperatures from COMSOL to a result indicative of the situation seen by the IR camera.

In order to adjust the simulated temperatures to represent the temperatures that would be seen by the IR camera 4, 2-dimensional arrays of temperatures were used corresponding to each of the 4 layers of KMPR present in our devices. The temperature profiles were provided in a 5 μm grid size and imported into MATLAB. Using the Stefan-Boltzmann law (power per unit area = $\epsilon\sigma T^4$, where ϵ is the effective emissivity and σ is the Stefan-Boltzmann constant) the temperatures were converted to an emitted power. For every x-y position represented by these arrays it was determined whether or not any metal was present between the first and second layers of KMPR and whether or not the position was within the radius of the PCR chamber (where the third layer of KMPR would not be present). Once these conditions were established, the

total power reaching the IR camera was calculated for every x-y position by determining an effective emissivity for each layer at that point by assuming the Al was 100% reflective and that for every layer of KMPR the IR radiation passed through it lost 10% of its power (resulting in the effective power being radiated by each layer being attenuated by a factor between 0 and 1). The sum of the effective power emitted by each layer was then converted back to a temperature by reversing the equation. The result was plotted in order to produce a representation what an IR camera would see if the temperature profile of the devices was equal to the simulated temperature profile. The result can be seen in Figure 5.7 and the result confirms the observed trends of the areas above the heater tracks appearing hotter than the other areas of the device and the area within the radius of the PCR chamber appearing cooler than the area around it.

5.2 Chapter Summary

This chapter has discussed the work that has been performed to validate the operation of KMPR-aluminium devices that were fabricated in the previous chapter. Of particular interest has been the physical stability of the metal films when the devices are heated, along with the long-term stability and electromigration resistance of the aluminium heaters during high-temperature operation with tests indicating the stability of the heaters for over 41 hours of operation at current densities of 14.2 mA/μm^2. The TCR of the devices was also measured using a hotplate to control the temperature of the heaters. Multiple devices from different fabrication batches have been tested and confirmed to have a consistent TCR of 0.002 K^{-1}, which can potentially simplify the calibration of devices in the future by avoiding the need to test every device. An

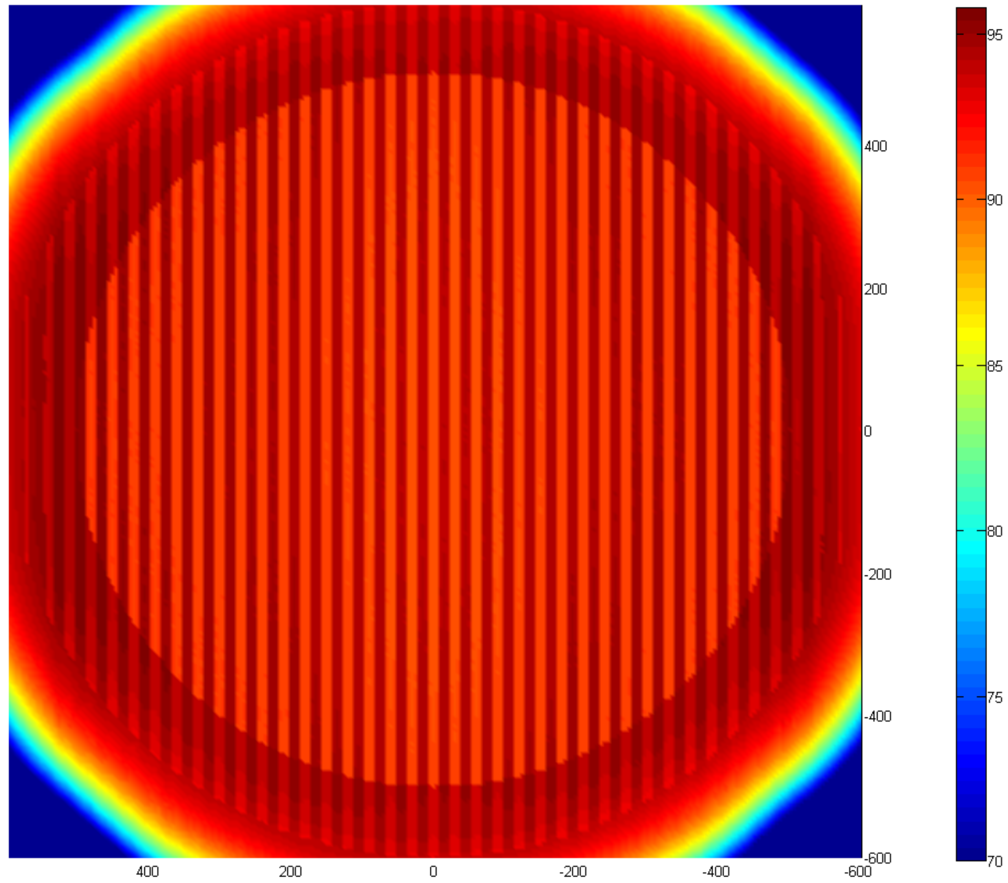

Figure 5.7: “Calibrated” COMSOL simulation data to compensate for imaging artifacts related to the presence of the Al film within the KMPR structure. The anomalous trends observed by the IR camera (tracks appearing significantly hotter than the surrounding area, and the areas outside the chamber radius appearing hotter than the area inside the chamber) are reproduced using this calibration.

IR camera was also used in order to study the actual temperature uniformity of the heaters during operation.

The greatest concern for these devices is their stability when operating in a moist environment. When heated in the presence of water the heater structures wrinkle and suffer a significant increase in resistance. Any future work on these devices will need to begin with an in-depth analysis of this failure mode in order to avoid this problem during operation of the chips. If this behaviour cannot be prevented through future development it will be necessary to consider alternative methods of heating and/or temperature sensing during PCR.

Chapter 6

Conclusion

KMPR is a negative photopolymer material developed by Microchem Corp. in 2004 as an alternative to their popular SU-8 resist. Studying the literature related to KMPR it is clear that there is a significant lack of information available on its physical properties. In order to remedy this a number of different properties of KMPR were studied including its T_g, modulus, thermal stability and the effect of processing conditions on these properties. Based on these studies it was determined that in order to produce reliable physical properties in the material the films should be exposed to at least 2 J/cm^2 of UV light and baked for at least 60 minutes at temperatures of at least 150^oC. Young's modulus for well-baked KMPR was measured to be between 2.0 and 2.7GPa, depending on the baking conditions. The polymer chains were also shown to begin crosslinking in the absence of UV light when baked at temperatures greater than 150^oC, requiring any high temperature bakes to be performed after development is completed. Using TGA KMPR was also shown to degrade significantly when exposed to temperatures above 200^oC.

With a better understanding of the physical properties of KMPR, the next step was to develop KMPR LOC devices. After developing a fabrication pro-

cess capable of producing 20 μm thick KMPR films with better than 1 μm surface uniformity a reliable thermo-compressive bonding was developed to be produce multi-layer KMPR microfluidics. Metal structures were also fabricated within the polymer structures taking advantage of the superior metal film adhesion to KMPR films. Any metal structures in previous LOC devices have had to be fabricated directly onto the silicon or glass substrates resulting in a high loss of power due to the substrate's high thermal conductivity compared to the polymer films. By fabricating heater structures within the polymer film the power required to heat the fluidics to PCR temperatures (up to 95°C) is greatly reduced. Utilizing these developments devices were fabricated containing an embedded Al film for the purpose of performing rapid temperature cycling. Design elements were included for the purpose of future development to achieve PCR and CE on chip.

Once the devices were fabricated they could be tested to ensure they operated as expected. Due to lithography resolution issues the exposure dose of the fluidic layers was reduced in order to avoid non-specific exposure of KMPR due to scattering effects. This lower dose does result in a lower and unpredictable T_g value for those layers, but this has not proven to be a concern as of yet as all tested devices have met specifications for channel filling (described in Chapter 4). Bonding of the devices have also met specifications as indicated by a lack of delamination in the bonded films during tape tests. The heaters have been confirmed to have survived the bonding process with the heater resistances falling within the range of acceptable resistance specifications, although tighter control over the film thicknesses would be beneficial to improve the accuracy of the device resistances. The TCR of the heater films was measured using a hotplate and has been confirmed to be repeatable between devices, allowing for the determination of the average temperature of

the heater structures during operation. In order to study the actual thermal uniformity of the heater structures a high resolution IR camera was used with the results showing a reasonable agreement with the simulated heaters after accounting for imaging artifacts. Dicing of the chips is discussed primarily in Appendix F, but also meets the required specifications for accuracy of the diced dimensions.

The only remaining outstanding issue with these devices is their stability when operating at PCR temperatures in the presence of water. The aluminium films consistently wrinkle after several minutes of operation in a moist environment at 95°C, resulting in an unstable resistance value for the heaters. This behaviour is unexpected as previous work in our research group [68] has successfully fabricated and tested aluminium heaters under these conditions. There are a number of hypotheses that may explain this behaviour in our devices. The first possible cause of this failure is due to a reduction of the physical stability in the KMPR films when heated in the presence of moisture causing any residual stress in the aluminium film to deform and wrinkle the structure. This issue may also be related to changes in the KMPR mechanical properties between the previous work and the current process such as the difference in film thickness, fabrication conditions or age of the KMPR. These differences have resulted in a difference in the mechanical properties of the films and further study of these differences may yield further information as to the cause of these failures. It may be discovered that the lower T_g resulting from our previous fabrication process may actually be beneficial for the operation of the heaters by allowing the polymer film to better absorb any residual stresses in the metal film, although care would have to be taken to ensure the devices are still able to withstand the bonding process as our previous tests did not include a thermo-compressive bonding step in the fabrication of the

heaters.

Residual stresses in the Al films either from deposition or from the lift-off process may also be contributing to the problem and studies into reducing the film stress could provide a solution as well. If necessary other alternatives such as using a more stable floor material or the inclusion of a moisture blocking layer may be studied for possible solutions. Regardless of the source of this issue, until devices can be produced capable of maintaining a sufficiently stable resistance in order to enable temperature measurements accurate to within 1°C the devices cannot be used for any applications above 50°C where moisture is present in the system.

This thesis set out to develop a KMPR-based LOC system for performing genetic analysis by utilizing an integrated thin film heater to perform genetic amplification. Although most of the outlined specifications for these devices have been met, lingering problems with the operation of the heaters in a moist environment at PCR temperatures must be resolved before these devices will be able to operate as specified.

6.1 Future Direction

This section will briefly discuss some of future challenges and opportunities that will arise during any further development of these KMPR LOC devices. The immediate challenges presented for the operation of these devices is discussed, followed by discussion of some alternatives to the current fabrication process that will allow for some new possibilities for devices.

6.1.1 Issues Related to Wet Operation of the Devices

The most immediate issue facing these devices is the operation of the heaters while a sample is loaded into the chip. As discussed in Chapter 5, tests have shown that with the current structures the heater metal heavily wrinkles when heated in the presence of moisture. This is a serious issue that must be solved before these devices will be able to serve any useful function. There are several possibilities that can be explored in order to address this issue. The first step should be study the differences between these devices and similar devices produced in the past by our research group [68] in order to identify the cause of the wrinkling. This may involve further studies into the baking conditions and the thicknesses of the KMPR films, along with determining if the lift-off process is a possible source of film stress and damage. Quantitative studies into the film stresses of the metal films sputtered onto KMPR may also lead to further information useful in solving the problem.

Solutions such as replacing the floor layer of KMPR with a more stable material (such as SU-8) in order to prevent the aluminum from wrinkling or introducing a moisture barrier between the heater and the PCR chamber may also serve to solve this issue. If wrinkling continues to be a problem it may be necessary to avoid fabricating the heaters on a polymer layer altogether at the cost of power requirements for heating the PCR chamber.

6.1.2 Airgap Structures

One possibility to reduce the power requirements for heating the PCR chamber is to introduce an airgap beneath the chamber in order to reduce the heat loss to the substrate. Producing a stable airgap in KMPR will prove to be quite a challenge. The biggest concern in producing the gap will be minimizing any deflection in the floor of the chamber which would no longer be be

supported from below. Simulations discussed in Appendix B show that posts will certainly be required to reduce the deflection to a manageable level, but the successful fabrication of posts will certainly prove to be a challenge and their effect on the uniformity of the heating will have to be addressed as well.

Besides the thermal effects of the airgap the fabrication of the heater devices is also complicated by the presence of the airgap. There are two additional considerations to account for when fabricating the heaters: how can the metal be deposited onto the KMPR and how well the metal will survive any deflection of the KMPR membrane. Currently the metal is fabricated on top of an unpatterned KMPR film serving as the floor of the device. This same KMPR floor would be the layer in which the airgap is fabricated preventing the fabrication of the heater on top of it. Other possible options for fabricating the metal are to have it fabricated on the bottom of the fluidic floor layer (which would then be bonded on top of the airgap layer) or to split the fluidic floor layer into two layers and fabricate the heater in the middle. In either case the ability of the film to survive bonding, and to survive any deflection of the KMPR, is not guaranteed.

6.1.3 Alternate Fabrication Techniques

It would be extremely beneficial to be able to fabricate valve structures within the KMPR in order to control fluid flow through the chips. Appendix D discusses the concept behind using lithographic exposure to locally roughen the surface of KMPR prior to bonding and with further research it may be possible to use this technique to selectively inhibit bonding in certain areas of the devices, allowing for the fabrication of valve structures. Other possibilities for valves may be to include the use of an RIE step to create a gap between the films during bonding or using temporary release layers to prevent bonding

in the valve areas.

Another possible fabrication technique that could be used is a hot embossing method in order to pattern the KMPR structures. Hot embossing is a common method when producing structures in polymers [6, 54] and it should be possible to use this technique to produce a rapid, reliable fabrication process for KMPR. Embossing can allow for the production of complex structures, such as sloped sidewalls and three-dimensional structures, while allowing for a simplified fabrication process. This kind of technique could better lend itself to high-volume manufacturing than the current fabrication techniques.

Given recent difficulties with the lift-off patterning of the aluminium heaters it would be beneficial to the stability of the fabrication process to develop alternative methods for patterning the material, whether that be through a more reliable lift-off resist or by utilizing a wet (or dry) etch process that is compatible with the rest of the fabrication process.

Bibliography

[1] P. P. R. Patnaik, "Multi-unit Integration in Microfluidic Processes: Current Status and Future Horizons," *International Journal Bio Automation*, vol. 15, no. 2, pp. 77–84, 2011.

[2] M. L. Sin, J. Gao, J. C. Liao, and P. K. Wong, "System Integration - A Major Step toward Lab on a Chip.," *Journal of biological engineering*, vol. 5, p. 6, May 2011.

[3] C. D. Chin, V. Linder, and S. K. Sia, "Commercialization of microfluidic point-of-care diagnostic devices," *Lab on a Chip*, vol. 12, no. 207890, pp. 2118–2134, 2012.

[4] D. Mark, S. Haeberle, G. Roth, F. von Stetten, and R. Zengerle, "Microfluidic lab-on-a-chip platforms: requirements, characteristics and applications.," *Chemical Society reviews*, vol. 39, pp. 1153–82, Mar. 2010.

[5] P. Yager, T. Edwards, E. Fu, K. Helton, K. Nelson, M. R. Tam, and B. H. Weigl, "Microfluidic diagnostic technologies for global public health.," *Nature*, vol. 442, pp. 412–8, July 2006.

[6] G. S. Fiorini and D. T. Chiu, "Disposable microfluidic devices: fabrication, function, and application.," *BioTechniques*, vol. 38, pp. 429–46, Mar. 2005.

[7] C. Zhang, J. Xu, W. Ma, and W. Zheng, "PCR microfluidic devices for DNA amplification.," *Biotechnology advances*, vol. 24, no. 3, pp. 243–84, 2006.

[8] J. K. Luo, Y. Q. Fu, Y. Li, X. Y. Du, A. J. Flewitt, A. J. Walton, and W. I. Milne, "Moving-part-free microfluidic systems for lab-on-a-chip," *Journal of Micromechanics and Microengineering*, vol. 19, p. 054001, May 2009.

[9] R. N. Zare and S. Kim, "Microfluidic platforms for single-cell analysis.," *Annual review of biomedical engineering*, vol. 12, pp. 187–201, Aug. 2010.

[10] A. Webster, J. Greenman, and S. J. Haswell, "Development of microfluidic devices for biomedical and clinical application," *Journal of Chemical Technology & Biotechnology*, vol. 86, pp. 10–17, Jan. 2011.

[11] V. J. Sieben, C. S. Debes-Marun, L. M. Pilarski, and C. J. Backhouse, "An integrated microfluidic chip for chromosome enumeration using fluorescence in situ hybridization.," *Lab on a chip*, vol. 8, pp. 2151–6, Dec. 2008.

[12] A. Folch, *Introduction to BioMEMS*. Boca Raton, Fl: CRC Press, Taylor and Francis Group, 1 ed., 2013.

[13] G. V. Kaigala, M. Behnam, A. C. E. Bidulock, C. Bargen, R. W. Johnstone, D. G. Elliott, and C. J. Backhouse, "A scalable and modular lab-on-a-chip genetic analysis instrument.," *The Analyst*, vol. 135, pp. 1606–17, July 2010.

[14] P. Liu and R. A. Mathies, "Integrated microfluidic systems for high-performance genetic analysis.," *Trends in biotechnology*, vol. 27, pp. 572–81, Oct. 2009.

[15] D. Brennan, J. Justice, B. Corbett, T. McCarthy, and P. Galvin, “Emerging optofluidic technologies for point-of-care genetic analysis systems: a review.,” *Analytical and bioanalytical chemistry*, vol. 395, pp. 621–36, Oct. 2009.

[16] G. V. Kaigala, V. N. Hoang, A. Stickel, J. Lauzon, D. Manage, L. M. Pilarski, and C. J. Backhouse, “An inexpensive and portable microchip-based platform for integrated RT-PCR and capillary electrophoresis.,” *The Analyst*, vol. 133, pp. 331–8, Mar. 2008.

[17] T. B. Christensen, D. D. Bang, and A. Wolff, “Multiplex polymerase chain reaction (PCR) on a SU-8 chip,” *Microelectronic Engineering*, vol. 85, pp. 1278–1281, May 2008.

[18] J. Ferrance, Q. Wu, B. Giordano, C. Hernandez, Y. Kwok, K. Snow, S. Thibodeau, and J. P. Landers, “Developments toward a complete micro-total analysis system for Duchenne muscular dystrophy diagnosis,” *Analytica Chimica Acta*, vol. 500, pp. 223–236, Dec. 2003.

[19] R. G. Blazej, P. Kumaresan, and R. A. Mathies, “Microfabricated bioprocessor for integrated nanoliter-scale Sanger DNA sequencing.,” *Proceedings of the National Academy of Sciences of the United States of America*, vol. 103, pp. 7240–5, May 2006.

[20] S. R. Quake, “From Micro- to Nanofabrication with Soft Materials,” *Science*, vol. 290, pp. 1536–1540, Nov. 2000.

[21] J. M. Ruano-López, M. Agirregabiria, G. Olabarria, D. Verdoy, D. D. Bang, M. Bu, A. Wolff, A. Voigt, J. A. Dziuban, R. Walczak, and J. Berganzo, “The SmartBioPhone, a point of care vision under develop-

ment through two European projects: OPTOLABCARD and LABON-FOIL.," *Lab on a Chip*, vol. 9, pp. 1495–9, June 2009.

[22] C. Richard, A. Renaudin, V. Aimez, and P. G. Charette, "An integrated hybrid interference and absorption filter for fluorescence detection in lab-on-a-chip devices.," *Lab on a Chip*, vol. 9, pp. 1371–6, May 2009.

[23] Microchem Corporation, "KMPR 1000 Datasheet," *http://www.microchem.com/pdf/KMPRDataSheetver4_2a.pdf*, no. 617, pp. 2–5, 2011.

[24] P. Liu, X. Li, S. A. Greenspoon, J. R. Scherer, and R. A. Mathies, "Integrated DNA purification, PCR, sample cleanup, and capillary electrophoresis microchip for forensic human identification.," *Lab on a Chip*, vol. 11, pp. 1041–8, Feb. 2011.

[25] M. A. Burns, C. H. Mastrangelo, T. S. Sammarco, F. P. Man, J. R. Webster, B. N. Johnsons, B. Foerster, D. Jones, Y. Fields, A. R. Kaiser, and D. T. Burke, "Microfabricated structures for integrated DNA analysis.," *Proceedings of the National Academy of Sciences of the United States of America*, vol. 93, pp. 5556–61, May 1996.

[26] T. Fukuba, T. Yamamoto, T. Naganuma, and T. Fujii, "Microfabricated flow-through device for DNA amplification-towards in situ gene analysis," *Chemical Engineering Journal*, vol. 101, pp. 151–156, Aug. 2004.

[27] E. T. Lagally, C. A. Emrich, and R. A. Mathies, "Fully integrated PCR-capillary electrophoresis microsystem for DNA analysis.," *Lab on a Chip*, vol. 1, pp. 102–7, Dec. 2001.

[28] H. Van Lintel, F. Van de Pol, and S. Bouwstra, "A Piezoelectric Micropump Based On Micromachining Of Silicon," *Sensors and Actuators*, vol. 15, pp. 153–167, 1988.

[29] A. Manz, D. J. Harrison, E. M. J. Verpoorte, J. C. Fettinger, A. Paulus, H. Li, and H. M. Widmer, "Planar chips technology for miniaturization and integration of separation techniques into monitoring systems Capillary electrophoresis on a chip," *Journal of Chromatography*, vol. 593, pp. 253–258, 1992.

[30] R. Zengerle, J. Ulrich, S. Kluge, M. Richter, and A. Richter, "A Bidirectional Silicon Micropump," *Sensors and Actuators A: Physical*, vol. 50, pp. 81–86, 1995.

[31] A. Manz, N. Graber, and H. Widmer, "Miniaturized total chemical analysis systems: A novel concept for chemical sensing," *Sensors and Actuators B: Chemical*, vol. 1, pp. 244–248, Jan. 1990.

[32] A. Van Den Berg and T. S. J. Lammerink, "Micro Total Analysis Systems: Microfluidic Aspects, Integration Concept and Applications," *Topics in Current Chemistry*, vol. 194, pp. 22–48, 1998.

[33] E. T. Lagally, J. R. Scherer, R. G. Blazej, N. M. Toriello, B. A. Diep, M. Ramchandani, G. F. Sensabaugh, L. W. Riley, and R. A. Mathies, "Integrated portable genetic analysis microsystem for pathogen/infectious disease detection.," *Analytical chemistry*, vol. 76, pp. 3162–70, June 2004.

[34] M. Behnam, A. Olanrewaju, J. Martinez-Quijada, F. Hejazi, G. Banting, A. Bidulock, S. Groendahl, R. Johnstone, D. Glerum, and C. Backhouse in *14th International Conference on Miniaturized Systems for Chemistry and Life Sciences 2010 (MicroTAS 2010).*

[35] A. Wu, L. Wang, E. Jensen, R. Mathies, and B. Boser, "Modular integration of electronics and microfluidic systems using flexible printed circuit boards.," *Lab on a Chip*, vol. 10, pp. 519–21, Feb. 2010.

[36] K. R. King, C. C. J. Wang, M. R. Kaazempur-Mofrad, J. P. Vacanti, and J. T. Borenstein, "Biodegradable Microfluidics," *Advanced Materials*, vol. 16, pp. 2007–2012, Nov. 2004.

[37] M. D. Tang, A. P. Golden, and J. Tien, "Fabrication of Collagen Gels That Contain Patterned, Micrometer-Scale Cavities," *Advanced Materials*, vol. 16, pp. 1345–1348, Aug. 2004.

[38] C.-S. Chen, D. N. Breslauer, J. I. Luna, A. Grimes, W.-C. Chin, L. P. Lee, and M. Khine, "Shrinky-Dink microfluidics: 3D polystyrene chips.," *Lab on a chip*, vol. 8, pp. 622–4, Apr. 2008.

[39] V. Singh, Y. Desta, P. Datta, J. Guy, M. Clarke, D. L. Feedback, J. Weimert, and J. Goettert, "A hybrid approach for fabrication of polymeric BIOMEMS devices," *Microsystem Technologies*, vol. 13, pp. 369–377, June 2006.

[40] J. A. Lounsbury, A. Karlsson, D. C. Miranian, S. M. Cronk, D. A. Nelson, J. Li, D. M. Haverstick, P. Kinnon, D. J. Saul, and J. P. Landers, "From Sample to PCR Product in Under 45 Minutes: A Polymeric Integrated Microdevice for Clinical and Forensic DNA Analysis," *Lab on a Chip*, vol. 13, no. 7, pp. 1384–93, 2013.

[41] S.-R. Joung, C. J. Kang, and Y.-S. Kim, "Series DNA Amplification Using the Continuous-Flow Polymerase Chain Reaction Chip," *Japanese Journal of Applied Physics*, vol. 47, pp. 1342–1345, Feb. 2008.

[42] S. Liu, Y. Gu, R. B. Le Roux, S. M. Matthews, D. Bratton, K. Yunus, A. C. Fisher, and W. T. S. Huck, "The electrochemical detection of droplets in microfluidic devices.," *Lab on a chip*, vol. 8, pp. 1937–42, Nov. 2008.

[43] M. Zhang, J. Wu, L. Wang, K. Xiao, and W. Wen, "A simple method for fabricating multi-layer PDMS structures for 3D microfluidic chips.," *Lab on a chip*, vol. 10, pp. 1199–203, May 2010.

[44] G. Shao, Z. Cai, J. Wang, W. Wang, and Y. Lin, "A pneumatic actuated microfluidic beads-trapping device," *Electrochemistry*, vol. 7929, pp. 792908–792908–5, 2011.

[45] Y. Sheng and M. Bowser, "Size selective DNA transport through a nanoporous membrane in a PDMS microfluidic device," *Analyst*, 2012.

[46] F. J. Blanco, M. Agirregabiria, J. Garcia, J. Berganzo, M. Tijero, M. T. Arroyo, J. M. Ruano, I. Aramburu, and K. Mayora, "Novel three-dimensional embedded SU-8 microchannels fabricated using a low temperature full wafer adhesive bonding," *Journal of Micromechanics and Microengineering*, vol. 14, pp. 1047–1056, July 2004.

[47] L. Gutierrez-Rivera, J. Martinez-Quijada, R. Johnstone, D. Elliott, C. Backhouse, and D. Sameoto, "Multilayer Bonding using a Conformal Adsorbate Film (CAF) for the Fabrication of 3D Monolithic Microfluidic Devices in Photopolymer," *Journal of Micromechanics and Microengineering*, vol. 22, no. 8, 2012.

[48] M. Reynolds, A. Elias, D. G Elliott, C. Backhouse, and D. Sameoto, "Variation of thermal and mechanical properties of KMPR due to pro-

cessing parameters," *Journal of Micromechanics and Microengineering*, vol. 22, p. 125023, Dec. 2012.

[49] H. Miller, D. Johnson, and S. Mori, "KMPR Photoresist Process Optimization Using Factorial Experimental Design," *Journal of Photopolymer Science and Technology*, vol. 17, no. 5, pp. 677–684, 2004.

[50] L. Convert, V. Aimez, P. Charette, and R. Lecomte, "Rapid prototyping of integrated microfluidic devices for combined radiation detection and plasma separation," in *Microsystems and Nanoelectronics Research Conference, 2008. MNRC 2008. 1st*, pp. 105–108, IEEE, 2008.

[51] T. Ray, H. Zhu, I. Elango, and D. Meldrum, "Characterization of KMPR 1025 as a masking layer for deep reactive ion etching of fused silica," in *Micro Electro Mechanical Systems (MEMS), 2011 IEEE 24th International Conference on*, pp. 213–216, IEEE, 2011.

[52] T. Ray, H. Zhu, and D. R. Meldrum, "Deep reactive ion etching of fused silica using a single-coated soft mask layer for bio-analytical applications," *Journal of Micromechanics and Microengineering*, vol. 20, p. 097002, Sept. 2010.

[53] D. Gamzina, L. R. Barnett, F. Yaghmaie, A. Baig, and N. C. Luhmann, "UV Lithography and Molding Fabrication of Ultrathick Micrometallic Structures Using a KMPR Photoresist," *Journal of Microelectromechanical Systems*, vol. 19, pp. 683–689, June 2010.

[54] S. R. Nugen, P. J. Asiello, and A. J. Baeumner, "Design and fabrication of a microfluidic device for near-single cell mRNA isolation using a copper hot embossing master," *Microsystem Technologies*, vol. 15, pp. 477–483, Aug. 2008.

[55] C. H. Lee and K. Jiang, "Fabrication of thick electroforming micro mould using a KMPR negative tone photoresist," *Journal of Micromechanics and Microengineering*, vol. 18, p. 055032, May 2008.

[56] A. Baig, D. Gamzina, M. Johnson, C. W. Domier, A. Spear, L. R. Barnett, N. C. Luhmann, and Y.-m. Shin, "P2-25 : Experimental Characterization of LIGA Fabricated 0 . 22 THz TWT Circuits," in *Vacuum Electronics Conference*, pp. 275–276, 2011.

[57] M. Ynsa, P. Shao, S. Kulkarni, N. Liu, and J. van Kan, "Exposure parameters in proton beam writing for KMPR and EPO Core negative tone photoresists," *Nuclear Instruments and Methods in Physics Research Section B: Beam Interactions with Materials and Atoms*, vol. 269, pp. 2409–2412, Oct. 2011.

[58] C. Salm, V. M. Blanco Carballo, J. Melai, and J. Schmitz, "Reliability aspects of a radiation detector fabricated by post-processing a standard CMOS chip," *Microelectronics Reliability*, vol. 48, pp. 1139–1143, Aug. 2008.

[59] K.-S. Ou, H.-Y. Yan, and K.-S. Chen, "Mechanical Characterization of KMPR by Nano-Indentation for MEMS Applications," *Strain*, vol. 44, pp. 267–271, June 2008.

[60] R. Feng and R. J. Farris, "Influence of processing conditions on the thermal and mechanical properties of SU8 negative photoresist coatings," *Journal of Micromechanics and Microengineering*, vol. 13, pp. 80–88, Jan. 2003.

[61] X. Wei, C.-H. Lee, Z. Jiang, and K. Jiang, "Thick photoresists for electroforming metallic microcomponents," *Proceedings of the Institution of*

Mechanical Engineers, Part C: Journal of Mechanical Engineering Science, vol. 222, pp. 37–42, Jan. 2008.

[62] V. Blanco Carballo, J. Melai, C. Salm, and J. Schmitz, "Moisture resistance of SU-8 and KMPR as structural material," *Microelectronic Engineering*, vol. 86, pp. 765–768, Apr. 2009.

[63] J. Park, J. Fattaccioli, H. Fujita, and B. Kim, "Fabrication of aluminum/alumina patterns using localized anodization of aluminum," *International Journal of Precision Engineering and Manufacturing*, vol. 13, pp. 765–770, May 2012.

[64] K. Wouters and R. Puers, "Determining the Young's modulus and creep effects in three different photo definable epoxies for MEMS applications," *Sensors and Actuators A: Physical*, vol. 156, pp. 196–200, Nov. 2009.

[65] B. Schoeberle, M. Wendlandt, and C. Hierold, "Long-term creep behavior of SU-8 membranes: Application of the timestress superposition principle to determine the master creep compliance curve," *Sensors and Actuators A: Physical*, vol. 142, pp. 242–249, Mar. 2008.

[66] A. Mata, A. J. Fleischman, and S. Roy, "Fabrication of multi-layer SU-8 microstructures," *Journal of Micromechanics and Microengineering*, vol. 16, pp. 276–284, Feb. 2006.

[67] S. R. Oh, "Thick single-layer positive photoresist mold and poly(dimethylsiloxane) (PDMS) dry etching for the fabrication of a glassPDMSglass microfluidic device," *Journal of Micromechanics and Microengineering*, vol. 18, p. 115025, Nov. 2008.

[68] J. Martinez-Quijada, S. Caverhill-Godkewitsch, M. Reynolds, L. Gutierrez-Rivera, R. Johnstone, D. Elliott, D. Sameoto, and

C. Backhouse, "Fabrication and Characterization of Aluminum Thin Film Heaters and Temperature Sensors on a Photopolymer for Lab-on-Chip Systems," *Sensors and Actuators A: Physical*, vol. 193, pp. 170–181, Jan. 2013.

[69] M. Chinmulgund, R. Inturi, and J. Barnard, "Effect of Ar gas pressure on growth, structure, and mechanical properties of sputtered Ti, Al, TiAl, and Ti3Al films," *Thin Solid Films*, vol. 270, no. 1-2, pp. 260–263, 1995.

[70] J. R. Black, "Electromigration-A Brief Survey and Some Recent Results," *IEEE Transactions on Electron Devices*, vol. 16, no. 4, pp. 338–47, 1969.

[71] M.-B. Lin, *Introduction to VLSI Systems: A Logic, Circuit, and System Perspective*. CRC Press.

[72] J. W. C. Devries, "Temperature and thickness dependence of the resistivity of thin polycrystalline aluminium, cobalt, nickel, palladium, silver and gold films," *Thin Solid Films*, vol. 167, pp. 25–32, 1988.

[73] J. Kim, D. Byun, M. G. Mauk, and H. H. Bau, "A disposable, self-contained PCR chip.," *Lab on a chip*, vol. 9, pp. 606–12, Feb. 2009.

[74] K. Wouters and R. Puers, "Diffusing and swelling in su-8: insight in material properties and processing," *Journal of Micromechanics and Microengineering*, vol. 20, no. 9, p. 095013, 2010.

[75] S. Schmid, S. Kuhne, and C. Hierold, "Influence of air humidity on polymeric microresonators," *Journal of Micromechanics and Microengineering*, vol. 19, no. 6, p. 065018, 2009.

[76] J. Hossenlopp, L. Jiang, R. Cernosek, and F. Josse, "Characterization of epoxy resin (su-8) film using thickness-shear mode (tsm) resonator under

various conditions," *Journal of Polymer Science*, vol. 42, no. 12, pp. 2373–2384.

[77] M. Spivack and G. Ferrante, "Determination of the water vapor permeability and continuity of ultrathin parylene membranes," *Journal of the Electrochemical Society*, vol. 116, no. 11, pp. 1592–1594.

[78] R. G. Denning, C. F. Blanford, H. Urban, H. Bharaj, D. N. Sharp, and A. J. Turberfield, "The Control of Shrinkage and Thermal Instability in SU-8 Photoresists for Holographic Lithography," *Advanced Functional Materials*, vol. 21, pp. 1593–1601, May 2011.

[79] "Disco dicing saw specifications." `http://www.disco.co.jp/eg/products/dicer/300.html`. Accessed: 2013.

Appendix A

Fabrication Protocols

A.1 KMPR 1 Layer (Sub-Floor)

A.1.1 Substrate Preparation

1. Scribe the back of the substrates with a unique identifier (Use 4, 4” Silicon Test Grade wafers per run)

2. Piranha clean the substrates for 15 min in hot, fresh piranha (3:1 H_2SO_4:H_2O_2).

3. Dump Rinse the substrates for 5 cycles.

4. Spin-rinse and dry the substrates.

5. Bake the substrates for 15 minutes at $> 100°C$ to dehydrate them (either use an oven or a hotplate, I haven’t noticed any difference between the two).

A.1.2 Spin and Soft-Bake

1. Turn on fumehood hotplates to 100°C (set to ∼155°C). The hotplates take 15-20 minutes to reach a stable temperature.

2. Center the first substrate on the spin chuck.

3. Pour KMPR (KMPR 1025, portioned into small amber bottles by the Nanofab) onto the center of the substrate to form a puddle 6∼7cm in diameter. Pour carefully to avoid bubble formation.

4. Spread step - 2000 RPM, 1 second ramp, spin for 2-3 seconds until substrate is covered (manually stop the spin). It's usually a good idea to hold a lid over the spinner to prevent splashing of KMPR.

5. Wait 1 minute for the KMPR to settle and smooth out before proceeding to the spin step. Program the spinner for the next step while waiting.

6. Spin Step - 4000 RPM, 10 second ramp, 60 second spin

7. Wait 2 minutes for the KMPR to settle before baking.

8. Place substrate on a hotplate at 100°C for 10 minutes. Film thickness should be approximately 20 μm.

9. Allow the substrate to cool for 30-60 seconds on a cleanroom wipe before placing back in a cleanroom box.

10. Repeat this process for each substrate. Note that after pouring the KMPR onto the substrates it's common to have bubbles form in the bottle itself. These bubbles may pour onto other substrates if not first removed. Using a plastic pipette (same ones used in the Nanofab for PDMS mixing) remove the bubbles from the bottle in between each spin.

A.1.3 Blanket Exposure and PEB

1. Determine exposure length (dose of 1,333 mJ/cm^2, only use 365nm intensity) for the floor layer based on the calibrated intensity of the mask

aligner you are using.

2. No mask is used for this exposure, just place the substrate on the chuck and begin exposure.

3. Post exposure bake (PEB) the substrates for 180°C for 60 minutes on a hotplate. The first few batches of devices were fabricated using a PEB of 120°C but experienced wrinkling of the aluminium during the bonding process (different wrinkling than due to wet operation of the devices, this wrinkling could also be smoothed out by baking the devices at 100°C on a hotplate after bonding). Baking at 180°C prevents this wrinkling.

4. Allow substrate to cool on a wipe for 30 seconds

A.2 Cr protection layer

A.2.1 Deposition of Cr Layer with Bob

1. Following the Nanofab SOP (see the end of this appendix), vent and open the chamber, ensure Cr target loaded in gun #1 and load the substrates.

2. Determine the deposition time in order to aim for a 100 nm film (using the deposition rates provided by the Nanofab, typically between 12 and 13 nm/min). The exact film thickness is not critical at this step but a thick enough layer of Cr should be used to prevent cracking of the KMPR film during the Al lift-off process.

3. Pump out the system until a base pressure of 1-2 μTorr is reached (should take about an hour).

4. Use an Ar pressure during deposition of 8.5 mTorr to avoid cracking due to film stress. Depending on target lifetime (and probably other

environmental factors as well), this pressure may need to vary slightly (+/-0.1 mTorr steps) over time in order to avoid cracking of the film. Deposition power should be 300 W and the deposition voltage should be between 350 and 370 V.

A.2.2 Patterning Cr Layer

1. Spin-coat a layer of HPR 504 photoresist onto the Cr-coated substrates (spin speed of 4000RPM, soft bake at 110 degrees for 90 seconds on a vacuum hotplate, allow 15 minutes for the film to rehydrate before exposure by placing the substrates in a closed wafer box).

2. The exposure time will need to be calculated every time fabrication occurs in order to account for drift in the lamp intensity over time but will usually be around 2-3 seconds on MA #1. The exposure time can be determined by preparing the photoresist as above and exposing for an initial length of time and checking the resolution of the film after development. If resolution needs to be improved the resist can be stripped with Acetone and IPA and another film can be prepared at a new exposure dose.

3. Use the heater mask for these exposures and ensure good contact is obtained to ensure good resolution.

4. Develop the films for 15-20 seconds in 354 developer. Take care not to over-develop (remove as soon as visual endpoint is reached).

5. Inspect the pattern using a microscope and check features to make sure they are well defined, especially the tighter features around the heater grids. Adjust the exposure time as needed to properly define the pattern (if features are not fully defined either a higher exposure dose or

a longer develop time is needed, if features are washed out a lower exposure dose/develop time is needed). The good thing about 504 is that acetone can be used to remove the resist and try again with little wasted time. Trial and error is pretty much required here as the lamp intensity can vary by up to 10% in between the monthly calibrations done by the nanoFab.

A.2.3 Etching Cr Layer

1. Place the substrates individually in Cr etch (available from the Nanofab, commercial Cr etch from Fujifilm Electronic Materials USA) and agitate the etchant while observing the metal on the substrate. The reported etch rate for Cr etch is 3.7 nm/second, so etching should only require about 20 seconds to complete (note, if over-etching is proving problematic it is possible to dilute the Cr etch with water to slow the etch rate).

2. The difference in color between Si and Cr is slight, but noticeable; once the visual endpoint has been reached remove the substrate, rinse with DI water for at least 60 seconds (wafer held by a clean pair of wafer tweezers and DI water sprayed across the surface of the wafer) and dry with nitrogen.

3. Inspect the substrate under the microscope to ensure etching is completed. If exposed Cr remains place the substrate back into the etchant for 5 seconds at a time until completed.

4. As a usual caveat when it comes to etching: under-etching is easy to fix, over-etching is permanent.

A.3 Heater Fabrication

A.3.1 Al Deposition - Bob Sputtering System

1. Prior to depositing the Al film the deposition rate of Al should be calibrated. Calibration should be performed on a bare Si wafer with a number of Xs drawn on the substrate using an Ultra-fine tip black Sharpie ("Sharpie lithography"). Follow standard procedures for pumping down the vacuum chamber for deposition, but only wait 15-20 minutes for the base pressure to reach 7-8 10^{-6} Torr instead of the hour to reach 1-2 10^{-6} Torr. The small amount of excess oxygen trapped in the film will have a negligible effect on the deposition rate but will save time for deposition (this is confirmed by comparing the film thickness of Al deposited at both base pressures). This calibration should be done every time a deposition is performed, unless no one else has used the sputtering target since the last time a deposition was performed.

2. Deposit the Al for 10 minutes with an Ar pressure of 7 mTorr and a power of 300 W.

3. After deposition remove the calibration substrate from the chamber. Apply IPA to the substrate and use a cleanroom wipe to gently wipe the surface in order to remove the Al deposited onto the sharpie marks. Use an Alpha-step profilometer to measure the step height and divide by 10 minutes to determine the deposition rate.

4. Once calibration is completed, load the Cr-patterned substrates into the chamber and pump-down to a base pressure of 1-2x10^{-6} Torr range (around 1 hour).

5. Deposition should be done at an Ar pressure of 7 mTorr and a power

of 300 W (voltage of 390-409 V), with the deposition time determined using the calibrated deposition rate and a film thickness of 150nm as the target (typical deposition rates are between 12 and 14 nm per minute).

6. Remove the substrates when completed.

A.3.2 Lift-off in Acetone

1. Place the sonic bath into the drop-deck and fill the main bath with DI water up to the fill line. Place the smaller metal bath into the main bath to account for the displacement of water during filling.

2. Place the first substrate into a wafer carrier and place the Al-coated side face-down in the carrier.

3. Fill the metal bath with Acetone to a level sufficient to cover the substrate in the wafer holder.

4. Turn on the sonic bath.

5. Every 3-4 minutes the substrate should be pulled out and examined for completeness of the lift-off process. After about 10 minutes all of the visible Al should be removed (not including the heaters).

6. Once this visual end-point is reached, rinse (at least 60 seconds of DI water) and dry the substrate before inspecting the tighter features with a microscope to ensure lift-off is complete. If sections remain, simply place the substrate back into the acetone for 2 minutes and inspect once more.

7. Repeat the lift-off process for each substrate.

A.3.3 Cr Strip

1. Once lift-off is finished place the substrates one at a time into a Cr etch bath to strip the remaining Cr from the substrate.

2. Rinse the substrates with DI water and dry with nitrogen, inspect under a microscope to ensure all the Cr is stripped.

3. Once all the visible Cr is stripped, place the substrates into a bath of Au etch for 10 seconds to remove any oxide residue left behind from the Cr. Rinse (60 seconds DI water) and dry (nitrogen) once more.

A.4 KMPR 2 (Fluidic Floor)

A.4.1 Spin and Soft-Bake

1. Proceed as in section A.1.2, but with a spin speed of 4000 RPM.

A.4.2 Exposure and PEB

1. Expose as in section A.1.3, except that appropriate mask should be used to pattern the electrical access pads. Ensure proper alignment is achieved between the heater layer and the KMPR layer.

2. PEB for 5 minutes at 100°C. Do not develop until the next layer has been patterned as well.

A.5 KMPR 3 (Fluidic Layer)

A.5.1 Spin and Soft-Bake

1. Proceed as in section A.4.2.

A.5.2 Exposure and PEB

1. Proceed as in section A.2, with 2 exceptions: first use the proper mask for the channels and chambers, second you need to use a lower exposure dose to avoid losing resolution of the channels. Resolution for the floor layer wasn't all that important given the size of the pads on the mask, but for the small channels you will run into problems with such a high dose. Use an exposure dose of 600 mJ/cm^2 for this exposure.

2. PEB for 5 minutes at 100°C.

A.5.3 Development

1. Develop in SU-8 Developer for 5 minutes using light agitation. After 5 minutes the substrate should be removed, rinsed (IPA, followed by DI water for 60 seconds), dried and inspected for completion of development. If further development is required, return the substrate to the developer solution and continue development in 2 minute steps. Over-development is not really an issue here. Note that MF-319 actually etches the Al film and cannot be used to develop KMPR when any Al is present.

A.6 Carrier Substrate - PDMS

A.6.1 Substrate Preparation

1. Using 4" square borofloat glass substrates, mark the tin side of the substrates with a diamond scribe.

2. Clean the substrates for 15 minutes in fresh piranha (3:1 H_2SO_4:H_2O_2).

3. After piranha cleaning the substrates dump rinse and spin-rinse the substrates.

4. Dehydrate the substrates for 15 minutes at ∼100°C (hotplate or oven). Note: the substrates can be prepared while de-gassing the PDMS in the next step to save time.

A.6.2 PDMS Preparation

1. Turn on the PDMS curing oven and set the temperature to 110°C. This takes about 1 hour to heat up.

2. The PDMS used for our purposes is Sylgard 184 from Dow Corning (supplied by the Nanofab), mixed in a 10:1 ratio of base to curing agent (by weight). Use the scale in the PDMS-dedicated fumehood to weigh out 18-20 g of PDMS base in the supplied plastic cups (the exact weight used is not important, but knowing the weight is). Add the curing agent with a weight equal to 10% of the weight of the base. Up to 4 mixtures should be prepared at once (1 per substrate).

3. Once the mixtures have been weighed out they need to be well mixed. Using plastic pipettes (supplied by the Nanofab) each batch should be mixed for 2 minutes, switching direction of stirring every 30 seconds. Once mixing is completed the PDMS will start curing (though very slowly at room temperature), and the remainder of these steps should be carried out with as little delay as possible.

4. Once mixing is complete the PDMS will be filled with bubbles (a sign of good mixing). The PDMS needs to be placed in the vacuum oven labeled for PDMS outgassing and held under vacuum (open the vacuum

valve fully and leave it open) for 40-60 minutes, or until all the bubbles have been cleared.

A.6.3 PDMS Spinning

Once the PDMS has been cleared of bubbles it is ready to be spun. Using the spinner in the Aisle 1 fumehood the PDMS should be spun with the following parameters:

RPM1 - 500

Ramp1 - 5

Time1 - 5

RPM2 - 3000

Ramp2 - 4

Time2 - 60

Time3 - 0 (ends program)

Note: Not all of the PDMS needs to be used to coat the substrates.

A.6.4 PDMS Curing

1. After spinning, the substrates should be placed on a cleanroom wipe and loaded into the PDMS curing oven (which should have been turned on to 110°C earlier).

2. Open the vacuum valve during the curing step to avoid any bubble formation.

3. Curing takes 1 hour at this temperature.

A.6.5 Deposition of Gold border

1. In order to reduce de-wetting effects while spinning KMPR onto PDMS a 0.5 cm wide gold border should be sputtered onto the PDMS using the Denton sputtering system (SEM room).

2. Sputter a 10 nm thick film of gold onto the substrate while using a glass substrate (with side length 1 cm shorter than the 4" substrate) placed in the middle of the PDMS film as a shadow mask to keep the majority of the PDMS film clear of gold (reduces contamination of the KMPR film). Note: The shadow mask can be re-used between substrates, just make sure you have the same side touching the PDMS each time or the gold will flake off onto the PDMS.

A.7 KMPR 4 (Fluidic Roof)

A.7.1 Spin and Soft-Bake

1. Follow the spin process in section A.1.2, but use a spin speed of 4000 RPM, and change the soft-bake to a 3 step process to reduce de-wetting effects as follows: 10 minutes @ 50°C, 10 minutes @ 80°C and 20 minutes @ 100°C. Be gentle during transfers to avoid de-wetting problems. Film should be $\sim$26 μm thick.

A.7.2 Exposure and PEB

1. Expose as in section A.1.3, but using the appropriate mask and an exposure dose of 900 mJ/cm^2 to avoid resolution problems with over-exposure. Alignment is obviously not an issue here, but make sure the pattern is as centered as possible on the substrate.

2. PEB for 5 minutes at 100°C.

A.7.3 Development

1. Develop for 8 minutes in MF-319 using light agitation. Once 8 minutes is completed remove the substrate, rinse with DI water for 60 seconds and dry with N_2. Inspect the substrate to ensure development is completed and continue development as needed in 3 minute steps. Over-development is not an issue here.

A.8 Bonding Process

A.8.1 Alignment

1. Clean the self-healing cutting mat with IPA, along with the 6" square glass plate (available next to the embosser) and the polycarbonate (PC) pieces used for bonding. The PC pieces should be cut approximately circular with a diameter equal to the diameter of the KMPR remaining on the Si substrates. The PC is ok to be a roughly cut circle, since as it will be easier for the machine shop to produce.

2. The bonding stack should be assembled as follows (bottom-to-top): glass plate, PC, Si device wafer (centered over the PC), glass carrier substrate (aligned to device wafer), PC (centered over KMPR pattern).

3. Alignment of the features between the carrier substrate and the device wafer should be performed under a microscope (the microscope in the glass bonding area is suitable), with care taken to align features across the substrate. This can be awkward and will likely take time, but accuracy is important. Alignment to within 5 μm across the substrates

should be possible.

A.8.2 Bonding

1. Turn on the Hot Embosser tool by first turning the large black switch, followed by the 2 smaller green switches (all of them are in the glass-fronted cabinet under the computer monitor).
2. Log into the HE computer.
3. Open the Hot Embosser application from the computer desktop. Note: If the temperature readings do not all load, restart the application.
4. Turn on the force unit at prompt by pressing the "On" button on the tool (to the right of the chamber).
5. Initialize force unit using the button in the HE application.
6. Open Safety Door.
7. Check the tool to ensure the proper components are correct (should have a 4" flat piece on top, and the clips on the bottom should be removed). If the top piece needs to be changed, use an Allen key to unscrew the piece (do not drop the screws) and switch it out. Some of the holes may be stripped, so you may only be able to use 3 or 4 of the 6 screws.
8. Clean the HE tool with IPA (top and bottom pieces should be cleaned).
9. Carefully place the stack into the center of the hot embosser without shifting the stack.
10. Carefully align (still taking great care not to change the alignment and position of any of the pieces) the stack with the 8 holes located on the

bottom part of the HE tool (there should be 2 holes on each side of the stack). Note: The force of the HE is applied primarily in the middle of the tool, so centering the stack is important to ensure the force is applied evenly.

11. Open the KMPR bonding Macro. Double check the macro against the expected settings (listed at the end of this appendix), especially the force (10 kN) and the top and bottom temperature (100°C).

12. Select "Process - Start at beginning" to begin the bonding process. Observe the force and temperature settings to ensure everything is going as expected and that none of the pieces in the stack are breaking.

13. Once the bonding process is completed, allow the stack to sit in the HE for ~2 minutes to cool.

14. Carefully remove the stack from the tool and place it on the cutting mat for another ~2 minutes to allow the stack to reach room temperature. Do not place the stack directly onto a metal surface, as the rapid temperature change may cause damage.

A.8.3 Substrate Separation

1. Remove the top PC piece, and the 6" glass from the stack (may require the use of a blade or substrate tweezers).

2. Using wafer tweezers, detach the top plate of borofloat by slowing trying to separate around the edge. Slowly work your way around and continue this until the PDMS completely releases from the KMPR. Note: Keep in mind, the Si substrate has a crystalline structure and will snap very easily in certain directions. Try to minimize/avoid applying force in those

directions or you will simply snap the wafer. A broken wafer doesn't necessarily make it useless, just awkward to work with when dicing.

3. Remove the bottom PC piece.

4. If no more substrates are to be bonded, return the substrate clips to the chamber.

5. Close the HE chamber door.

6. Close the macro, and then the HE application (the application may run a cooling macro prior to closing, let it do so).

7. Shut down the HE computer.

8. Turn off the power switches (2 small green switches first, then the large black switch).

9. Log off the HE tool.

A.9 Dicing

A.9.1 Preparation

1. Turn on the Disco Dicing Saw and the tape hotplate next to it.

2. On each substrate that is to be diced, cover the top surface of the chips with blue tape to protect them. If any substrates broke while separating after bonding, first place them face up on the hotplate and attempt to arrange the pieces as if the substrate was still in one piece. When you tape across the top of the substrate you can fix the pieces in place much the same as if the substrate was still in one piece. This can help rescue at least parts of the substrate for working chips.

3. Follow the setup procedure in the SOP (end of this appendix) for the dicing saw to prepare it for cutting, with the appropriate substrate diameter, substrate thickness and blade height entered. The feed speed for the cuts should be 15 mm/sec.

4. Place the first substrate on the hotplate (face down) and use blue tape to attach it to the appropriate cutting frame. Try to keep the substrate as centered as possible.

5. Load the first substrate into the dicing saw.

A.9.2 Horizontal Cuts

1. Following the dicing saw SOP, align the first cuts horizontally across the substrate. The dicing lines on the substrate are much wider than the blade, and the blade should be aligned such that the cut is performed as close to the top of the dicing lines as possible (i.e. close to the bottom of chips, next to the electrical contact pads). Consistent placing of the dicing cuts is required to ensure optimal accuracy in the dimensions of the diced chips.

2. Make each of the horizontal cuts across the substrate.

A.9.3 Vertical Cuts

1. Once the horizontal cuts are done, remove the substrate from the dicing saw, and tape up and load one of the pieces at a time back into the saw.

2. For each cut between the chips, two cuts should be made, as close to the edges of each chip as possible (i.e. every chip should be approximately minimum width without cutting off any of the chip features).

3. Repeat this process for each of the pieces produced by section A.9.2.

4. Once all the chips are diced, move onto the next substrate.

A.10 KMPR-KMPR Bonding Macro:

```
Close door( )

Open File Protocol(New, View, Print=0(0,1,2))

Open File Measure( )

Initialize ForceControl(true/false=0)

Close Chamber( )

Position relative(Position=17.0mm, Velocity=75.0mm/minute, MaxForce=1500N)

Show Chart Window(Show/Hide=11/0)

Force - Force controlled(Force=2000N, Velocity=6.0mm/min)

Evacuate Chamber( )

Force - Force controlled(Force=10000N, Velocity=1.0mm/min)

Heater(Top=110.0_C, Bottom=110.0_C)

Temperature >=(Temperature=90.0deg, Channel=12)

Heating(Top=100.0_C, Bottom=100_C)

Wait Time(Time=900.00s)

Cooling(Top=10.0deg, Bottom=10.0deg)

Temperature <=(Temperature=65.0deg, Channel=12)

Force - Force controlled(Force=2000N, Velocity=1.0mm/min)

Venting Chamber( )

Open Chamber( )

Close File Measure( )

Open door( )

Show Chart Window(Show/Hide=01/0)
```

```
Temper(Top=25.0deg, Bottom=25.0deg)
```

A.11 Process Changes Between Batches

Four different batches of chips have been fabricated over the course of this thesis, each with a single variation of parameters in order to improve at least one feature of the final devices. The changes applied to each batch is indicated as follows and summarized in Table A.1:

- The first batch of chips (Batch 1) to be produced followed a very similar protocol to the one listed in A.1-A.9 except for the location of the dicing cut (changed in Batch 2 in order to reduce the error in the dimensions of the diced chips), the exposure dose for patterning the fluidic structures was 1,333 mJ/cm^2 resulting in reduced lithography resolution, the thickness of the Cr protection layer was 50nm (which was later increased to further reduce cracking during lift-off) and the PEB temperature for the KMPR floor layer was only 120°C resulting in parts of the heater wrinkling during the compressive bonding step. The deposition voltage for the Al film was 402 V.

- Batch 2 was produced using the same process as batch 1 except batch 1 had been diced by casually placing the cuts near the "center" of the 300 μm wide dicing lines. In an effort to improve the accuracy of the diced chip dimension, batch 2 was diced by aligning the cut as accurately as possible to the edge of the dicing line, minimizing the error resulting from the user aligning the cuts and leaving only the error in the accuracy of the dicing saw itself. All future batches discussed in this thesis were diced in this same way. The deposition voltage for Al was 409 V.

- Batch 3 was produced using the same process as batch 2 except that the exposure dose for the KMPR layers 3 and 4 was reduced in order to improve lithography resolution. The first 2 batches were discovered to have the fluidic channels and vias being partially sealed due to insufficient development. It was determined that the cause was due to the high exposure dose (1,333 mJ/cm^2 and 2,000 mJ/cm^2 for the Si and glass substrates respectively) that was used to pattern the fluidic layers (A.5 and A.7) causing a decrease in resolution. In order to avoid this problem batches 3 and 4 were both fabricated using an exposure dose of 600 mJ/cm^2 for the KMPR 3 layer (on the Si device wafer) and a dose of 900 mJ/cm^2 for the KMPR 4 layer (on the glass handle wafer, due to reduced reflection from the substrate during exposure). After making this change multiple devices from this batch, as well as batch 4 were tested by placing a drop of water on one of the wells and confirming that the water was able to flow into the channels using capillary forces. The deposition voltage for the Al film was 400 V.

- Batch 4 was produced using the same process as batch 3 except for the thickness of the Cr protection layer and the PEB temperature of the KMPR floor layer. Each of the earlier batches suffered from wrinkling effects in the aluminium heaters during the bonding process. In an effort to avoid this problem the fabrication process was changed to use a PEB of 180°C for the KMPR floor layer (instead of 120°C, A.1) in order to increase the mechanical stability of the film and prevent the wrinkling of the heaters during bonding. Also for batch for the thickness of the Cr protection layer (A.2) during lift-off was increased to 100 nm in an effort to further reduce any cracking of the KMPR during the lift-off process. The deposition voltage for the Al film was 390 V.

Table A.1: Fabrication Process Changes Between Different Batches of Devices.

Batch #	Variation from Stated Protocol
4	Same as protocol provided earlier in Appendix A.1-A.9
3	Same as batch 4 except the PEB for KMPR 1 layer (A.1) was only 120°C and the Cr protection layer was only 50 nm thick (A.2).
2	Same as batch 3 except all of the KMPR layers were exposed with a UV dose of 2 J/cm^2
1	Same as batch 2 except that the dicing was performed by targeting the dicing cuts approximately in the center of the dicing lines instead of using the edges of the dicing lines as an accurate guideline

A.12 SOPs from nanoFab

The following pages contain the nanoFab SOPs that were used as part of the fabrication process as indicated previously in this appendix.

W1-60 ECERF Building Edmonton, AB, CANADA T6G 2V4
p: 780.492.0167 f: 780.492.1811 www.nanofab.ualberta.ca

BOB SPUTTERING TOOL

October 21 2013

Location: 10K PVD area
Primary Trainer: Les Schowalter (587-879-1516), les.schowalter@ualberta.ca)
Secondary Trainer:

OVERVIEW

A planar magnetron sputter system with three sources. The gun/substrate configuration is designed for sequential sputtering. The third source can be used for magnetic materials.

SAFETY PRECAUTIONS

When using the hoist to close the system take care that your fingers are not between the chamber lid and body. Some materials are not compatible with a vacuum system; if you aren't sure of your material please see the primary trainer.

If you are bringing any new materials into the NanoFab for use in your process, it is necessary to fill out a chemical import form (available on our website, http://www.nanofab.ualberta.ca) and supply an MSDS data sheet to Stephanie Bozic.

THE nanoFAB
Fabrication | Characterization | Expertise

W1-60 ECERF Building Edmonton, AB, CANADA T6G 2V4
p: 780.492.0167 f: 780.492.1811 www.nanofab.ualberta.ca

OPERATING INSTRUCTIONS

Opening & Loading

1.0 Press "emis" on the Multi Gauge controller to turn off the ion gauge and check to see if the filament is off; then press "channel" until TC-1 is displayed and nothing showing in the blue section.
2.0 Turn the Baratron valve clockwise until closed.
3.0 Close the cryopump valve clockwise until closed; there should be a solid click sound when closed. Also note the cryopump temperature, if it's not below 20K please inform nanoFAB staff.
4.0 Flip the chamber vent switch up. When the pressure readout is at 760 Torr the chamber should be at atmosphere and the chamber vent switch must be closed.
5.0 Lift the lever on the back of the chamber lid.
6.0 Press the up button on the hoist and raise the top of the chamber until the substrate holder is clear of the main chamber, and then move the chamber top away.
7.0 Please put gloves on for the next steps.
8.0 Check the inside of the chamber for flaking and other debris; vacuum as required.
9.0 If the glass view port is coated with metal, pull out and replace glass. Please use IPA to clean all six sides of glass before installing.
10.0 Change targets as required, check to see if the proper target is in the chamber or in the correct container. Sputtering the wrong material may set your project back.
11.0 Make sure the dark space shield has adequate spacing. Most targets are ¼" thick and the dark space shield shouldn't be on any notch, Targets such as Au and Pt are thinner and should go onto the smallest notch. Check spacing with the voltmeter, you should have an open circuit.
12.0 Close the shutters. Remove any particles around the main o-ring using a cleanroom wipe and IPA.
13.0 Load your substrate(s) and move the top over the chamber; move the lever down and press the lower button on the hoist. Make sure you hold onto the top section as it wants to move to the right. When the top meets the chamber stop pressing the lower button, it can't lower any further!

Pump down

1.0 Open the chamber roughing valve about one full turn and observe if the chamber pressure is dropping. If the pressure doesn't change, check to see if the lid is properly seated onto the chamber. If pressure still doesn't drop close roughing valve and find nano**FAB** staff to look into the issue.
2.0 Rough to about **350 Torr** then open the roughing valve all the way then close about a half turn. Rough out to **$3.0X10^{-1}$** (about five minutes depending on which roughing pump is used.) then close roughing valve.
3.0 Slowly open the cryo valve all the way by turning counterclockwise.
4.0 Open the Baratron valve by turning it counterclockwise.

W1-60 ECERF Building Edmonton, AB, CANADA T6G 2V4
p: 780.492.0167 f: 780.492.1811 www.nanofab.ualberta.ca

5.0: Press “**channel**” on the Multi gauge controller until BA-1 is shown in the blue section, then press “**emis**”.
6.0 Pumpdown takes about one hour to reach the low -6 Torr.
7.0 Write your deposition parameters in the logbook, and put the sputter system in use sign up.

Deposition

1.0 Press “**emis**” on the Multi Gauge controller, then press “**channel**” until aux 1 is shown in the blue section.
2.0 Pull and lift the power switch on the MKS controller, then lift switch 1 for Ar gas, close the cryo gate valve about four turns until the Multi gauge controller reads $7X10^{-3}$ Torr.
3.0 Put target selector switch to the desired target. Switch on the power on the back of the MDX 500 power supply; adjust the power setting required for the material you are depositing. Remember the power supply should only be used in power mode.
4.0 Set substrate rotation to the desired speed, three to four is normal. Press the rotation switch.
5.0 Set a timer for the deposition time plus preconditioning. Target conditioning is usually three minutes except for Pt and Au which is one minute.
6.0 Press start on the power supply to condition the target. Look in the chamber to make sure the shutter is closed.
7.0 After the target conditioning step is over gently open the shutter and deposit for the desired time. Remember to write the voltage in the logbook. Press stop on the power supply when the desired time is reached.
8.0 Close the shutter and repeat steps three to six if another metal is required.
9.0 After the deposition is completed, turn off MDX 500 power supply (switch at the back).
10.0 Stop substrate rotation.
11.0 Turn target selector switch to off.
12.0 Turn off Argon switch, and MKS master power.
13.0 Press “**channel**” on the Multi gauge controller to read TC-1 (nothing in the blue section).
14.0 Close the Baratron valve.
15.0 Close the cryo gate valve.
16.0 Flick the chamber vent switch to put a few Torr of N_2 in the chamber then wait five minutes before venting.
17.0 After venting, open chamber using the same instructions as opening and loading starting at step #5. Put gloves on after moving the chamber top, remove substrate(s) and inspect chamber for flaking. If flaking is discovered please vacuum.
18.0 If you used a Pt target, please remove it from the system.
19.0 Follow steps from pumpdown section. Please note that you don’t have to start with slow pump down.

THE nanoFAB
Fabrication | Characterization | Expertise

W1-60 ECERF Building Edmonton, AB, CANADA T6G 2V4
p: 780.492.0167 f: 780.492.1811 www.nanofab.ualberta.ca

TROUBLESHOOTING

If you can't get a plasma do the following:
Close the cryo gate valve to the point of causing resistance.
Change power setting to 50 watts.
If you still can't get a plasma find the trainer for the tool or other nanoFAB staff to look into the issue.

If you encounter an unexpected error or require assistance please contact the primary or secondary trainer listed above. Should they not be available, please contact any staff member for assistance.

APPROVAL

Qualified Trainer: Les Schowalter
Training Coordinator: Stephanie Bozic

DICING SAW (DISCO DAD 321)

LOCATION: 10K Area

PRIMARY TRAINER: Stephanie Bozic (2-6724, sbozic@ualberta.ca)
SECONDARY TRAINER: Jolene Chorzempa (2-4823, jolenec@ualberta.ca)

1. OVERVIEW

This tool is used for dicing (cutting) Si and similar substrates. The chuck can support 6” wafer (full size) and anything smaller than that. The substrates can be bare, with thin films or without, patterned or etched. If there is a delicate device on the substrate, thin layer of photo resist can be used for protection.

2. SAFETY PRECAUTIONS

If you are bringing any new materials into the NanoFab for use in your process, it is necessary to fill out a chemical import form (available on our website, http://www.nanofab.ualberta.ca) and supply an MSDS data sheet to Stephanie Bozic.

3. OPERATING INSTRUCTIONS

1. Begin by heating up the hotplate in between the disco and diamond touch dicing saws. Turn on high heat.
2. Mount the substrate (silicon wafer or piece) to be diced in the center of the correct metal frame.

a. Substrate is placed feature side down on the heated hot plate. Turn on the substrate vacuum. Place it as close to the center as possible.
b. The correct frame is placed around the substrate. Frames are kept separated in separate labeled boxes.
c. Match the notches on the frame to the shaped posts on the hotplate.
d. Pull the blue tape across the substrate and frame and press “Table Up”.
e. Roll/push out the air bubbles. The larger the air bubbles the less likely the pieces will stay stuck to the tape once cut.
f. Close the top and spin to cut the tape around the frame.
g. Raise the top, turn off the substrate vacuum, and remove mounted substrate and frame.

3. Turn on the Disco Dicing saw by turning the key to START until the green light comes on. Let go of the key and let it return to ON. (Just like starting a car). The screen will remain dark for a while.

4. Once the screen comes on it will read “Initialize System” at the bottom left. Press the SYS INIT button. The system will then initialize and once done will read “G007 Initialization complete”
5. Blade Setup
    a. Go to the Blade Maintenance menu (F5)
    b. Enter the Blade Setup menu (F3)
    c. Start the Non-Contact Setup (F3)
    d. When the bottom left of the screen reads “G074 Press the ENTER key to execute” press ENTER

e. When the bottom left of the screen reads “G173 !Attention: press ENTER, axis moving to setup point” press ENTER
f. When the bottom left of the screen reads “G173 !Attention” press ENTER, axis moving to 0 point”, press ENTER
g. Once completed, press EXIT twice to return to the main menu.

6. Load your substrate onto the chuck, now press the C/T VAC button, the frame should be against the two pins as shown below. The vacuum gauge should move from red to green, if it does not you will need to adjust your dicing frame and substrate until it does.

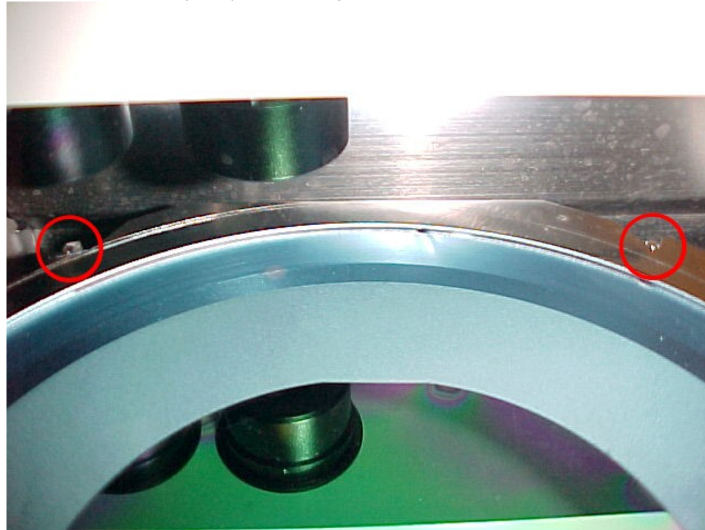

7. Select Device Data (F4) to choose a program. Scroll up and down and press ENTER when the one you wish to use is highlighted. Any program may be chosen and modified.
8. Using the up and down scroll through and change the program to suit your substrate or piece. Values are entered using the number pad and then pressing the arrow to replace the previous value.
    a. RND WORK SIZE: the diameter of the work area in millimeters.
    b. WORK THICKNESS: the typical thickness of a silicon substrate is 0.5000mm.
    c. TAPE THICKNESS: the thickness of the blue tape is 0.0700mm.
    d. BLADE HEIGHT: the blade is set to cut down to 0.0500mm.
    e. FEED SPEED: is the speed the blade moves, typically between 10-20mm/sec
    f. Y INDEX CH1: is the distance between the first set of cuts (not applicable if only one cut is being made)
    CH2: is the distance between the second set of cuts (not applicable if only one cut is being made or cutting in only one direction)
9. Press ENTER to save the changes to the program.
10. Press EXIT twice to return to the main menu.
11. In the main menu choose Semi-Auto (F2)
12. Press F8 to enter the measure view and see the substrate through the lenses.
13. Press EXIT once to return to the commands at the bottom of the screen.

14. The substrate can be moved using the X, Y, and Q keys. Use the SLOW key to make finer movements. The INDEX key will move the substrate the distance set in the program.

15. Choose a line that runs across the width of the substrate (or two features that are even). Using the movement keys, align to the three dashed lines across the screen.

16. Once the substrate is aligned, position the first cut. The cut is made between the three lines on the screen. To increase accuracy place the first cut at the end of the substrate closest to you.
17. Choose the cut direction: F5 if you are at the front of the substrate
    F10 if you are at the back of the substrate
18. Select START to start the cut.
19. The program may ask to verify the jog direction of the movement keys. Perform the verification by briefly touching the specified underlined key.
20. Reselect the cut direction and press START.
21. When the cut(s) are finished, dry off the substrate using the nitrogen gun. The cuts can be inspected by moving the substrate under the lenses.
22. To rotate the substrate exactly 90º select the INDEX and press the Q counter clockwise (ie. the one not underlined)
23. Repeat steps 16-20. The substrate does not need any additional aligning.
24. Exit to main menu.
25. Turn off chuck vacuum (C/T VAC).
26. Remove substrate, turn off dicing saw (key to OFF position), and ensure everything is clean and dry.

4. Troubleshooting

If you encounter an unexpected error or require assistance please contact the primary or secondary trainer listed above. Should they not be available, please contact any staff member for assistance.

6. Approval

Qualified Trainer: Jolene Chorzempa
Training Coordinator: Stephanie Bozic

Appendix B

Membrane Deflection

In order to further improve the power consumption of our LOC devices an airgap can be used to separate the heater element from the substrate in order to reduce the amount of power required to heat the KMPR above the heater. Instituting this kind of change introduces a wide range of complications into the fabrication and operation of the chips. This appendix will report on the possible issue of deflection of the membrane suspended above the airgap. These results may also be applied readily to other situations such as opening and closing valves using pneumatic pressure or other pressure-generating sources such as phase change or electrostatic valves.

Deflection was studied using COMSOL simulations to represent the physical structures of the chips under applied pressures.

B.1 Simulation Details

The initial simulation runs were set up as 3D Solid Mechanics simulations in COMSOL 4.3 with the structure of the KMPR generated to resemble the actual structures as closely as possible (Figure B.1). The fixed boundary conditions for the module assume that the silicon substrate is a rigid material, creating the

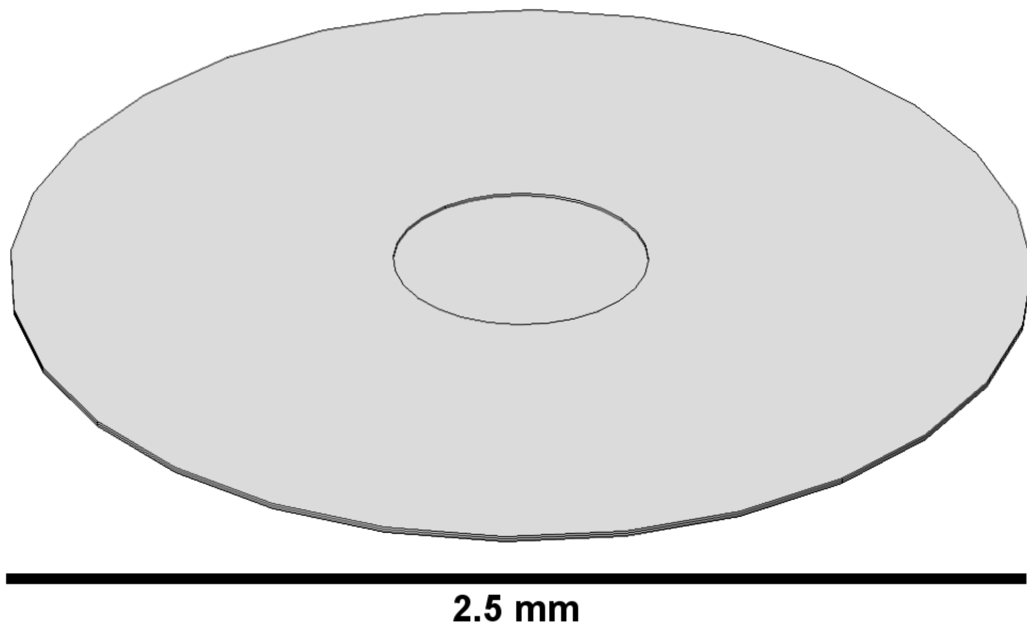

Figure B.1: KMPR geometry used in COMSOL simulations for membrane deflection under pressure. The first 3 layers of KMPR (airgap layer, membrane layer, chamber layer) are represented according the the expected fabricated dimensions (500 μm radius chamber, 600 μm radius airgap), with the bottom of the first layer being fixed under the assumption that the silicon substrate is rigid. The outer radius of the KMPR structures is 2.5 mm

Table B.1: List of Simulation Parameters.

Membrane Radius ($\mathbf{R}_{mem}$):	500 μm
Membrane Thickness ($\mathbf{t}_{mem}$):	10 μm
Post Radius ($\mathbf{R}_{post}$):	2.5 μm
Pressure Differential ($\mathbf{P}$):	101325 Pa

Radius of circles defining post positions = $\mathbf{R}_{px}$, where x is the series number.
Note: 6 posts around the circumference for x=1, 2, 3. 12 posts for x=4, 5, 6.

# of Posts	$\mathbf{R}_{p1}$	$\mathbf{R}_{p2}$	$\mathbf{R}_{p3}$	$\mathbf{R}_{p4}$	$\mathbf{R}_{p5}$	$\mathbf{R}_{p6}$
7	266 μm					
25	172 μm	261 μm	347 μm	366 μm		
55	125 μm	220 μm	237 μm	320 μm	365 μm	420 μm

boundary condition of the bottom of the lowest KMPR layer being fixed. In order to control the amount of deflection posts were placed inside the airgap to provide physical support. These posts were defined as fixed structures attached to the bottom of the membrane. A membrane radius of 500 μm and a thickness of 10 μm was used to coincide with the fabrication process the airgap was being targeted for. Post radius was defined as 2.5 μm corresponding to the minimum size produced by the anticipated fabrication process and also representing the worst-case scenario for the posts since larger posts would serve to reduce membrane deflection. The positioning of the posts was determined by placing the first post at the center of the chamber and placing further posts around the first in sets of either 6 or 12 posts evenly spaced around the circumference of a circle of a defined radius. The goal of the simulations was to reach a maximum membrane deflection of less than 0.5 μm under 1 atm of differential pressure (applied across the membrane area as a boundary load). These target values were chosen as a conservative estimate for the viability of an airgap. See Table B.1 for a full list of parameters.

For a further discourse on the assumptions used and their validity to the actual physical situation see the final section of this appendix.

Table B.2: Simulation Results for Membrane Deflection

# of Posts	Maximum Deflection of Membrane*
0	421.83 μm
1	58.819 μm
7	8.6503 μm
25	1.5216 μm
55	0.4176 μm

* There was no limit placed on the deflection of the membrane, either by the membrane hitting the bottom of the airgap or the membrane bursting. Since the goal was to achieve less than 0.5 μm deflection there was little need to include these complications into the simulation.

B.2 Simulation Results

The results of the simulations can be seen in Figures B.2 - B.6 and are summarized in Table B.2.

B.3 Simulation Matching the Fabrication Process

With a foundation of understanding of the limitations and requirements established for building an viable airgap the simulation geometry could be expanded to match the fabrication process. The initial simulations assumed that posts could be placed arbitrarily throughout the airgap however limitations of the targeted fabrication process restrict the post positions and sizes.

The pattern of the post layout will likely end up having to be a rectangular or square grid with the actual pitch determined by the heater layout due to the fabrication process requiring holes in the metal layer while fabricating the posts. The number of posts required should be kept as low as possible in order to minimize the power requirement for the heater design. More posts

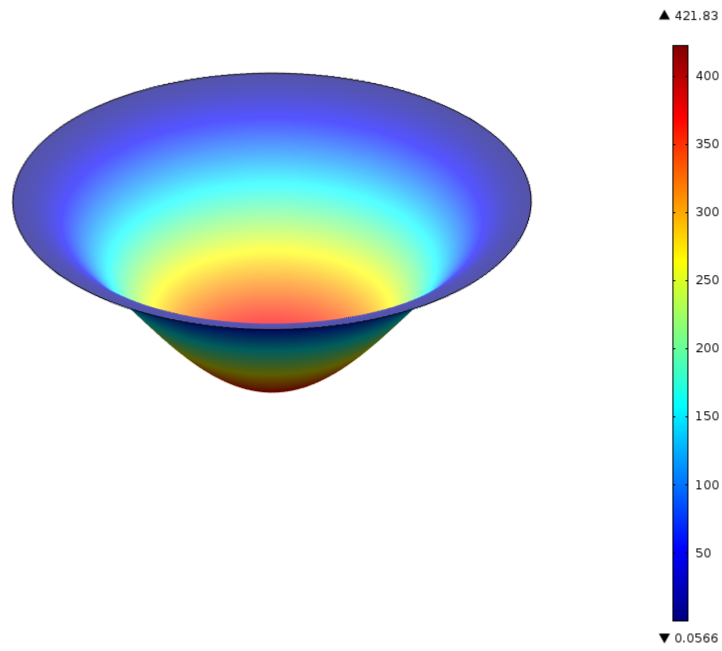

Figure B.2: Simulation Result for 0 Posts.

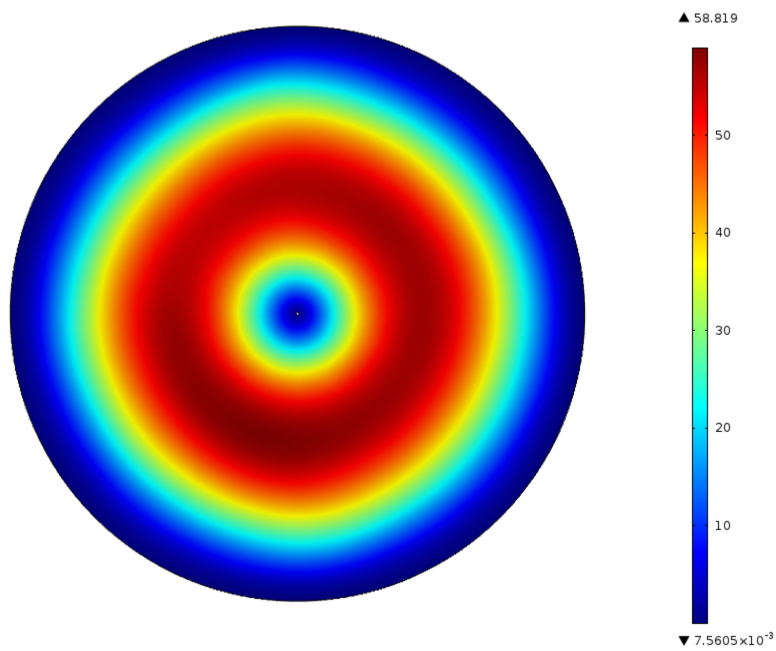

Figure B.3: Simulation Result for a Post Placed in the Center of the Chamber.

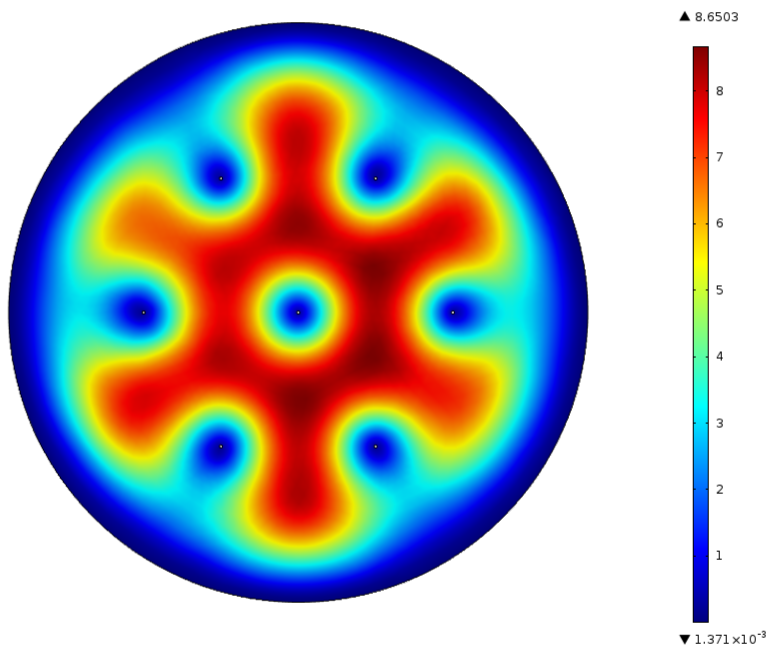

Figure B.4: Simulation Result for 7 Posts.

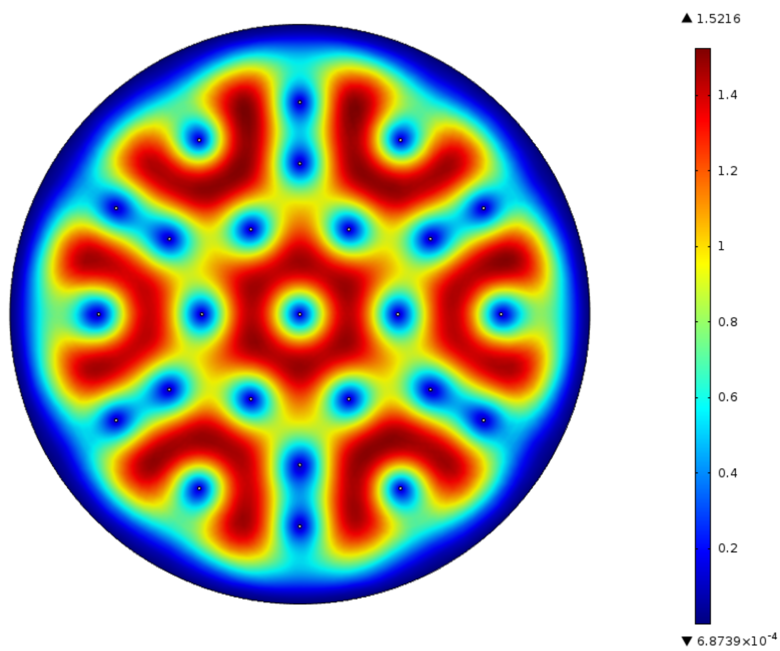

Figure B.5: Simulation Result for 25 Posts.

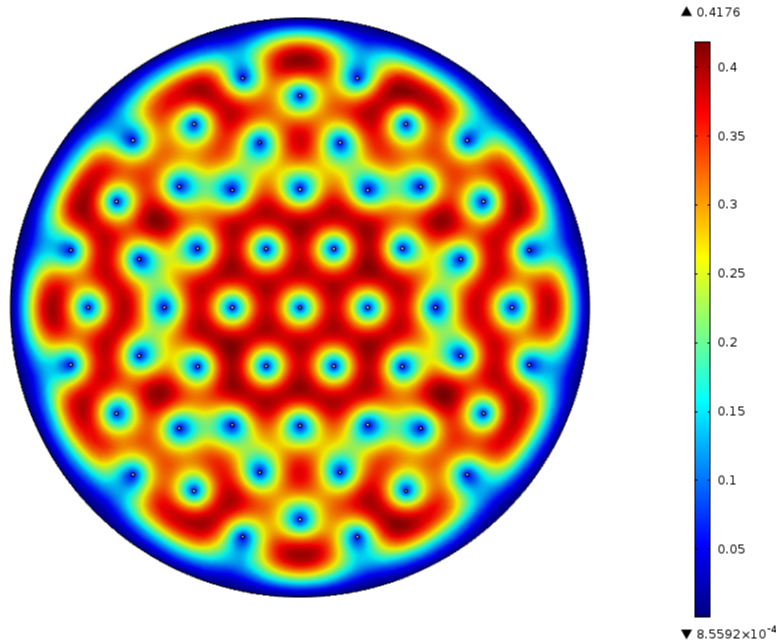

Figure B.6: Simulation Result for 55 Posts.

in the airgap means a greater amount of heat transfer down to the substrate which means that the pitch between posts should be kept at a maximum. To accomplish this two factors must be considered: the pitch (of a rectangular grid) required to reduce the membrane deflection within tolerance and the highest pitch that the fabrication process allows.

B.3.1 Maximum Pitch - Membrane Deflection

Simulations using a square grid of posts show that a post pitch of 109 μm (x and y directions, Figure B.7) results in a maximum membrane deflection of less than 0.5 μm. For a rectangular grid of posts (different X and Y pitches) a grid of 96 μm by 116 μm also yields suitable deflection values (Figure B.8). A value greater than 115 μm could probably also be achieved but is unnecessary as shown in the next section.

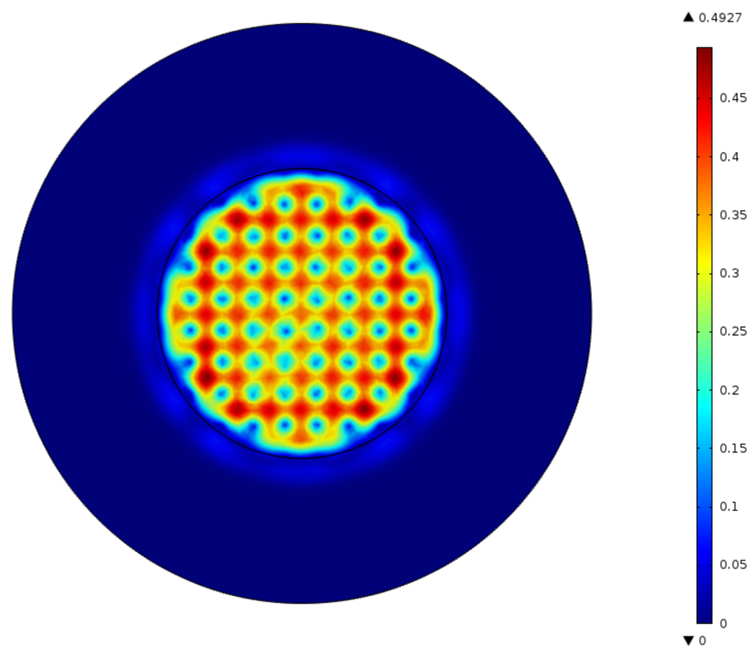

Figure B.7: Simulation results for a square grid of posts with a pitch of 109 μm.

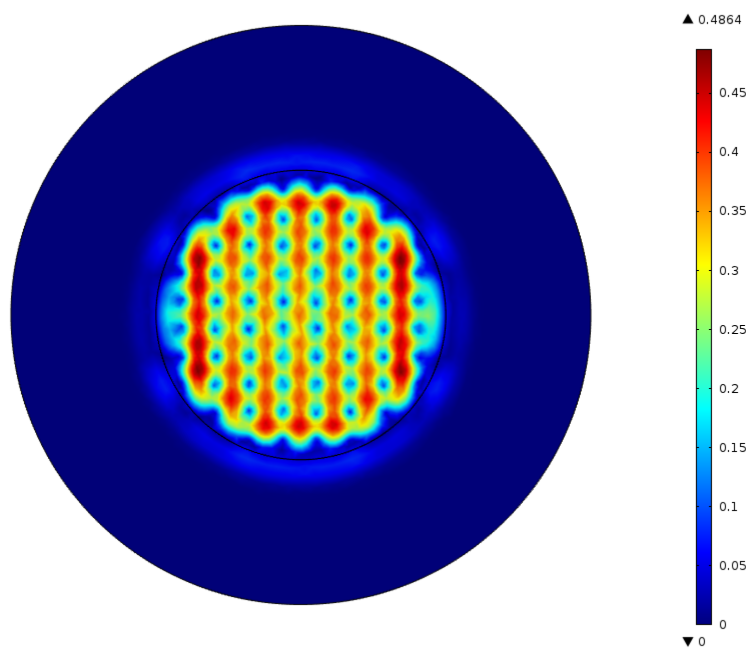

Figure B.8: Simulation results for a rectangular grid of posts with a pitch of 96 x 116 μm.

B.3.2 Maximum Spacing - Etch Holes and Heater Pitch

The fabrication process to be used for the airgap and the posts involves the use of 5 μm diameter holes in the Al metal layer through which an 18-22 μm isotropic etch is performed to remove the KMPR underneath the chamber. Post are formed by removing specific etch holes to produce an area of the airgap beyond the etch radius around the remaining holes. As a result of this process the holes must be spaced such that the maximum length of the diagonal between holes is 40 μm. The minimum spacing between holes to ensure structural stability was taken to be 5 μm.

Using a rectangular grid in order to maximize the pitch for the heater traces a grid spacing of 10.6 μm x 38.57 μm yields a diagonal length of 50 μm (by removing 4 holes total) which will allow for the formation of a 5 μm wide post with a 20 μm etch radius (Figure B.9). This grid spacing also allows for a post pitch of 95.4 μm x 115.7 μm which matches the limitations for membrane deflection.

Alternatively a grid of hexagonal posts has also been suggested in order to reduce the effect of any variation in the etch rate as well as to avoid any sharp angles during fabrication. See Figure B.10 for a simulated example of the hexagonal posts.

B.4 Membrane Deflection Assumptions

A number of assumptions were made when simulating the deflection of a membrane under a differential pressure. These assumptions were made for 1 of 3 reasons: their effect on the situation was minor (e.g. linear elastic material), we lacked the proper information (e.g. using some of SU-8's physical properties), or to simplify the situation (e.g. the position of the posts). Each of the

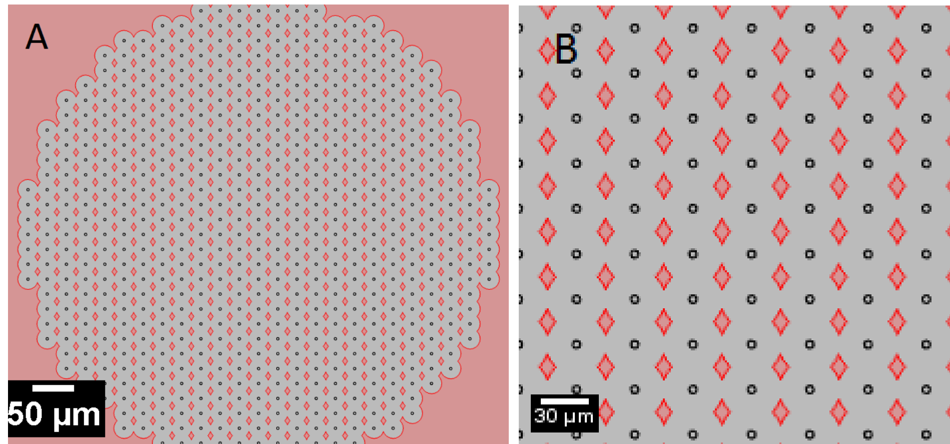

Figure B.9: Simulated formation of posts by performing an isotropic etch step through etch holes. The airgap is created using the removed parts of the KMPR film (image A). The posts themselves are approximately diamond shaped due to the etch process, with the etch originating from 2.5 μm radius holes (image B).

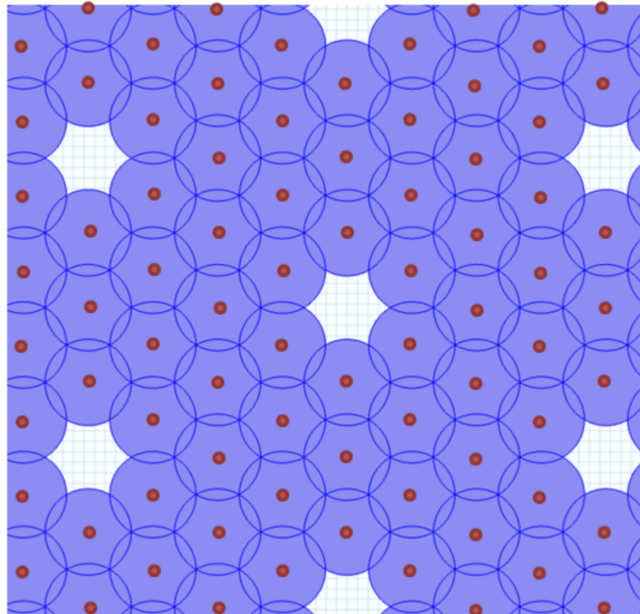

Figure B.10: Simulated formation of hexagonal posts by performing an isotropic etch step (represented by the large circles) through etch holes (smaller circles). The posts are produced by the removal of a single etch hole from the hexagonal array of holes.

assumptions made will be discussed here.

B.4.1 Pressure

The pressure used to determine the membrane deflection was 101325 Pa (1 atm). This value hopefully represents a "worst-case" scenario for the pressure exerted on the membrane during operation, but the actual pressure exerted here is a rather complicated function. If the top of the PCR chamber consist of a valve membrane pneumatically controlled by a helper chip then the most obvious source of pressure on the bottom of the PCR chamber (the membrane being simulated) is the force exerted through the fluid contents of the PCR chamber from the top membrane. There is also the fact that we are heating a sealed volume of liquid, which will obviously want to expand outwards while heating resulting in a further increase in pressure and/or deflection.

The pressure used to seal the valves and the PCR chamber is expected to be 15 PSI (1 atm). So it's likely that the pressure exerted through the chamber will be around this value (in the absence of pressure matching in the airgap).

B.4.2 Mechanical Properties

The value for Modulus used in these simulations was the room temperature modulus measured for KMPR. Although there is some evidence to suggest that this modulus value remains largely unchanged at PCR-operating temperatures (given extreme enough processing conditions), it's just as likely that the modulus will rapidly decrease by an order of magnitude or more if the glass-transition temperature of the material is too low.

The value for Poisson's ratio used was that of SU-8 as I was unable to find any references to the value for KMPR. The value (0.22) is probably reasonable given that they are both the same class of material, but without confirmation

this value may be significantly off target.

B.4.3 Post Placement

These simulations were run assuming that the posts could be placed purely arbitrarily throughout the airgap. This isn't actually valid given the limitations imposed by the expected fabrication process and they will likely have to be shifted around in order to fit into a more rectangular grid. This change is likely to affect the number of posts required to minimize the maximum deflection. From the fabrication process the expected minimum post pitch will be as low as 40 μm, which is smaller than the current pitch produced by these simulations (one of the reasons these simplified simulations were worth running), so the goal of less than 0.5 μm deflection should still be achievable.

B.4.4 Linear Elastic Material

The simulations involving very few posts result in an extremely large deflection of the membranes (421.83 μm for no posts in the airgap). Obviously this kind of deflection is unrealistic as COMSOL is running these simulations assuming KMPR is a linear-elastic material no matter how much it is being deformed. For small displacements this is a reasonable assumption (i.e. our target deflection of less than 0.5 μm), but for the very large displacements suggested by some of the simulations it's likely the membrane will have either left the linear elastic stage or simply burst apart. It's not worth accounting for this behaviour since by the time the membrane has deformed enough for this to be a problem, it will have already deformed well beyond the point that we find acceptable for operating these devices (not to mention the airgap will only actually be 2 μm high, so the membrane would simply hit the bottom of the gap!). We must keep this assumption in mind for the extreme cases, but there

is no need to complicate the simulation to account for non-linear stretching of the membrane as entering that regime is already a sign that the membrane is deflecting too far.

Appendix C

Selective Bonding

In this appendix I will discuss the various experiments that have been performed in an attempt to accomplish selective bonding (SB) of KMPR to fabricate valve structures. The idea behind these attempts was to achieve a localized increase in cross-linking level in the KMPR in order to reduce the effectiveness of bonding in those areas. Numerous attempts were made in order to accomplish this process and the results will be discussed here. Throughout this appendix bonding quality is assessed based on the percentage of bonded area not displaying any delamination effects following the bonding process. Any bonded substrate with at least 90% of the area successfully bonded is considered a good bond. This typically equates to 2 or less defects present, depending on the size of the defects.

C.1 Experimental Results

C.1.1 60°C PEB

The first experiments involved device wafers fabricated with 120°C PEBs for 20 minutes and carrier wafers fabricated on PDMS and silanized glass with

PEBs at 60°C. The first thing to determine was the PEB time required for the exposed pattern to be defined at 60°C. The end point used was for the pattern to be visibly discernible (as specified in the KMPR data sheet). For the first substrate fabricated (on PDMS), 30 minutes at 60°C was enough to define the pattern, this time was repeated for the next 2 substrates (one PDMS, one silanized glass) and was found to be sufficient. Development was performed for 8 minutes on the first two substrates (both PDMS) to remove the unexposed KMPR successfully. It should be noted that under a microscope there was some signs of delamination of the KMPR around the dicing lines. A PEB was started at 60°C to attempt to dry out the KMPR a little before bonding, but this quickly proved to be a very bad idea. Within minutes the KMPR began to badly delaminate. Both substrates were removed from the hotplates immediately after noticing the problem. The first substrate (20111019-A) had a large amount of delamination across the entire substrate and there was little point to attempting to bond the substrate. The second substrate (20111019-B) only had significant delamination on a few of the features along one edge of the substrate, so those parts of the KMPR were removed with tweezers and bonding the substrate was still attempted despite the greatly increased risk of the substrate breaking. Bonding was performed to the device wafer 20111024-A at a force of 5750N and a temperature of 70°C. As expected, the carrier wafer broke and bonding quality was poor, with most of the substrate not bonding properly. However, 2 of the structures remained bonded to the device wafer, so it was decided to apply pressure to those chips to see what would happen, expecting the bonded KMPR to simply delaminate. It was a pleasant surprise when, under a pressure of ∼10 PSI, the the SB-exposed parts of the KMPR released properly (Figure C.1), while the chip remained sealed around the deflected membrane. This is the exact result that was looked for

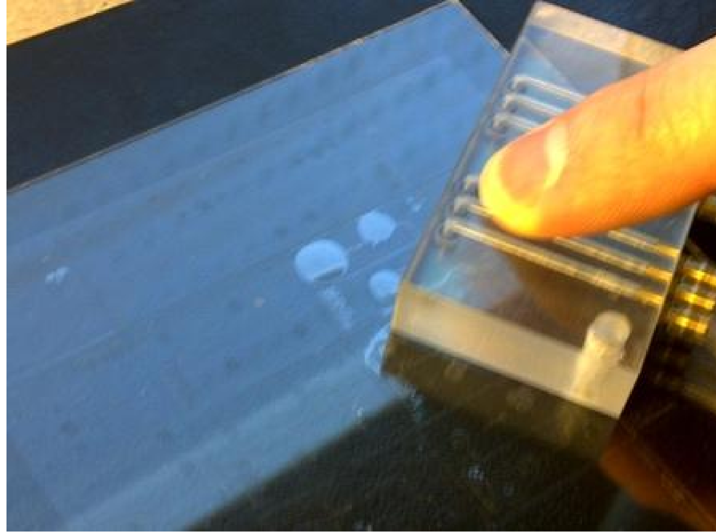

Figure C.1: SB Result - 60°C PEB, but with a broken substrate during bonding. When pressure is applied to the channels the selectively bonded areas covering the channel outlets successfully release and deflect upwards. Although this is a positive result, the broken substrate during bonding means that this result is not repeatable.

to prove the functionality of the SB process, although the result includes a broken substrate.

Moving onto the third prepared carrier wafer (on silanized glass, which had yet to be developed), the KMPR was developed with the plan of not performing any PEB step. 8 minutes into the development it was paused (rinsed and dried with nitrogen) in order to inspect the substrate. The substrate still contained residual KMPR to develop away and was also starting to display delamination around the edges of features. Developing was continued for 2 more minutes with the expectation of the development being completed, but when drying the substrate with pressurized nitrogen the KMPR started blowing off the substrate (Figure C.2). Apparently film stress along with the deliberately poor adhesion to carrier wafers will make PEBs at 60°C a greater challenge then expected.

Figure C.2: Delamination post develop of 60°C PEB KMPR on silanized glass (4" borofloat glass substrate). From this result is it clear that a higher temperature PEB must be used during fabrication.

C.1.2 70°C PEB

Given the problems related to fabricating carrier wafers with 60°C PEBs, the next bonding experiments were performed using 70°C bakes to avoid the delamination effects. 2 quick tests have been performed (using the two device wafers that were to be used in the 60°C tests). One substrate was fabricated on PDMS, the other using silanized glass. Both substrates were spun using the same protocol as the 60°C experiments, with the exception of the PEB temperature. Upon development there was a slight hint of delamination at the corners of the dicing lines, but the KMPR held firm to the substrates. The PDMS carrier wafer was bonded first, using a temperature of 75°C and a force of 5750 N in the embosser for 15 minutes. 4 of the membranes to be fabricated on the chip had water-soluble ink applied to them to encourage SB. During bonding, there was no breakage of the carrier wafer. While releasing the carrier wafer, it was clear that the bonding strength was quite poor, and much of the KMPR didn't release from the PDMS. However, despite the fairly

Figure C.3: SB Result = 70°C PEB, 75°C bonding temperature. Once again the desired areas release and deflect when pressurized, but this result is overshadowed by the fact that the bonding quality was poor (much of the bonded area was delaminated).

poor bonding, 3 of the structures remained on the device substrate. Applying 5-10 PSI of pressure to the open well of the structures actually yielded surprisingly effective results; the SB-exposed membranes released successfully from the KMPR surface while the surrounding KMPR remaining bonded, much the same result as the 60°C experiment previously, except without the broken substrate (Figure C.3).

Given this positive result, but with the presence of poor bonding, the next substrate (fabricated on silanized glass) was bonded at 80°C, 5750N, for 15 minutes. Once again there was no breakage of the substrate. Unfortunately the bonding quality was once more quite poor, and this time no structures remainied to study. In fact poking around the released carrier wafer with a scalpel actually showed the KMPR to be fairly strongly attached to the substrate, much more so than usual. At this stage, given the varying results of silanized substrates it was decided to return to using only PDMS as a low-

adhesion layer until the fabrication process has been stabilized.

C.1.3 85 and 90°C Bonds

Two more sets of substrates (2 device wafers and 2 carrier wafers) were fabricated on PDMS with a PEB temperature of 70°C. The substrates had no problems with delamination during fabrication. There were slight problems with dewetting of the KMPR during the 120°C bake (which has been fairly common during these tests). Dewetting has been a common problem around spinning defects in the KMPR (this issue does not present as readily on the full 4-layer process as the SB exposed KMPR is spun on top of another KMPR layer instead of straight on top of the PDMS release-layer). Bonding of the first substrate pair was performed at 90°C and 5750N for 15 minutes. 6 (out of 18) of the SB-exposed membranes had water-soluble ink applied to them. Once the bonding process was completed (the substrate didn't break), the carrier wafer was detached from KMPR. Unlike the bonding trials at 70 and 80°C, all the KMPR released from the PDMS, although the KMPR at the corners of the substrates displayed poor bonding (see Figure C.4), as well as the areas near dewetted features. As for SB results, the inked membranes released properly for pressures up to 30 PSI, at which point the bonded KMPR delaminated as far as the chip edges on some of the designs. None of the non-inked membranes were able to fully release (some would partially release).

The second prepared substrate pair was bonded at 85°C and 5750N for 15 minutes (same fabrication procedure). Once again 6/18 valves were inked. Once more the substrate did not break during bonding, although the bonding quality was noticeably worse (noticeable around the edges of the substrates and around defects in the KMPR). All the KMPR still released from the PDMS when the carrier wafer was removed (See Figure C.5). The SB results from

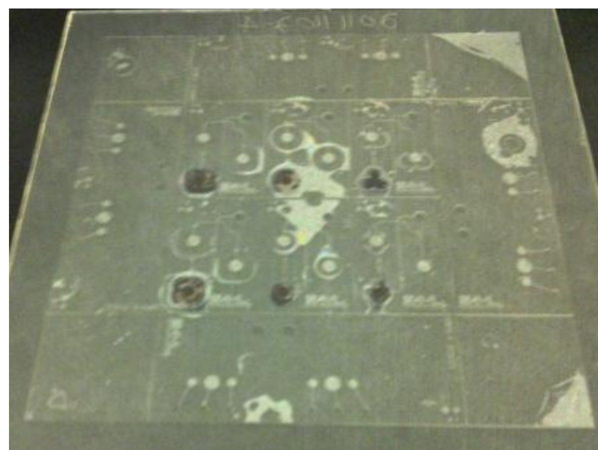

Figure C.4: Post-Release, PEB at 70°C, bonded at 90°C, 5750N, 15 minutes. The amount of delaminated area classifies this as poor bonding quality.

this bond showed that all of the membranes released for pressures up to 15 PSI, at which point delamination occurred to the dicing lines of the chip.

These 2 bonding experiments (85 and 90°C) were repeated November 4th to verify their results. Bonding performed a second time at 85°C once again showed marginal bonding (this time 3 of the structures didn't release from the carrier wafer; Figure C.6). The structures remaining on the substrate showed that the inked membranes (3 remaining on the substrate) released fine at 5 PSI, and delaminated to the chip edge by 10 PSI. The non-inked membranes did not fully release prior to the inked membranes delaminating to the edge of the chip.

Repeating the 90°C bonding experiment once more showed much better bonding quality (everything released from the PDMS; Figure C.7). Unlike the previous bond, 12 of the 18 membranes had ink applied to them (not expecting non-inked membranes to release). Applying pressure to the open well showed that the inked membranes all released properly (12 out of 12) for pressures as low as 5 PSI, and held firm up to 15 PSI (with the exception of 1 membrane that did not seal properly following bonding). The non-inked membranes were

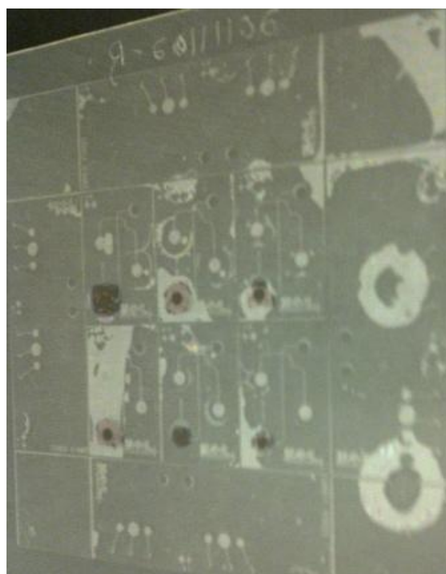

Figure C.5: Post-Release, PEB at 70°C, Bonded at 85°C, 5750N, 15 minutes. Again the bonding quality was quite poor due to the amount of delaminated area requiring different parameters to be needed for a reliable bonding process.

not able to fully release.

The next set of bonding trials involved extending the bond time to 20 minutes at 85°C, and reducing the bond time to 10 minutes at 90°C, with the expectation that longer bond times improves bond quality (strengthening the weak bonding at 85°C) and shorter bond times improves selective bonding at 90°C (with minimal sacrifice to bond strength). Bonding at 90°C for 10 minutes however yielded significantly worse bonding (not everything was able to release from the PDMS), and when applying pressure to the structures, the membranes were only able to handle up to 10 PSI before delamination occurred (inked membranes released at 5 PSI, non-inked membranes didn't release). Bonding for 20 minutes at 85°C yielded far better results, with poor bonding only being exhibited around defects in the KMPR on the carrier wafer. Applying pressure to the structures showed the inked membranes (10 of them) all releasing easily at 5 PSI, with delamination beginning to occur at 20 PSI.

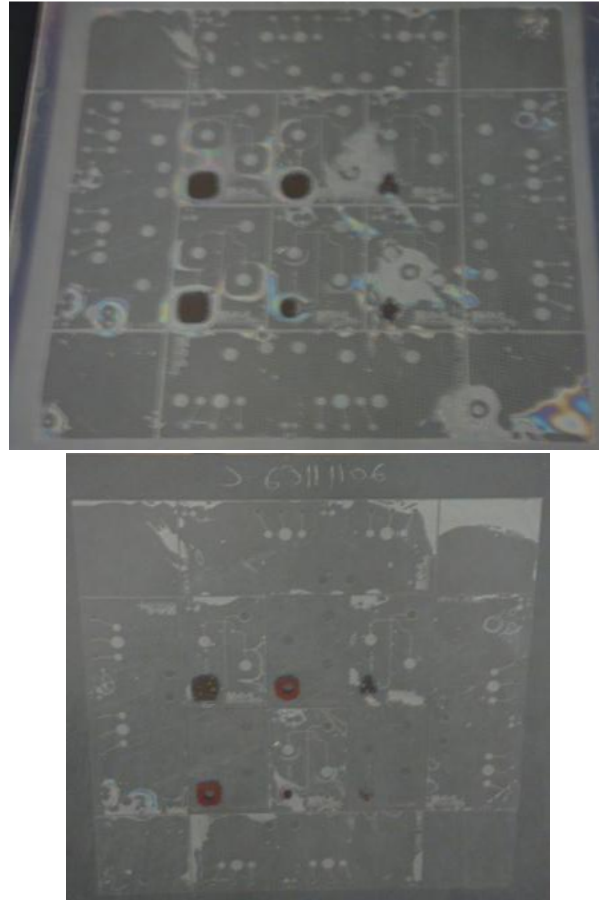

Figure C.6: Substrate bonded at 85°C for 15 minutes at 5750N. The second image shows the substrate after release of the carrier wafer; 3 of the structures did not release (poor bonding quality).

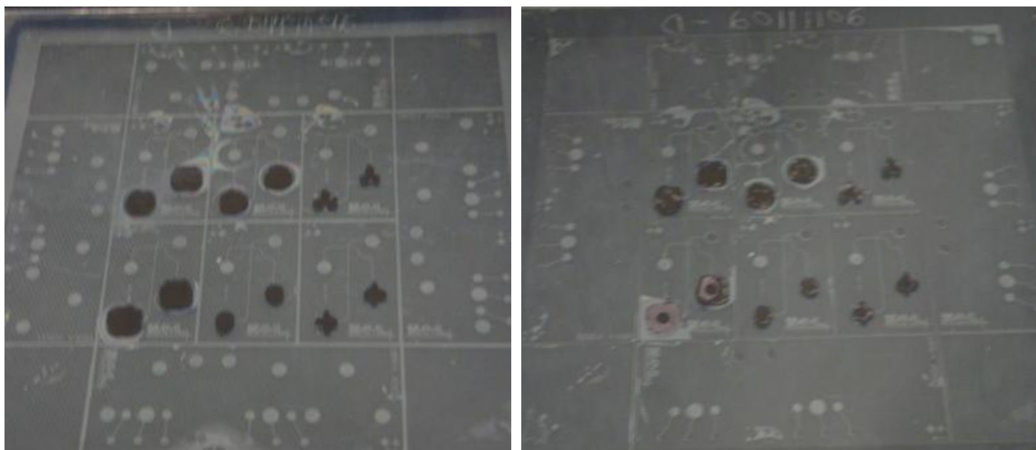

Figure C.7: Substrate bonded at 90°C for 15 minutes at 5750N. The second image shows the substrate after release of the carrier wafer. The bonding quality in this case was acceptable, though the selective bonding result was negative.

At 20 PSI, the non-inked membranes were only able to partially release (less than half of the membrane area would deflect).

These two bonded substrates were then baked at 100°C (fumehood hotplates) for 10 minutes in an attempted to improve bond strength. For the substrate bonded at 90°C the bond qualities (SB or otherwise) showed little change (delamination at 10 PSI, only inked membranes released). For the 85°C bonded substrate, applying pressure after baking showed the inked membranes releasing at $\sim$ 10 PSI, the non-inked membranes releasing at $\sim$ 20 PSI, and delamination not occurring until 45 PSI! This is currently the most promising SB result that has been attained and needs to be repeated for confirmation).

2 more sets of substrates were fabricated to repeat the previous result with one set seeing a PEB of 130°C and the other seeing the same fabrication parameters as the previous result (120°C SB bake temperature). Unfortunately the PEB of 130°C for the SB exposure yielded significant dewetting on the PDMS, severe enough to prevent bonding (Figure C.8). The 120°C set was bonded at 85°C for 20 minutes (5750N). The bond quality was not as good as

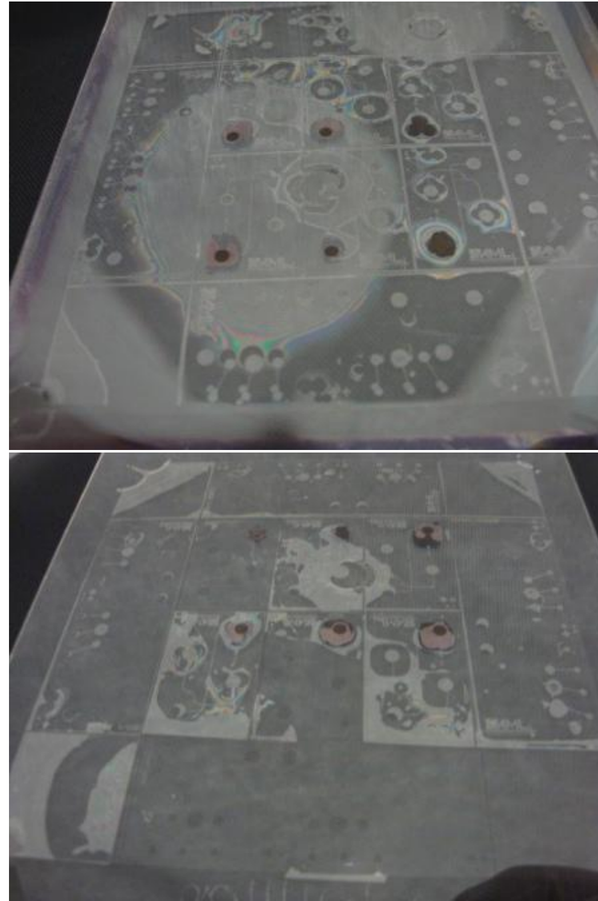

Figure C.8: Substrate bonded at 85°C for 20 minutes at 5750N. The substrate displayed very poor bonding quality with many areas not releasing from the carrier wafer.

previously (3 of the structures showed significant delamination upon release of the CW, although they did all release from the CW; see Figure C.9). The structures remaining had 5PSI of pressure applied to them to release all the membranes (inked or not, they all released). The entire substrate was then baked at 100°C for 10 minutes, before having further pressure applied. After baking, 15PSI was sufficient to release all 9 of the membranes, and the bond was able to hold for applied pressures of 20, 25, and 30PSI, before delaminating at 40PSI.

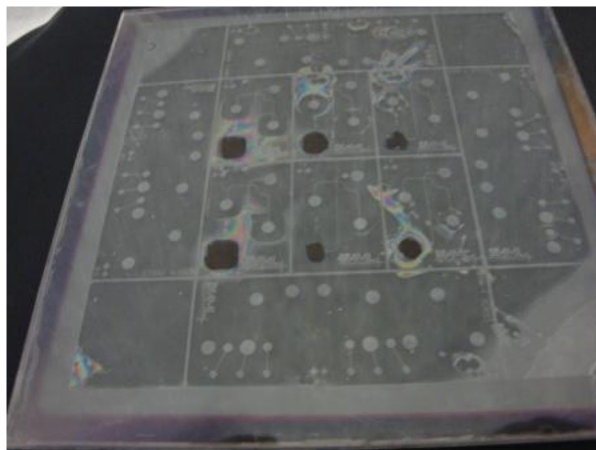

Figure C.9: Substrate bonded at 85°C for 20 minutes at 5750N. The bonding quality would still be considered poor due to the amount of delaminated area.

C.1.4 Full PC5k Fabrication

Given the previous results, I decided to move forward to attempting to fabricate the full PC5k chips (including actual valve structures). Based on previous results, I will use 2 different bonding protocols for these tests, both using SB PEB at 120°C, and fluidic layer PEB at 70°C. The first protocol will bond the substrate at 90°C, 5750N, and 15 minutes, based on the previous results of inked membranes functioning under these conditions. The second bond will use 85°C, 5750N, for 20 minutes, based on the positive results for both inked and non-inked membranes. One point of mention from the fabrication was that for CW 2 (with 2 layers of KMPR spun on top), the act of spinning the 2nd layer on top of the exposed and post exposure baked first layer caused a lot of small ripples around the features in the first layer (I have observed in the past that exposed and baked KMPR will have small bumps at the edges of features). These small features proved to be problematic during the bonding. The first bond for each DW worked wonderfully (11500N, 100°C, 15 minutes), with the exception of around a few defects which were present on the substrates from spinning (but the areas of poor bonding were contained to the

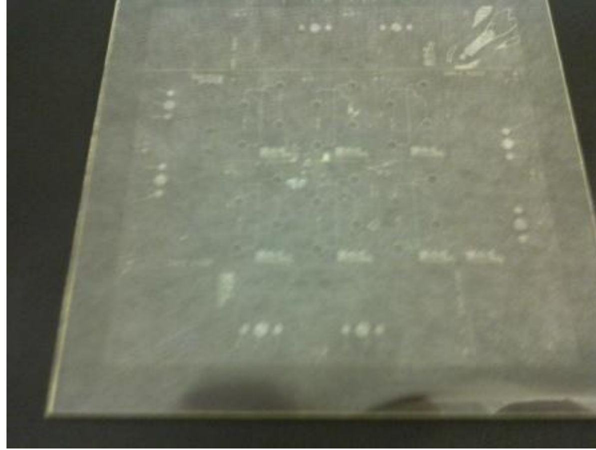

Figure C.10: First Bond of the full PC5k chips. The bond was performed at 100°C for 15 minutes, followed by a bake at 120°C for 15 minutes to facilitate SB. The bonding quality is acceptable, with the only delamination visible due to the presence of the defect in the KMPR film (top right of the substrate)

areas of the defects; Figure C.10). Following the first bond step, each of the substrates was baked at 120°C for 15 minutes to facilitate selective bonding (all SB was done with the DW having been baked at 120°C).

The problems arose during the second bond step. The first substrate was bonded at 90°C for 15 minutes with a force of 5750N. Immediately following bonding however, it was obvious that very poor contact had been obtained, especially in the center of the substrate. The pattern of poor contact certainly appears to possess a certain amount of radial symmetry, suggesting the problem was certainly due to the extra ridging in the dual layer of KMPR. When attempting to release the carrier wafer only very small pieces of KMPR actually released (see Figure C.11).

In an attempt to improve the bonding quality for the second substrate the bonding force was doubled to 11500N (with the expectation that greater force will create better contact). Now the bonding protocol for the second substrate was 85°C for 15 minutes under a force of 11500N. Although the bond quality was higher in this case (especially around the edges of the substrates - the PC5k

Figure C.11: Second bond of the full PC5k structure. Bond was performed at 90°C for 15 minutes with a force of 5750N. In this case the bonding quality was poor due to the 120°C bake performed after the first bonding step.

Chips), the substrate still suffered from poor contact (Figure C.12). Upon attempting to release the carrier wafer, 3 of the PC5k structures remained on the DW, with the remainder of the structures not releasing. This is certainly an improvement over the previous bond (especially considering the use of a lower bond temperature), but still not very good. It should be noted however that on the 3 structures that remained, it was possible to use capillary forces, combined with a bit of syringe-powered valve actuation, to fill IPA from one well, through 6 valves and the PCR chamber, to reach another well (Figure C.13 shows the filling of the PCR chamber in the middle). But the result still isn't all that trustworthy given the poor bond quality overall.

These experiments we repeated with the bonding pressure of the second bond increased to 23kN in order to improve contact. Once more the first bond worked extremely well (Figure C.14). But once more problems arose with the second bonding stop. As can be seen in Figure C.15, contact is improved with the increased pressure, except around spin defects in the carrier wafer (this second bond step appears to be far less forgiving with bonding around defects

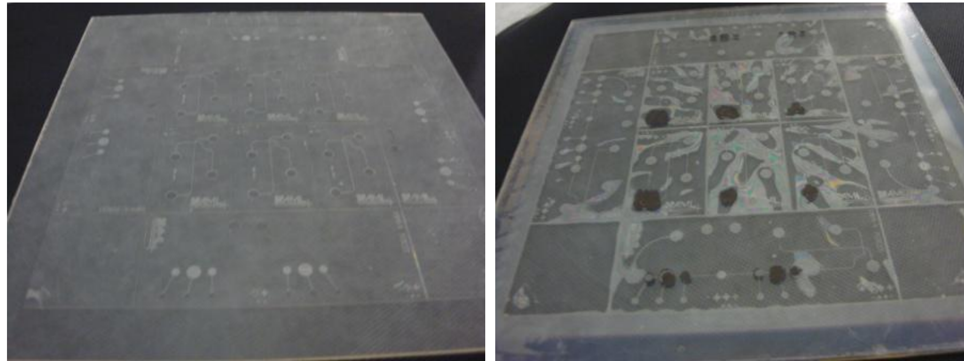

Figure C.12: First and second bond of the full PC5k structure. The second bond was performed at 85°C for 20 minutes with a force of 11500N. Despite the increased bonding force poor contact continued to be made resulting in a poor bonding quality.

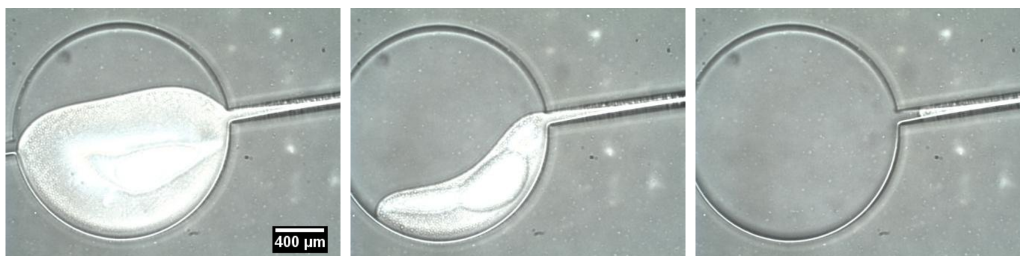

Figure C.13: Filling of the PCR chamber with IPA through the bonded valves. This shows that the valves were not completely sealed shut, though it is hard to say exactly how much they opened.

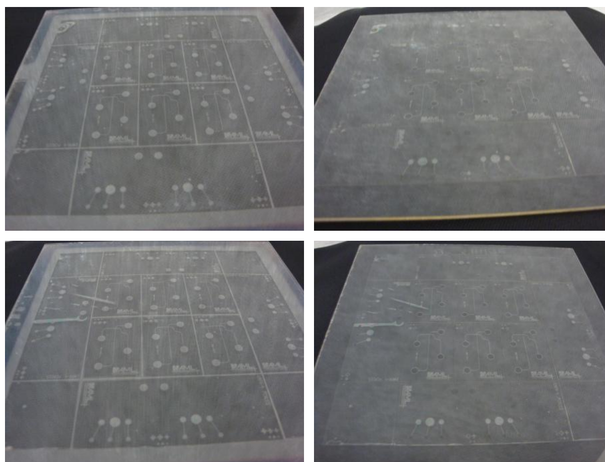

Figure C.14: First bond (2 different substrates) at 100°C for 15 minutes and 11500N of force. From left to right, top to bottom: Pre-release and post release of the first substrate, followed by pre-release and post-release of the second substrate. In both of these cases the bonding quality was good.

than the first step). Unfortunately, despite the much improved contact, the bonding strength was very weak and most of the KMPR was unable to release from the carrier wafer.

C.1.5 Dual SB Exposures

The next tests performed involved exposing both the membrane and the fluidic layers of KMPR with the SB mask (in addition to their own masks) in an attempt to promote stronger bonding while still facilitating selective bonding. The hope was that in the areas where bonding was to be avoided that both layers would have been baked at 120°C, while the remainder of the layers would be prepared at lower temperatures, allowing them to bond together more effectively. To accomplish this method, the first bond step (between the pneumatic layer and the membrane layer) was performed at 80°C (both substrates were prepared with 70°C PEBs). The hope was that this low bond temperature would allow the membrane layer to maintain a low Tg and cross-

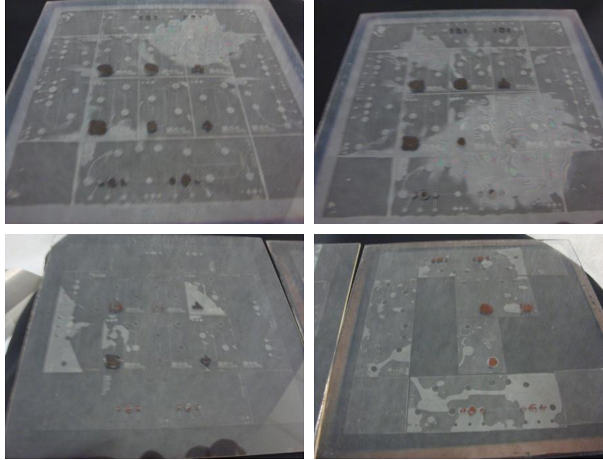

Figure C.15: Second bond. From left to right, top to bottom: 1) 90°C for 15 minutes, 2) 85°C for 20 minutes, 3) post-release of (2), 4) carrier wafer from (2). Once again the bonding quality for this second bond step was poor.

linking level.

Results from the first bond step were surprisingly good. In fact, while cooling the substrates down to room temperature following bonding, the carrier wafers for both trials detached themselves from the membrane layer of KMPR. The bond quality was as good as has been seen to date, with the only significant non-bonded areas being present immediately surrounding some film defects in the second bond trial and around some of the selectively exposed areas (see Figure C.16).

As for the second bond step, the first substrate to be bonded also worked quite well, with the carrier wafer once again detaching itself upon cooling. The bond quality was high, but selective bonding wasn't achieved (Figure C.17).The second bonded substrate did not have such good bonding quality, with parts of the KMPR not releasing from the carrier wafer. The parts that did remain did not show selective bonding (could not release the membranes above the structures, Figure C.18).

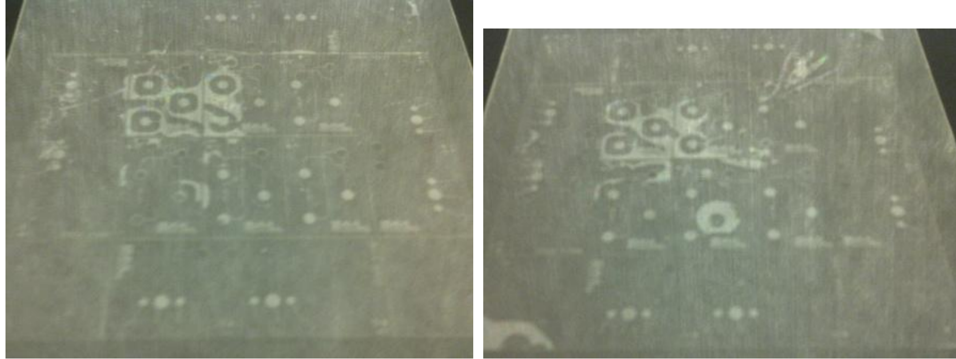

Figure C.16: The first bond step resulting from an 80°C bonding temperature (two trials). The second image shows small non-bonded areas around some large film defects (comet tail and dewetted circle). The bonding quality was marginal, but good enough to move onto the second bond test.

Figure C.17: Result of the second bond step, bonded at 90°C. The bonding quality remains marginal, the same as the first bond.

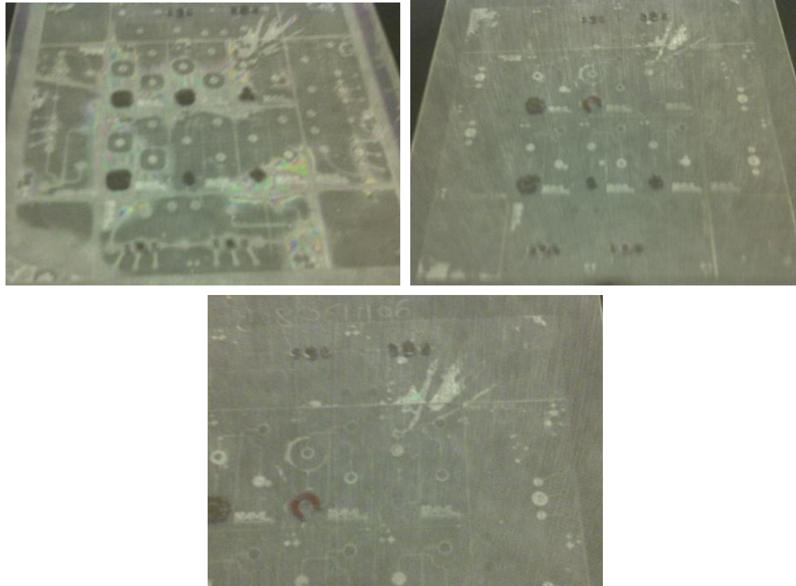

Figure C.18: Images of the second bonded substrate (2nd bond step). The first image shows the substrate before release the CW, the second image shows the substrate following release, and the third image is a close up of some of the non-bonded areas. The bonding quality was acceptable, with only small areas of delamination.

C.2 Conclusions

Following this lengthy set of experiments, it still appears that selective bonding is possible, although with the lack of consistency in achieving positive results it does not seem feasible to perform this process using the current equipment (especially the hotplates) present in the nanoFab. It would not be surprising if the error in temperature for the hotplates being used to be as high as 10°C (in either direction) and as a result it is doubtful that SB will be able to achieved in the nanoFab. However, this work has greatly improved the reliability of the bonding process, even at bonding temperatures as low as 80°C, and any bonding process not requiring selective bonding can likely be performed with a workable rate of success. Perhaps a redesign of the fluidic systems to operate without requiring the use of normally-closed valves could yield positive results.

The summary of results related to finding an operating window for SB

follows.

- 60°C PEB temperature produces serious delamination problems during fabrication of the carrier wafers. A lower PEB should allow for an increased bonding yield at lower bonding temperatures. Delamination may be less of an issue if the KMPR layer were spun on another layer of KMPR (i.e. the current 4-layer process), so we may still be able to reach this temperature in our final process. For the time being though we are limited to 70°C PEB temperatures.

- A Bonding temperature of 80°C (with 120°C SB and 70°C PEB) yields very weak/unsuccessful bonding (though successful SB; note: DW in this case is baked at 100°C or higher), bonding at 85°C yields weak bonding (though still partially successful) along with promising SB, bonding at 90°C yields good bonding, but with poor SB (ink required). Note: 2-layer process notes, in the 4-layer process the bond quality of the second bond is greatly reduced.

- For the 4-layer bonding process, poor bonding quality is obtained in the second bond step using 85°C (20 minutes) and 90°C bonding temperatures (23kN). Note: DW is baked entirely at 120°C for 20 minute following the first bond step.

- Post bond bakes at 100°C for 10 minutes serves to strengthen bonding performed at 85°C, with minimal effect on the SB results.

- SB baking at 130°C starts to cause problems with developing KMPR. Anything higher than 130°C would likely prevent developing at all.

- Bonding pressures less than 23kN during the second bond step of the 4-layer process yields quite poor contact. Pressures of 5750N and 11500N

yield acceptable contact during the first bond step.

- Bonding at 10 minutes yields poor bonding at 90°C, where bonding for 20 minutes at 85°C yields successful bonding for a 2 layer process.

- When both substrates are prepared at 70°C baking temperatures, bonding quality is high at temperatures as low as 80°C. Selective bonding results have not been achieved however, even when areas on both sides of the bond are selectively exposed.

Reducing the PEB temperature to 60°C would likely help open the window further, as would increasing the SB bake temperature to 130°C. Just how much effect this would have has yet to be seen. Another issue is that of strengthening the bonded KMPR (15-30 PSI bond strength is not very good) while not bonding the SB-exposed areas. Baking for extended periods of times (20 minutes) at 90°C or more begins to reduce the SB yield for substrates bonded at 85 and 90°C, but shorter post-bond bakes (10 minutes) at 100°C serves to strengthen the bond, while producing a minimal effect on SB yield (observed on substrate bonded at 85°C).

Increasing the bonding time to 20 minutes at 85°C increases the bond quality, while still allowing for a reasonable SB yield, especially when coupled with a post-bond bake. A 10 minute bond at 90°C yielded poor results. There is an issue of consistency for bonding at this temperature, but with minor tweaking (bond pressure, temp, time) it should be possible to find a more stable point.

It has also been confirmed that even after passing through the bonding process the water-soluble ink washes off the KMPR simply by running water over it (tested on KMPR which did not release from the carrier wafer following bonding).

Appendix D

Lithographic Roughening

D.1 Introduction

This appendix contains information related to an observed behaviour of KMPR following exposure and baking. At the edges of exposed features roughening of the surface could be produced using only UV exposure and baking steps (no developing or etching required). This appendix will include the motivation behind this work, along with a list of possible applications, the fabrication methods used and the results of the experiments.

D.2 Motivation

After more than 6 months of working on selective bonding of KMPR to produce valves, with little success, it because clear that another technique would be needed to prevent bonding in selected areas of KMPR structures/substrates. The idea behind selective bonding was to increase the polymer cross-linking level in certain areas of the KMPR (i.e. where the valves are located) in order to prevent any bonds from occurring across the interface between the two layers. Unfortunately this technique met with very limited success and alter-

native methods are required. It would be most beneficial if a method could be developed that doesn't require any new fabrication technologies to be used, hopefully minimizing the development time.

In the course of working with KMPR it has been noticed on multiple occasions that KMPR tends to "pile up" at the edges of exposed features creating a short ridge typically between a few tens of nanometers and several hundred nanometers high (Figure D.1). The height of this ridge seemed to be proportional to the temperature and duration of the post-exposure bake. It is hoped that this effect could be manipulated to limit the contact area during bonding. In order to use this technique it is necessary to determine what factors are involved in producing this effect and how it can be controlled to produce a viable selective bonding process.

D.3 Method

The key concept behind this technique is the decrease in thermal expansion coefficient (TEC) of KMPR during crosslinking. It has been demonstrated in SU-8 that when the resist heats at the beginning of a PEB it will expand (almost equally between exposed and non-exposed resist), however when the sample is cooled down following the PEB the cross-linked resist has a significantly reduced TEC, causing the exposed resist to contract less upon cooling [78] (Figure D.2). Ridges, which appear as localized increases in film thickness at the edges of exposed features, are caused by surface tension effects where exposed KMPR (which expands slightly less than non-exposed KMPR during heating) is pulled upwards towards the higher, non-exposed KMPR. Upon cooling the KMPR is unable to reflow due to the reduced temperature and as the KMPR retracts, the ridge remains, with approximately half of the

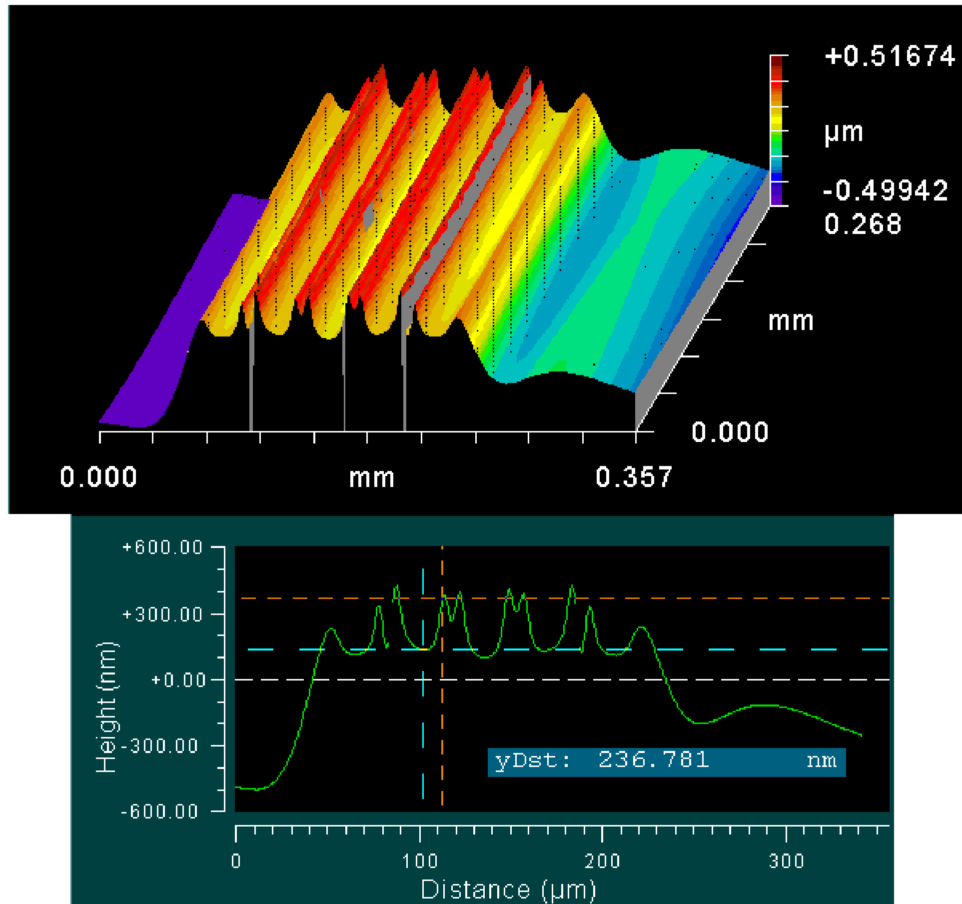

Figure D.1: Optical profilometer measurements of the surface profile of a set of 6 parallel lines that were exposed and hard-baked. No development has been performed on the film, and all localized non-uniformities are as a result of the exposure and baking of the film.

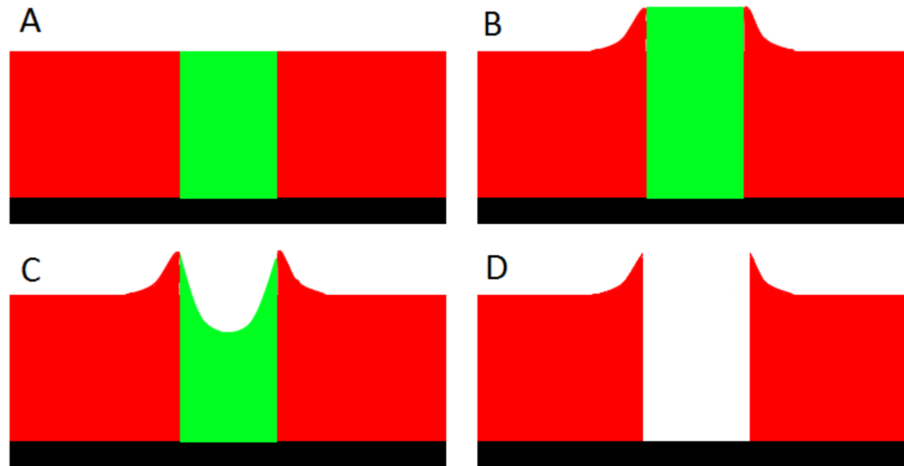

Figure D.2: Visual example of the surface structure of exposed (red) and unexposed (green) resist during exposure (A), heating (B), cooling (C) and developing (D). The ridges are clearly demonstrated to form in the exposed resist by flowing up to the higher, non-exposed resist.

ridge consisting of exposed KMPR and the remainder of the ridge composed of un-exposed KMPR (held up by the same surface tension effects that created in the ridge in the first place).

Assuming this mechanism is accurate, it stands to reason that the higher the temperature and the faster the temperature ramp of the PEB, the more exaggerated the thickness difference will be. It is also likely that as features are brought closer together that these effects will begin to overlap, and further manipulate the effect. It seems possible that 200nm height difference could actually be created in as simple a process change as adding a single exposure and bake step.

The first experiments to confirm this effect involved 4" square Borofloat glass substrates, spin coating a 20 μm film of KMPR (3000 RPM) and soft-baking the films at 100°C for 10 minutes. The KMPR was then exposed to a pattern including a variety of different shapes, sizes and pitches using a number of different dose intensities across each substrate. Each substrate was then

placed on a hotplate at either 80°C, 100°C, 120°C or 150°C for 30 minutes. Following the bake step the substrates were then removed from the hotplates and allowed to cool to room temperature. The substrates were then blanket exposed to several different dose intensities (resulting a grid of different exposures across the substrates, with each section of the substrate being exposed to a different combination of pattern and blanket doses). Following these blanket exposures, the substrates were all placed on hotplates at 100°C for 5 minutes. Once the substrates were allowed to cool, the surface profiles were studied using a Zygo optical profilometer. The substrates were coated in a 20 nm film of gold from a Denton desktop sputtering system to improve the profilometer measurements. An overview of the fabrication process used is shown in Figure D.3.

D.4 Results and Discussion

This section will start with the following definitions to ease the wording of the rest of the section:

- Dose 1: The pattern dose - applied to the substrate through the photomask. KMPR exposed to this dose will be referred to as "patterned" or "A" KMPR.

- Dose 2: The blanket dose - applied to the entire substrate without the use of a photomask. Although all of the KMPR (including patterned KMPR) is exposed to this dose, only the KMPR being exposed exclusively by this dose (i.e. all the KMPR not exposed to Dose 1) is referred to as "blanket-exposed", "blanket" or "B" KMPR.

Measurements were taken for each of the 4 different PEB temperatures, with the doses examined involving the lowest and/or the highest doses applied

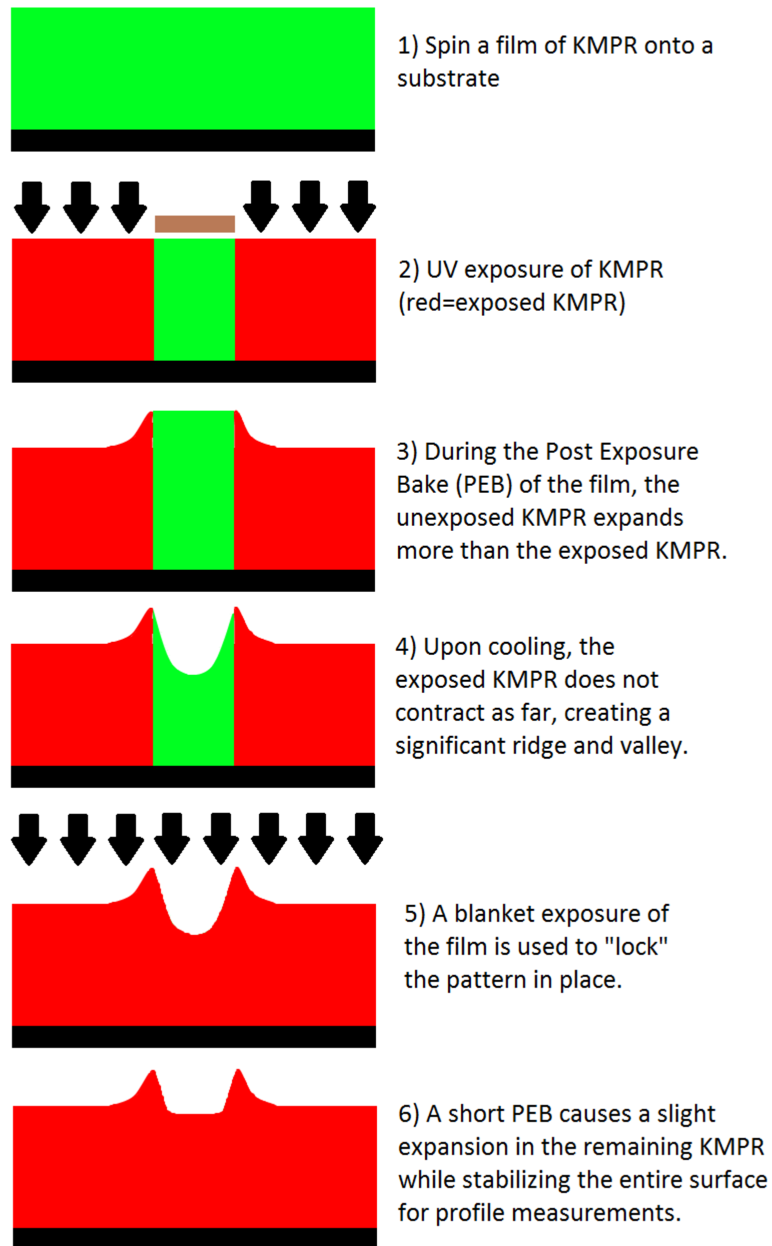

Figure D.3: Fabrication overview for lithographic roughness tests.

Table D.1: Lithographic Roughness Results. All measurements are peak-to-peak height difference of patterned features. Dose 1 is the pattern dose, Dose 2 is the blanket dose. The "Ridge?" column states either "Yes" or "No" depending on if a ridge is visible at the edges of features. The bake temperature is the PEB temperature after Dose 1 (30 minute bake). After Dose two, all PEBs were at 100°C for 5 minutes.

Bake Temp	Dose [J/cm^2]		Roughness (Peak-to-Peak) [nm]			
^{o}C	Dose 1	Dose 2	15μm Square	Ridge?	30μm Square	Ridge?
80	0.8	0.8	123	Yes	282	Yes
	2.2	0.8	216	No	691	Yes
	1.2	1.8	269	No	428	Yes
	2.2	1.8	171	No	923	No
100	0.8	0.8	36	Yes	147	Yes
	1.8	0.8	210	No	236	Yes
	0.8	1.8	42	Yes	172	Yes
	1.8	1.8	259	No	325	Yes
120	0.8	0.8	29	Yes	221	Yes
	1.8	0.8	125	No	202	Yes
	0.8	1.8	41	Yes	226	Yes
	1.8	1.8	222	No	344	Yes
150	0.8	0.8	315	Yes	1178	Yes
	1.8	0.8	707	No	794	Yes
	0.8	1.8	285	Yes	1317	Yes
	1.8	1.8	982	No	886	Yes

to the substrate in either the first or second exposures. The measurements were taken from areas patterned with either 15 μm or a 30 μm checkerboard pattern (alternating pattern exposed and blanket exposed squares). Results are shown in Table D.1. Note that the dose combinations for the 80°C bake temperature are slightly different than for the rest, this was due an attempt to use 5 different dose levels on the first substrate, but some of the features were too close to the edge of the substrate (edge bead would skew the results). After the first substrate, the number of doses was reduced to 4 to avoid this problem.

Analyzing these results in order to understand the mechanisms involved (and therefore to be able to predictably use this technique) is quite complicated, as there are a lot of overlapping effects occurring here which make for some rather complicated trends.

Based on an analysis of the results the following list of interpretations can be made as to what is occurring during this process. While listing these it will be stated whether they are directly from and/or derived from literature support or whether they are based on the intepretation of the data.

1. The TEC of cross-linked KMPR is lower than that of non-crosslinked KMPR (TEC decreases as cross-linking level increases). This is directly from Denning [78].

2. Ridges form as a result of un-exposed KMPR expanding more than exposed KMPR when heated (due to the onset of cross-linking reactions, and from contraction due to cross-linking) and surface tension effects "pulling up" the exposed KMPR to form a smooth interface. When cooling, the KMPR becomes too rigid to fully re-flow as the KMPR contracts. This is also from Denning [78].

3. The exposure dose determines the amount of expansion experienced by KMPR during heating; i.e. higher doses result in a higher cross-linking rate during heating, resulting in the TEC decreasing at a faster rate. This effect would result in greater ridging for a higher Dose 1. This is not specifically mentioned in Denning [78], but is no great stretch from their conclusions.

4. A 100°C bake for 5 minutes (PEB for Dose 2) has a significantly smaller effect on the TEC of KMPR than the 30 minute baked applied after Dose 1. This is a conclusion based on the aquired data. A higher dose

would also have a greater effect on the TEC during the second PEB than a lower dose (faster cross-linking rate).

5. For features with a small pitch and exposure/baking conditions resulting in large step heights, the ability for B KMPR to contract upon cooling may be limited by surface tension effects (resulting in a parabolic-type shape) preventing the B KMPR from contracting as much as would be expected for features spaced further apart. This assumption is not stated by Denning but makes physical sense; much like a doubly clamped beam with a uniformly distributed load, the maximum deflection experienced by the beam is proportional to the length of the beam squared.

6. In many situations B KMPR is able to start pulling down the ridges while the KMPR is at a raised temperature and the height of the B KMPR is less than the height of the ridge. This effect is greater when A KMPR is only lightly cross-linked (80^oC PEB), or when the B KMPR is beneath the level of the ridges even after heating (when Dose 2 PEB temperature is less than Dose 1 PEB temperature). This is not mentioned by Denning but explains some trends seen in the results and does make physical sense.

7. As an extension of the last points, the more "pull-down" that occurs, the greater the distance between the ridges of two adjacent pattern edges and therefore the B KMPR is able to contract lower (in cases where surface tension was limiting the contraction of B KMPR). Using the beam equation as an approximation, the increase in the ability of B KMPR to contract is proportional to the square of the increase in distance between the ridges. Given that the ridges are much wider than they are tall (as demonstrated by Denning), the height of the ridges will decrease by less than the increase in the distance between the ridges during pull-down.

As a result, pull-down of the ridges by B KMPR will result in an increased overall step height (note: only in cases where surface tension was limiting the ability of B to contract). Using the trends found in the results, the step heights above which surface tension has a pronounced effects appear to be at approximately 100nm for the 15 μm squares, and approximately 200nm for 30 μm squares. This "pull-down" effect also varies according to the presence of distinct ridges at the edges of features, in cases where the ridges are able to overlap (for tighter features) pull-down will have a greater effect on the distance between peaks than for cases where the ridges are separated into tall, sharp peaks.

Given the amount of information currently obtained it is not possible to state for certain how accurate these assumptions are and further work is needed to understand this situation. What this does confirm is that localized surface roughness is possible using only lithographic exposures and baking.

Appendix E

Heater Metal Choices

When deciding what choice of metal is best suited for use as a resistive heater embedded within our polymer microfluidic structures, there are a number of properties that must be taken into account. In order to reduce the current requirements for heating a higher resistivity is preferred, the higher the better. In order to function as a temperature sensor as well as a heater, the metal must also have a TCR high enough to detect the change in resistance for temperatures between 20°C and 100°C. Given the high currents required for this heating, electromigration resistance is also of interest in order to allow for long-term use of the heaters. Any metal to be used must also be compatible with KMPR during deposition and patterning of the heaters. The heaters must also be able to resist corrosion during operation, as it is likely that moisture from the microfluidics will migrate through the KMPR to the heater during heater operation.

E.1 Aluminium

Aluminium is a common metal used in CMOS devices and as such is a readily available option for the development of CMOS-integrated LOC devices. The

Table E.1: Some properties of interest for different prospective material choices for the development of a resistive heater/temperature sensor embedded within KMPR microfluidic structures. Some materials do not have an accepted electromigration threshold, but are considered to be resistant to electromigration in the current ranges of interest to us (Labeled in this table as having a "Large" electromigration threshold. Temperature for the listed electromigration limits is around 70°C.

Material	Resistivity [Ω-nm]	TCR [K^{-1}]	Electromigration Threshold	Power Density at EM Threshold (150nm film)
Al	27.1	0.0039	1 mA/μm^2	4 kW/m^2
TiW	700	0.02	Large	n/a
TiN	1500	0.0003	Large	n/a
Pt	107	0.00392	Large	n/a
Cu	17.1	0.0068	10 mA/μm^2	257 kW/m^2
Cr	126	-0.0001	Unknown	Unknown
Poly-Si	Varies*	Varies*	Large	n/a

*Value of resistivity and TCR for poly-Si is dependent on B and P dopant concentrations.

resistivity and TCR of Al (Table E.1) is acceptable for the production of a resistive heater, although the current requirements for heating up to 100°C are above the current density threshold (1 mA/μm^2 [71]) where electromigration damage is expected. Simulations predict current densities between 10 and 30 mA/μm^2 would be required to produce the required heating. These currents will result in a reduced lifetime of the heaters, but may not necessarily prevent the use of Al as the heater material.

Al films can be deposited by standard sputtering processes which are compatible with KMPR films, and can be patterned by wet etching using a mixture of phosphoric acid, nitric acid and acetic acid. Other options for patterning, such as lift-off, dry etching, or other wet etchants, are available if needed. Aluminium is typically considered to be resistant to corrosion and oxidation as a result of its thin, self-terminating oxide layer, although heating the film in the presence of moisture may be a potential cause for concern, perhaps requiring

the use of a moisture barrier layer.

E.2 TiW

A titanium-tungsten alloy (W/Ti, 90/10 wt%) is another possibility as a heater material. The resistivity and the TCR of TiW is much higher than that of Al (Table E.1), and it has a much greater electromigration resistance than Al. TiW can be deposited by standard sputtering processes using a single sputtering target for consistent films. Etching of TiW is performed using H_2O_2, although lift-off is another possibility as well. Two concerns arise when considering TiW: its resistance to moisture, especially when heated, and the ability to deposit films without cracking on KMPR. A moisture barrier would be required in order to use TiW in this particular application in order to avoid damage to the heaters during operation. Additionally, numerous attempts have been made in an attempt to deposit TiW on KMPR without the film suffering cracks, with no success being demonstrated. This issue would require significant work to overcome before being able to use TiW in these devices.

E.3 TiN

TiN has also been suggested as a possibility for a heater material. It has a very high resistivity (1500 Ω-nm) compared to Al and TiW, however its TCR is very low (0.0003 K^{-1}) which would make temperature sensing extremely difficult. Wet etching involves a hot solution of ammonium hydroxide, hydrogen peroxide and water which would likely prove problematic for the KMPR films. Dry etching is also possible ($CF_4/BCL_3/N_2$), but the effect on the underlying KMPR film would need to be determined. Moisture resistance of TiN should not be a concern in these devices, and electromigration is not an expected

issue.

E.4 Platinum

Platinum is a commonly used material for this type of application owing to its positive resistivity and TCR (Table E.1), high stability and high electromigration resistance. Platinum can be deposited by a standard sputtering process, although wet etching requires the use of Aqua Regia (hot HCL, HNO_3) which would almost certainly damage the underlying KMPR film. Lift-off patterning is possible with platinum, however experience with a lift-off process with platinum suggests that the process is too slow and would risk serious damage to the underlying KMPR film. Platinum processing is also very expensive due to the high cost of the metal.

E.5 Copper

Copper is another possible alternative material for these devices. Its resistivity is slightly lower than Al (Table E.1), although its TCR is higher. Copper is not typically used with CMOS processes due to its tendency to diffuse into surrounding materials (especially silicon). It is unknown how copper will respond in the presence of KMPR. Copper also tends to oxidize quite readily, which could prove problematic during device operation. Copper also suffers from electromigration issues, although not as severely as Al, with a current density threshold of 10 mA/μm^2 [71] (compared to 1 mA/μm^2 for Al). Copper can be deposited by standard sputter deposition processes, and can be wet etched using nitric acid.

E.6 Chromium

Chromium has been suggested as another alternative material due to its good resistivity (126 Ω-nm) and simple processing. Cr can be deposited by sputtering and wet etched using a solution of ceric ammonium nitrite and nitric acid (compatible with KMPR). Stability of Cr films should not be an issue given the expected operating conditions, although there is little information available as to the electromigration resistance of the material. The main concern with Cr films is the very low TCR (-0.0001 K^{-1}), which would prevent accurate temperature measurements using the resistance change of the heaters.

E.7 Poly-Silicon

Poly-silicon has also been suggested as a heater material. The resistivity of poly-Si is highly variable, depending on the processing and doping conditions of the film, and can be kept extremely high in order to reduce the current requirements of the heaters. The TCR is also dependent on the dopant concentrations, but is generally considered to be quite low (0.0004 K^{-1} is commonly reported), but could still allow for temperature measurements to be made. Electromigration should not be an issue for the operation of the heaters, especially given the possibility for high resistivity (and therefore low current requirements) of the material. Films can be grown using CVD techniques, although the compatibility of the deposition process with KMPR is unknown. Etching can be performing either by RIE processes, or by wet etching (KOH or TMAH), which may lead to issues with compatibility.

Appendix F

Dicing Accuracy

This appendix outlines and discusses the dicing process which uses the Disco DAD 321 dicing saw in the University of Alberta nanoFab. Images will be included that demonstrate the ability of the saw to align to known features on a substrate with final reference given to the actual accuracy of the dicing cuts.

F.1 Dicing Process

The dicing saw uses a pair a optical microscopes operating in stereo to allow for accurate rotational alignment of the dicing cuts (Figure F.1). The system overlays a target reticle over the stereo images to provide a set of 3 fixed, straight lines to use for aligning the cuts (Figure F.2).

Once the substrate is mounted into the substrate the rotational alignment is achieved by using a feature (or features) on the substrate that are known to be at the same "y" position. These two features are then viewed simultaneously in both microscopes and the features are aligned between the images (Figure F.3).

With the rotational alignment established it is time to move on the positioning of the cuts themselves. In the case of the KMPR PC2 devices dicing

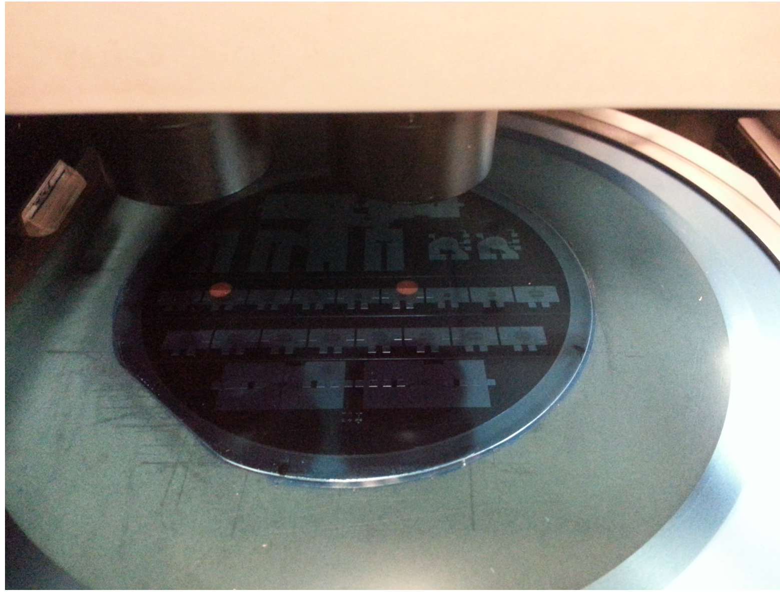

Figure F.1: Substrate mounted on the dicing saw, showing the location of the stereo alignment microscopes.

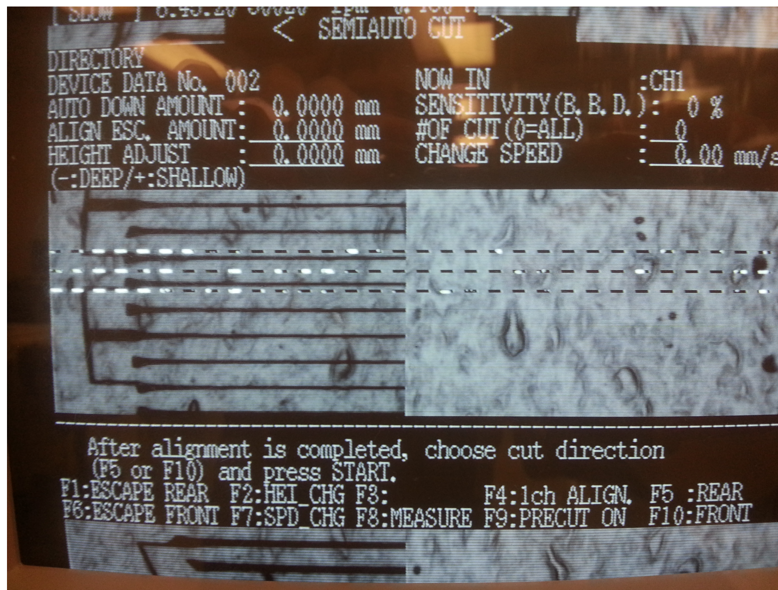

Figure F.2: The dicing system overlays a targeting reticle (3 parallel dashed lines) over the center of the two microscope images. Notice the left and right sides of the image are actually different images, this will be the case for all images displayed on screen. The heater traces are displayed on the left to give an idea as to the scale of the image. The thickness of each dicing line is around 5-10μm.

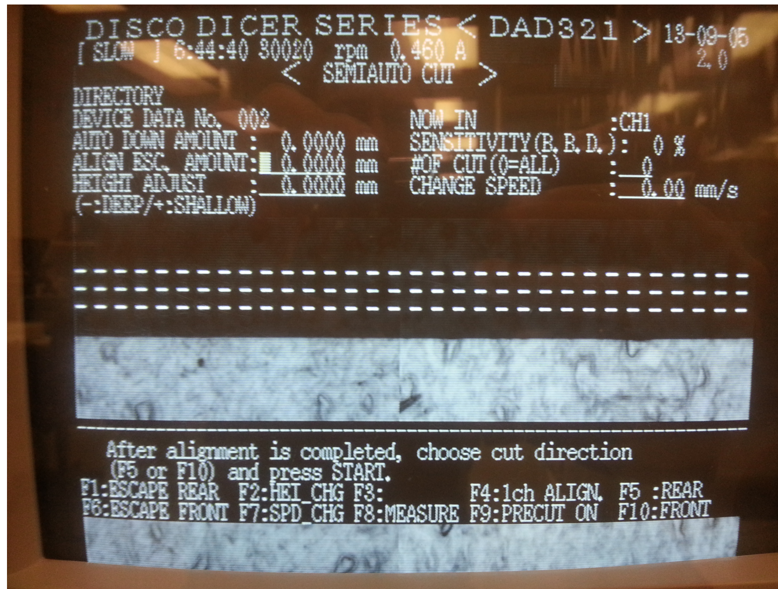

Figure F.3: Rotational alignment is achieved by lining up two features on opposite ends of the substrate, in this case the top edge of the aluminium of two different devices. Notice the lack of seam present between to images (the target reticle is not used at this stage).

lines have been included on the substrate in order to provide a fixed location for the cuts to be applied. Although the dicing lines are only present in the KMPR layers the line edges are clearly discernible to the alignment microscopes (Figure F.4). Given the size of the lines in the target reticle position of the substrate can easily be achieved with an accuracy of at least 10μm (approximately the size of the reticle). Every cut that is performed on these devices is aligned to features that are at least as visible as the dicing line (in the case of cuts aligned to a metal feature it is even easier to see the feature).

F.2 Discussion

The initial devices that were designed and fabricated (Batch 1, described in Appendix A) were produced with minimal consideration given to the accuracy of the device dimensions. As a result the initial dicing was performed by

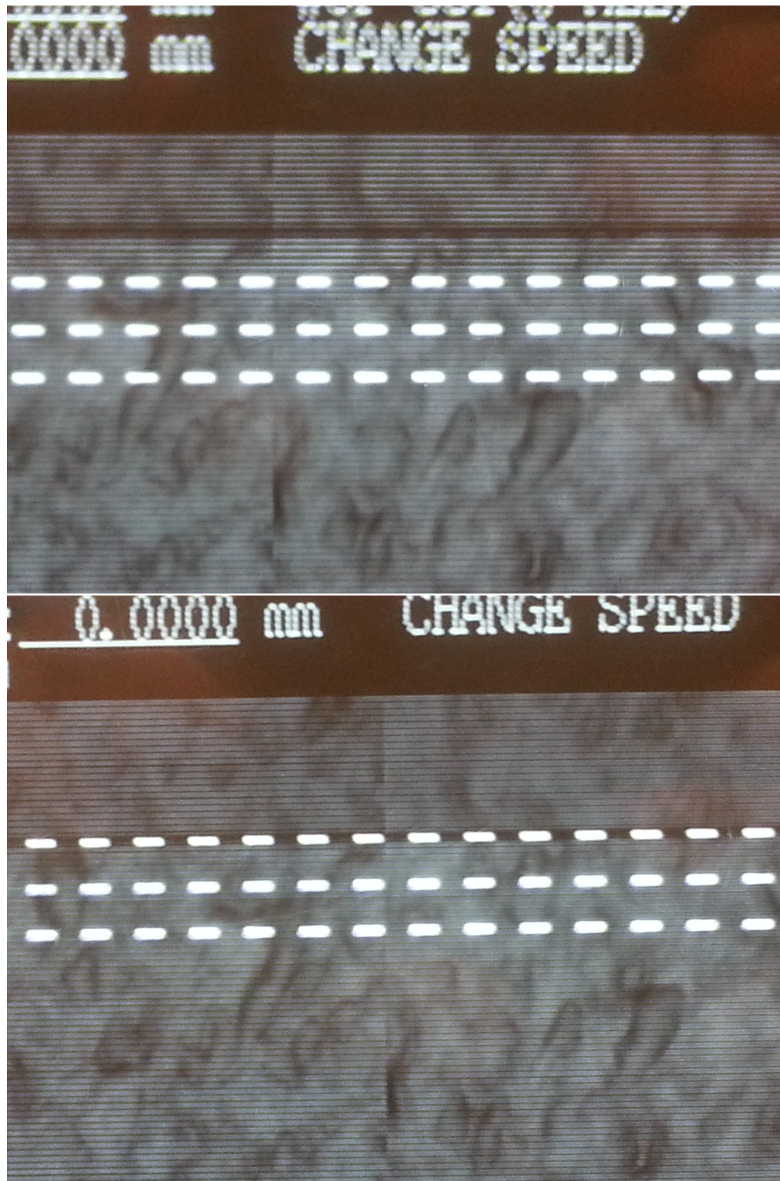

Figure F.4: The edges of the dicing lines are easily observed using the alignment microscopes (top image). The target reticle can be aligned to the edge of the dicing line to provide a consistent target position (bottom image - it may be difficult to see due to the picture quality, but the top line of the reticle is positioned directly over the dicing line).

casually locating the cuts within a 300 μm wide area patterned between the designed devices. After this first batch was produced it was decided that the dicing process should be changed to provide device dimensions that were as accurate as possible with respect to the designed dimensions of the chips.

As shown in the previous section alignment using the stereo alignment microscopes is possible to achieve with accuracy better than 10 μm. According to the system's specifications published by the manufacturer [79] the expected error in positioning the stage is +/- 8 μm. When combined with the manual alignment error each cut could be expected to have an error of approximately 18 μm. When comparing the distance between two cuts the maximum expected error would be twice this, or 36 μm. Given this information the specification for the dicing accuracy was tentatively identified as being +/- 40 μm from the designed dimensions.

Unfortunately we have discovered that despite this expected level of precision the actual diced dimensions of the final devices have varied by much more than this. Chips from each batch (Batch 2, 3 and 4) have had their device dimensions verified using a micrometer. In each of the 3 batches that have been fabricated since the dicing protocol was changed the width of the diced chips have been measured to be between 8.87 mm and 9.03 mm, with the designed width being 8.95 mm (the actual designed device width was 8.93 mm but a bias of 10 μm was intentionally added to each side of the chip in order to avoid the removal of any of the electrical contact pads). Based on this information the actual variation in the dimensions of the chip is +/- 80 μm.

This actual inaccuracy cannot be caused by a constant offset in the position of the dicing blade (if every cut had the same offset then the final diced dimensions would be unchanged). The software operating the dicing saw also seeks to avoid problems with the stage motors by ensuring the final movement dur-

ing alignment is always in the same direction (sometimes stage control motors have a "dead" space where they do not move immediately when the movement direction is changed). Discussions with multiple experienced users of the tool have also failed to yield any techniques to improve the dicing accuracy. Given the measured variation in the final diced dimensions the logical explanation for the additional error is the system's inability to consistently position the dicing blade for each cut, resulting in a seemingly random deviation every time a cut is made.

The most likely explanation for the discrepancy between the expected error (36 μm) and the actual error (80 μm) is considered to be the age of the tool resulting in a reduced accuracy in the positioning motors. A refurbishment of the tool might serve to increase the reliability of the motors otherwise the only available option for improving the dicing accuracy would be to send the devices to an external facility for dicing. Until another method for dicing is implemented the current specifications for the accuracy in the dimensions of the diced chips is taken to be within 100 μm of the designed dimensions in order to provide a margin of error in the alignment of any chips to any external systems that will be used in the operation of these devices. This is the specification that was listed in Chapter 4.